# USING ELECTRICAL RESISTIVITY TOMOGRAPHY TO CALIBRATE SEAWATER INTRUSION MODELS ALONG THE ALABAMA GULF COAST

by

NATHAN L. COBURN

NATASHA T. DIMOVA, COMMITTEE CHAIR
CHUNMIAO ZHENG, COMMITTEE CO-CHAIR

GEOFFREY R. TICK
NEIL ANDERSON

A THESIS

Submitted in partial fulfillment of the requirements
for the degree of Master of Science
in the Department of Geology
in the Graduate School of
The University of Alabama

TUSCALOOSA, ALABAMA

2015

Copyright Nathan L. Coburn 2015
ALL RIGHTS RESERVED

LIST OF ABBREVIATIONS AND SYMBOLS

ERT Electrical Resistivity Tomography

SI Seawater Intrusion

*In-situ* In position

G-H Ghyben-Herzberg

MODFLOW Modular Finite Difference Flow Model

MT3DMS Modular Transport Three Dimensional of Multi-Species Model

USGS United States Geological Survey

UCODE Universal Code

EPA Environmental Protection Agency

ER Electrical Resistivity

RMS Root Mean Square

AGI Advanced Geophysical Instruments

2-D Two Dimensional

3-D Three Dimensional

PEST Parameter Estimation

TDEM Time Domain Electromagnetics

Km Kilometers

m Meter

GPS Global Positioning Satellite

# ABSTRACT

Numerical models (e.g., MODFLOW/SEAWAT) are commonly used to quantify the extent and magnitude of seawater intrusion (SI). Since coastal communities must account for SI into local aquifers, numerical models can be an effective planning and management tool as coastal populations increase. While these models tend to be limited by the availability of hydrological data, uncertainty in these results can be substantially reduced through the integration of field geophysical measurements. Field measurements employing electrical resistivity tomography (ERT) were utilized to calibrate a density-dependent groundwater flow model for Gulf Shores, Alabama. Specifically, six independent ERT profiles were produced within a modeled area adjacent to a shallow lake and along the near-shore boundary. The ERT methods were employed to a depth of 95 meters, encapsulating two aquifer systems with previously identified SI concerns (*Chandler et al*, 1986; *Murgulet and Tick*, 2008). Results from the ERT deployments were compared to previously developed models' near shore density boundary constructed from local borehole data, then utilized to calibrate the model freshwater/saltwater mixing zone. Other geophysical investigations employing similar methodology (e.g. Time-Domain Electromagnetics) have been used to calibrate SI models and to explore the extent of SI in a number of coastal regions. This study expands upon previous research through the integration of a 3-D groundwater flow model with greater resolution ERT measurements to more accurately determine the extent of SI, and delineate the near shore freshwater/seawater boundary zone.

# DEDICATION

This thesis is dedicated to those most important to me during my time as a graduate student: my wife, Adah Coburn, children: Faith and AJ, my parents: Luke and Charlene, and my friends, whose support made this possible.

# ACKNOWLEDGMENTS

Funding for this project was provided by the University of Alabama, Department of Geological Sciences Johnson Fund and the Lindahl Endowment and the AWRI and the US Geological Survey (contract #) via Dr Geoffrey Tick and Dr. Natasha Dimova. The author would like to give special thanks to the Evgeniy Torgashov from the Missouri University of Science and Technology (MST Rolla) who provided the ERT equipment for the field measurements and expertise to complete this research. John Ellis, currently at the US Geological Survey in the Oklahoma Water Science Center, contributed significantly by providing his groundwater flow model for this work and helped with locating wells. I would like to thank Dr. Natasha Dimova, who spent countless hours encouraging me and getting exasperated with me. She is a devoted researcher to whom I am very grateful.

CONTENTS

LIST OF ABBREVIATIONS AND SYMBOLS ..... ii

ABSTRACT..... iii

DEDICATION..... iv

ACKNOWLEDGMENTS .....v

LIST OF TABLES..... viii

LIST OF FIGURES ..... ix

1. INTRODUCTION .....1

a. Objectives.....3

2. BACKGROUND .....5

a. Site Description.....5

b. Hydrogeology .....5

c. Methodology .....7

i. Field data collection.....8

ii. ERT-derived salinity assessments .....9

iii. MODFLOW/SEAWAT calibration procedure.....19

iv. Calculating salinity from resistivity and location of the freshwater-seawater interface.....20

3. RESULTS AND DISCUSSION.....24

a. ERT imaging field results from Gulf State Park, Gulf Shore, AL……..24

b. Converting ERT profiles to salinity profiles: uncertainties and assumptions…….35

c. MODFLOW/SEAWAT: variable-density groundwater flow model …53

d. Validating or refuting the existing SI models .....55

e. Predictions Based on SI Model developed for this Study.....66

4. CONCLUSIONS.....71

REFERENCES .....73

APPENDIX.....77

LIST OF TABLES

Table 1 Constants for calculating salinity from conductivity (from *Fofanoff and Millard Jr.*, 1983)…….10

Table 2 Typical resistivity values of different substrates (from *Zohdy and Jackson* [1969] and *Dimova et al.*, 2012)……12

Table 3 Effective porosities for sedimentary material (from *McWorter and Sunada* [1977])…….15

Table 4 Cementation factors for sand to sandstone (from *Bateman* [1985])…….15

Table 5 Range of formation factors (*F*) for sand to sandstone calculated using *McWorter and Sunada* (1977) and *Bateman* (1985)…….16

Table 6 ERT array characteristics and identified regional aquifer layers…..….35

Table 7 Depth, resistivity, and GPS coordinates of pore-water from sampled boreholes used for the calibration in this study.……..38

Table 8 Position of *G-H relation* Depth of Z to observed h and calculated h.….49

Table 9 Comparing of constant concentration boundary *Ellis et al.* (in prep.) model to the model parameters used in this study…….61

LIST OF FIGURES

Figure 1 Typical coastal aquifer system set up showing the fresh - seawater interface in the subsurface modified from *Barlow et al.*, (2003) and *Cooper et al*., (1964)……..……2

Figure 2 Maps showing the boundaries of the research area .....5

Figure 3 Cross-sectional fence diagram illustrating different hydrologic units in the study area…….....6

Figure 4 Flowchart presenting the main steps in completing this study.....8

Figure 5 Isopleth plot of clean sand with low salinity porewater *Worthington et al.,* (1974) .....13

Figure 6 Example using ERT profile "a" taken near the beach Perpendicular to the shore.....14

Figure 7 Shaly/Clay sand core conductivity behavior, after *Waxman and Smits* (1968). (*Thomas et al.*, (2010), *Jin et al.*, (2007)) ....17

Figure 8 Determination of profile salinity from nearby wells is accomplished using two described methods. .....21

Figure 9 Study site (Gulf State Park) with ERT arrays and previous studies' SI extent presented .....25

Figure 10 ERT images of arrays carried out within the study area .....35

Figure 11 Map of porewater sample borehole locations along with illustrated extrapolated salinity projections .....38

Figure 12 Example 1 of discerning stratagraphic layers from resistivity results (clean sand and clay layers in freshwater).....40

Figure 13 Example 2 of discerning stratagraphic layers from resistivity results (seawater in clay layers) .....40

Figure 14 Resistivity-derived salinity profiles superimposed on the lithological makeup of the aquifer system in the study area.....45

Figure 15 Interpolated extent of SI (ppt) in Aquifer A1(13a) and Aquifer A2a-c .....52

Figure 16 Illustrated SI profile extents of by previous studies as compared to ERT derived results .....57

Figure 17 Scatter diagram showing the goodness of fit between the observed and calculated heads for 2013 produced by the model developed in this study.....62

Figure 18 Comparison of the seawater extent between *Ellis et al.*(in prep.) and this study .....64

Figure 19 Current (year 2013) seawater intrusion extent for aquifers as determined by *Ellis et al,* (in prep.). .....65

Figure 20 Seawater intrusion extent for aquifers as determined by this study.....66

Figure 21 Predicted extent of SI by this study for Aquifer A2a for 2036 .....68

Figure 21 Predicted extent of SI in AquiferA2a for 2113 for 100 years of "zero" pumping.....69

## 1. INTRODUCTION

Assessing the extent of seawater intrusion is critical for predicting groundwater deterioration and managing water resources of coastal aquifers. Numerical models (e.g., MODFLOW/SEAWAT) are commonly used to quantify the extent and magnitude of seawater intrusion (SI) and have become effective planning and management tool as population increases and puts higher demand on freshwater resources in coastal areas. While these models tend to be limited by the availability of hydrological data, uncertainty in these results can be substantially reduced through the integration of field geophysical measurements. Previous studies have demonstrated the ability of electromagnetic (EM) data to determine the extent of saltwater intrusion at many sites in the world (e.g., *Fitterman and Stewart,* 1986; *Goldman et al.*1991; *Frohlich et al,* 1994; *Duque et al*, 2008). Recently, *Herckenrath et al* (2013) demonstrated that time-domain electromagnetic methods (TDEM) can be used successfully to calibrate saltwater intrusion model. Interpretation of the results is very complex because of high level of heterogeneity of these coastal aquifer systems. High-resolution geophysical field data sets supported by good understanding of hydrogeology of the study area is imperative for adequate results.

Seawater intrusion is the movement of seawater into fresh water coastal aquifers. It is result of differences in water densities and can be triggered by natural processes and human influence where fresh groundwater resources are over exploited, rendering groundwater unsuitable for use. The first physical formulation of saltwater intrusion was given by *W. Badon-Ghijben* (1888, 1889) and *A. Herzberg* (1901) (thus called the "*Ghyben-Herzberg relation*").

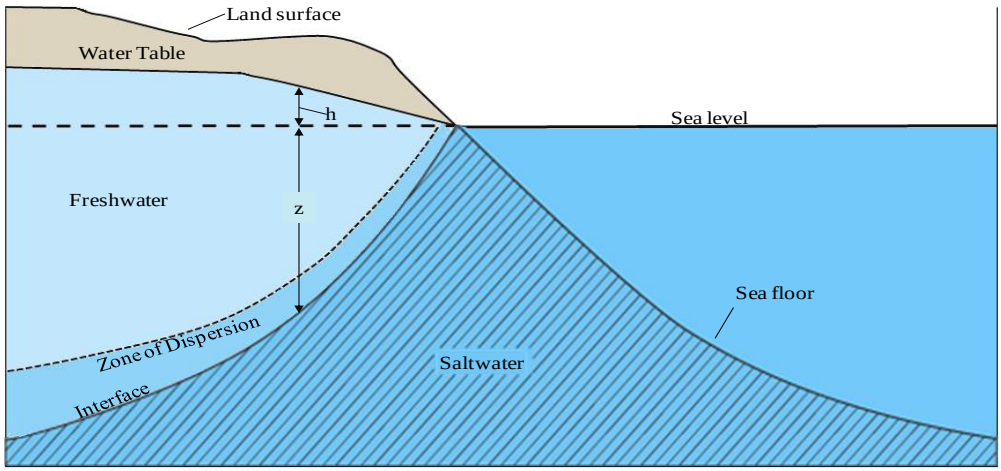


**Figure 1** Typical coastal aquifer system set up showing the fresh - seawater interface in the subsurface modified from *Barlow et al.*, (2003) and *Cooper et al*., (1964)

Locating the fresh-seawater interface, i.e. the relationship between the parameters in **Figure 1** (*h* and *z*), can be done using the *Ghyben-Herzberg* formula:

$$z = \frac{\rho_f}{(\rho_s - \rho_f)} \times h \quad (1)$$

Where *h* is the thickness of the freshwater zone above sea level and *z* the thickness of the freshwater layer below sea level. The two thicknesses *h* and *z*, are related by $\rho_f$ and $\rho_s$, where $\rho_f$ is the density of freshwater and $\rho_s$is the density of saltwater. Since freshwater has a density of about 1.000 grams per cubic centimeter (g/cm$^3$) at 20 °C and seawater is about 1.025 g/cm$^3$, Equation 1 can be simplified to:

$$z = 40 \times h \quad (2)$$

The Ghyben-Herzberg ratio states that for every foot of fresh water in an unconfined aquifer above sea level, there will be forty feet of fresh water in the aquifer below sea level.

Seawater intrusion is caused by decreases in groundwater levels or by rises in seawater levels. To evaluate seawater intrusion (SI) in coastal aquifers along the Alabama coast, we investigated an area previously subject of SI investigation, namely Gulf Shores, Baldwin County, AL (*Lin et al*, 2008; *Murgulet and Tick*, 2008; *Chandler et al*, 1996). For consistency, all SI investigations, regardless of specific model boundaries and approach, use initial conditions as described by *Chandler et al.*, (1985). In this study, we utilized field geophysical measurements employing electrical resistivity tomography (ERT) to calibrate a density-dependent groundwater flow model (MODFLOW/SEAWAT) that was previously developed by *Ellis et al* (in prep.). We selected this study site to test our approach because: (*i*) previous studies by *Lin et al*, 2008 and *Murgulet and Tick*, 2008 have indicated larger scale saltwater intrusion in the area; (*ii*) this area is relatively small (45.5 $km^2$) and thus manageable to perform high resolution ERT measurements that will be used for calibrating SI numerical model; (*iii*) recently, *Ellis et al* (in prep.) had revised and re-constructed the hydrogeological set up of the aquifer system and this give us confidence that the framework is very well known. As such, this study expands upon previous research through the integration of a 3-D groundwater flow model with greater resolution ERT measurements to more accurately determine the extent of SI.

### a. Objectives

The goal of this study is to accomplish three main objectives:

1) Perform high resolution deep ERT measurements subsurface in areas with previously predicted SI and re-construct subsurface salinity distributions in the local coastal aquifer system
2) Calibrate the most recent groundwater flow model in the study area

(MODFLOW/SEAWAT) by *Ellis et al* (in prep.) using observed ERT/salinity values.

3) Evaluate the current extent of the fresh-seawater interface and forecast future trends.

## 2. BACKGROUND

### a. Site Description

This study utilizes the same rectangular-shaped groundwater study area (**Figure 2a&b**) of *Ellis et al.* (in prep.). The area includes the city of Gulf Shores in southern Baldwin County, extending northward to the outskirts of Foley, bound on the north by Cypress Bend Drive, on the south by the Gulf of Mexico, in the east by Powerline Rd, and in the west by West 6$^{th}$ Street. The north side of Gulf Shores is mostly agricultural as is the majority of Baldwin County. Although the city of Gulf Shores has relatively small population of 9,795 (*US Census Bureau. 2010*), a significant portion of 4.6 million tourists visit Gulf Shores annually, with tourist population peaking during the summer months (*Alabama Gulf Coast Region Chamber of Commerce. 2010*).

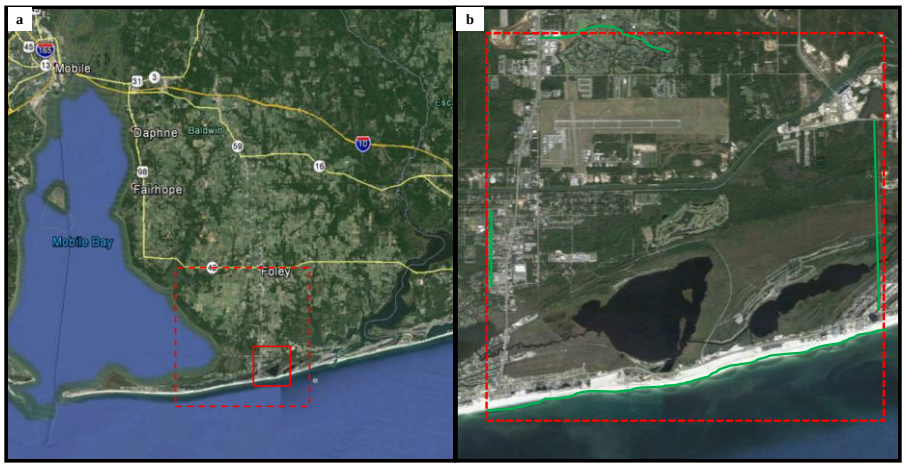


**Figure 2** Maps showing the boundaries of the research area. **(a)** Red dashed line on the map shows the boundaries of previous study by *Lin et al* (2008) solid line box represent this research area of this study **(b)** Close look map of the research area; dashed line box shows approximately the boundaries of SI model used in this study.

### b. Hydrogeology

The geologic age and aquifer-zone designation of the hydrogeologic units of the study area has been described in several previous studies (*Chandler et al.*, 1985, *Lin et al.*, 2008). The most

recent reconstruction of the Alabama coastal aquifer system was performed in 2013 by *Ellis et al (in prep.)* and is presented in **Figure 3**.

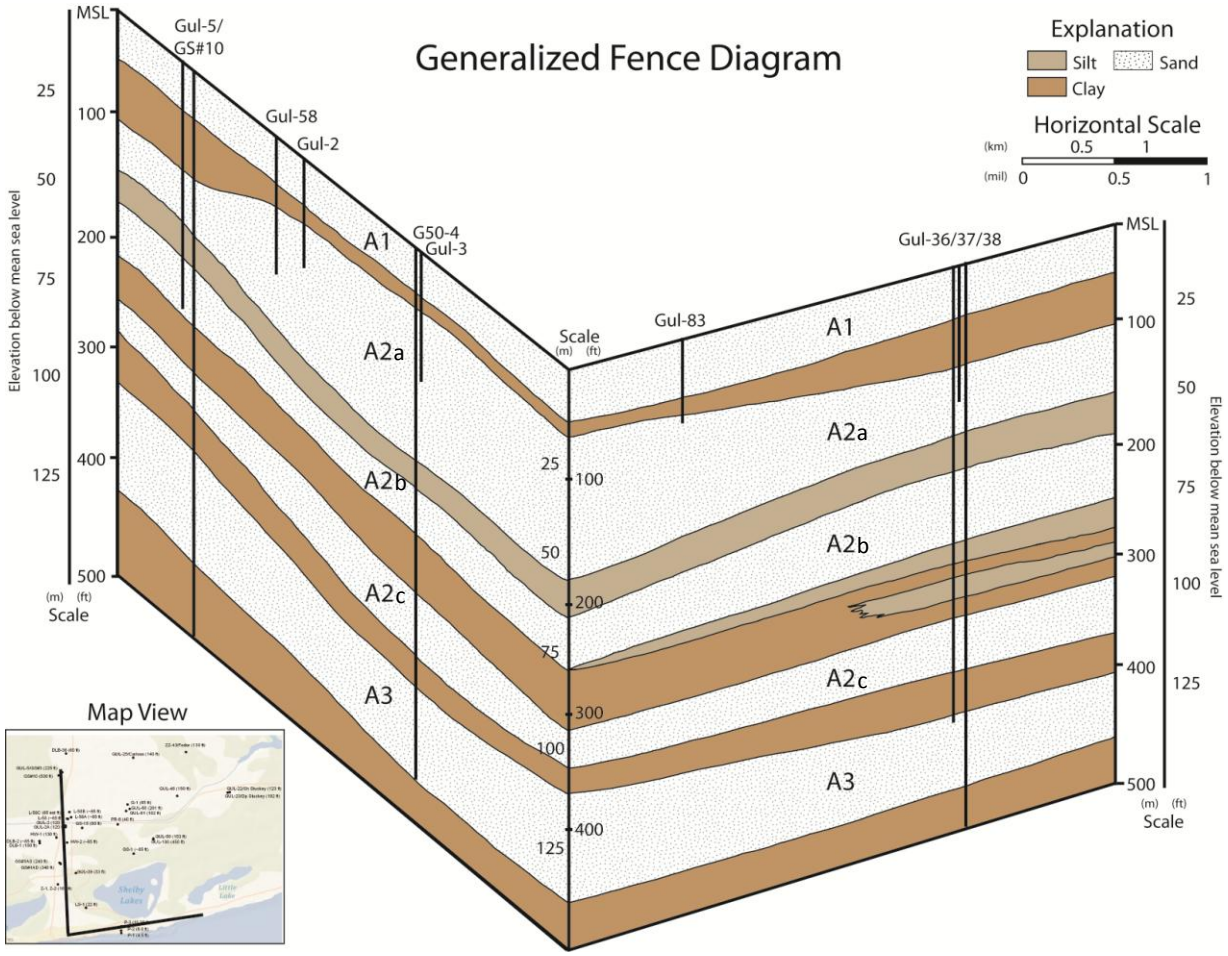


**Figure 3** Cross sectional fence diagram illustrating different hydrologic units in the study area. The coastal aquifer consists of three major aquifer units (A1, A2 and A3). Recent data indicates that aquifer unit A2 is heterogeneous and has been separated into three sub units. Three aquitard clay layers (C1, C2 and C3) separate the A1, A2 and A3 layers (from *Ellis et al (in prep*.))

The uppermost aquifer zone is A1 (also called the ‘‘*Beach Sand aquifer*’’) and it consisting of alluvial, low terrace, and coastal deposits (*Chandler et al.*, 1985). The A1 unconfined aquifer occurs in the entire study area with depths ranging from 12 m to 18 m (**Figure 3**). Underlying A1 is the confining bed C1 aquitard that in turn is immediately underlain by aquifer zone A2.

The A2 aquifer, also referred to as the "*Gulf Shores Aquifer*" in *Walter and Kidd.,* 1979, is up to 76 m thick, primarily consisting of sand and clay with inter-bedded gravel and shell-hash (*Chandler et al.,* 1985, *Lin et al*., 2008), and is unconfined north of the study site, but is confined where it is overlain by the C1 aquitard. Additionally, this aquifer is subdivided (*Chandler et al*., (1985) documents two subdivision ) as the A2 aquifer approaches the coastline by the C2 aquitard clay layer (*Chandler et al*., (1985)). However, interpolations from boreholes drilled since this time show evidence of a three subdivisions (**Figure 3**) with C2 aquitard divided into an upper silt layer and a lower clay layer with additional A2 Aquifer layer sandwiched between the silt and clay. The A2 aquifer is a significant source of freshwater in southern Baldwin County, with a potential yields up to 5,451.0 $m^3$ /day per well (*Chandler et al*., 1985; *Chandler et al*., 1996; *Lin et al.,* 2008). The C3 aquitard underlies the A2 Aquifer that is underlain by the A3 aquifer consisting of undifferentiated sediments. This artesian aquifer has a potential yield greater than 8,176.5 $m^3$ /day per well and is considered the primary source of freshwater in the region (*Chandler et al.,* 1985; *Chandler et al.,* 1996).

### c. Methodology

The approach used in this study follows the flowchart presented in **Figure 4**. The development of the SI model in accomplished through three stages: (*i*) hydrogeological data collection; (*ii*) groundwater flow model development and (*iii*) ERT field data collection and interpretation and model calibration. Since the first two steps of this approach were previously developed by *Ellis et al* (in prep.), the goal of this study was to calibrate *Ellis*' model using high resolution ERT data and salinity interpretations through site-specific formation factors.

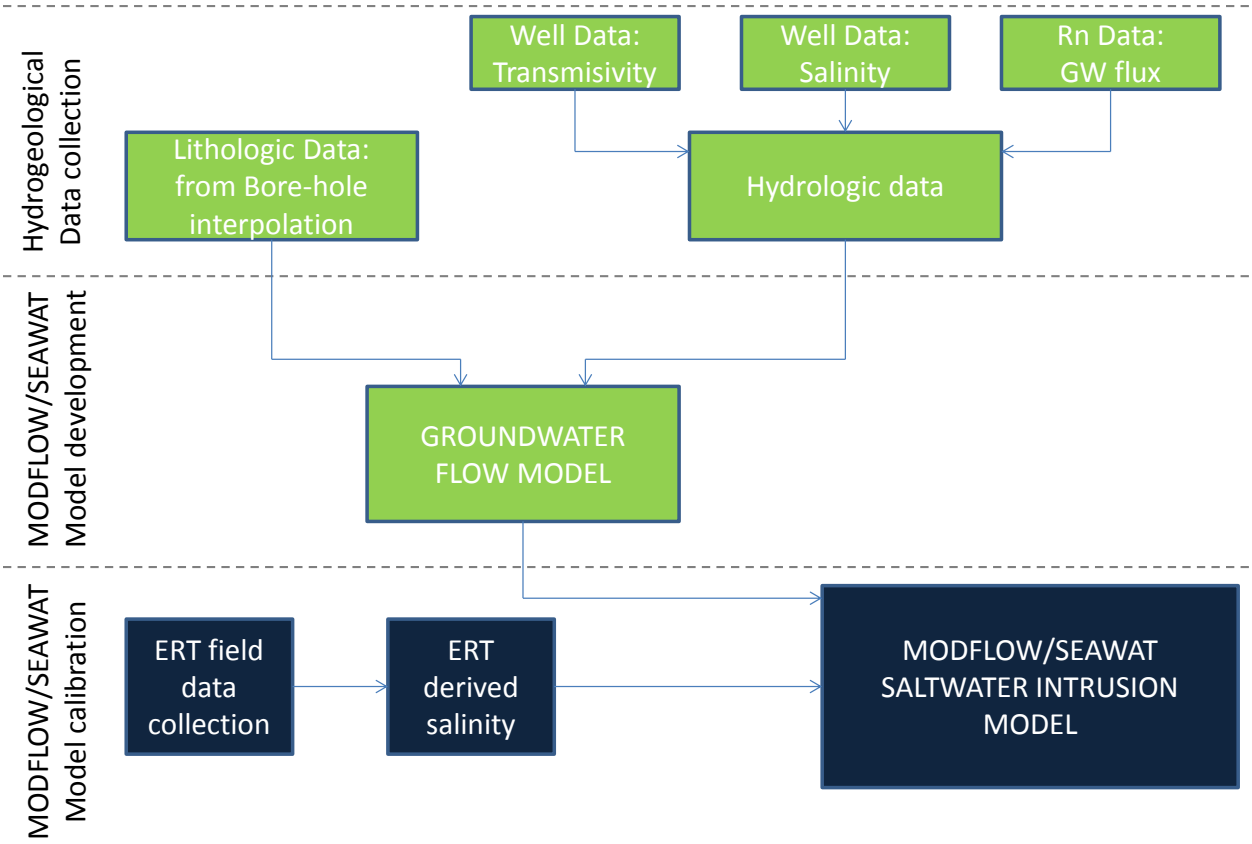


**Figure 4** Flowchart presenting the main steps in completing this study. Green boxes present previously collected data and model developed as a framework for this work. Salinity distributions from field ERT measurements were calculated using Archie's Law. The data was then implemented into a groundwater flow model previously developed by *Ellis et al* (in prep.)

### i. Field data collection

The field ERT measurements for reconstructing the geometry of the SI line were carried out using an eight-channel electrical resistivity meter (*R8 SuperSting, AGI*) interfaced with multi-electrode cables. For each ERT array both *Dipole-Dipole* and *Wenner-Schlumberger* array configurations were used. Specifically, in four of land-based ERT arrays we used 56 active electrodes and 28 passive while the two marine arrays used 56 passive electrodes only. Throughout the fieldwork performed for this study, the electrode spacing ranged between 1.5 and 3.8 meters. For the land-based arrays *Wenner-Schlumberger* electrode configuration provided

both horizontal and vertical resolution with better vertical resolution than the *Dipole-Dipole* array configuration, though the opposite was true for the marine based arrays. The 2D resistivity models were inverted using last updated software of *EarthImager ( AGI)*. The algorithm produces apparent resistivity values from direct values produces resistivity distribution in the subsurface. Briefly, the algorithm divides the subsurface into rectangular blocks based on a smoothness-constrained least-squares method and the resistivity within the blocks is then smoothed to minimize iterative difference between the calculated and the measured resistivity values. The root mean square (RMS) and L2 errors are utilized to qualify this difference (*Loke and Barker*., 1996; *Sasaki et al*., 1991).

### ii. ERT-derived salinity assessments

In order to evaluate distribution of salinity in the coastal aquifer system, salinity values were first calculated using resistivity and site-specific formation factor (*F*) inferred from ERT measurements and data for resistivity of collected pore-water from boreholes at the areas where the ER measurements were acquired. The formation factor is a site-specific characteristic of the mineral composition of an aquifer, its porosity and composition of the saturated fluids. The relationship between formation factor and porosity is given by Archie's law (*Archie*, 1942):

$$F = a \times \varphi^{-m} \tag{3}$$

Where φ is the porosity of the media (%), *F* is the formation factor of the subsurface (dimensionless), and the two coefficients, tortuosity "*a*", and cementation factor "*m*," also known as Archie's coefficients, reflect the physical properties of the aquifer (*Winsauer et al.,*1952; *Keller and Frischknecht*, 1966; *Jackson et al.*, 2002).

Archie's coefficients often vary over a large range and are difficult to evaluate due to natural heterogeneity of the subsurface (*Jackson et al*., 2002; *Worthington*, 1993). However, for fully saturated substrate Archie's law can be expressed also as:

$$\rho_w = \frac{1}{F} \times \rho_o \tag{4}$$

Where $\rho_o$ in the resistivity of the porous medium measure by ER instrumentation (Ohm.m) also referred to as formation resistivity, and $\rho_w$ is the resistivity (Ohm.m) of the pore fluid. For the purpose of our calculations we used formation factor values obtained from Equation (2) and ER data of the porous medium ($\rho_o$) to calculate the resistivity of the pore fluid ($\rho_w$) for each individual data point of our ER time series. The ERT profile is then converted to a salinity profile using equations developed by *Fofanoff and Millard Jr*. (1983) (**Equations 5 and 6**).

$$S = a_0 + a_1 R_t^{0.5} + a_2 R_t + a_3 R_t^{1.5} + a_4 R_t^2 + a_5 R_t^{2.5} + \Delta S \tag{5}$$

$$\Delta S = \left[\frac{T-15℃}{1+0.0162(t-15℃)}\right](b_0 + b_1 R_t^{0.5} + b_2 R_t + b_3 R_t^{1.5} + b_4 R_t^2 + + b_5 R_t^{2.5}) \tag{6}$$

**Table 1** Constants for calculating salinity from conductivity (from *Fofanoff and Millard Jr*., 1983)

| | | | |
|---|---|---|---|
| a0= | 0.0080 | b0= | 0.0005 |
| a1= | -0.1692 | b1= | -0.0056 |
| a2= | 25.3851 | b2= | -0.0066 |
| a3= | 14.0941 | b3= | -0.0375 |
| a4= | -7.0261 | b4= | 0.0636 |
| a5= | 2.7081 | b5= | -0.0144 |

Where: in equations (5) and (6), *S* is salinity of pore-water, $a_0$- $a_5$ and $b_0$-$b_5$ are empirical constants (**Table 1**) and $R_t$ is the conductivity ratio, which is the conductivity, C (at an unknown salinity S, known temperature T, and pressure of 1 ATM)of the sampled water over the standard conductivity of seawater, C ( S=35ppt, T=15$^o$C, and P= 1 ATM). A substitution of the

conductivity ratio ($R_t$) with a resistivity ratio ($R_r$) is done using Ohm's law of electrical conductivity.

The $\rho_w$ resistivity calculated with equation 4 is the variable resistivity and 0.207 Ohm.m is the constant resistivity at the average shallow groundwater temperature of $20.5^0$ C for the Gulf Shores, AL area (*EPA, Ecosystem Research, Athens, GA*); the constant resistivity is calculated from 4.84 S/m which is calculated from the conductivity equation for the temperature of seawater (*Fofanoff and Millard Jr*., 1983). The resistivity ratio ($R_r$) is substituted for conductivity ($R_t$) in equations 5 and 6 and the results is:

$$R_r = \frac{0.207}{\rho_w} \tag{7}$$

ΔS is the change in salinity from the standard salinity at $15^0$C, can then be calculated using the average groundwater temperature of $20.5^0$ C (EPA, Ecosystem Research, Athens, GA) and the constant 0.207 Ohm.m with the variable $\rho_w$ from the ERT model. The ΔS is the final defined variable, changing with each zone of the ERT cross-section, which enables the calculation of salinity in the corresponding zone. The calculated salinity in each zone is then cross referenced with observed values for sandy aquifers to ensure values are within acceptable values as determined in *Worthington et al*., (1976).

Near shore $\boldsymbol{\rho_o}$ values are expected below 1.0 Ohm.m in agreement with literature data for seawater intrusion, e.g. ~0.2 Ohm.m (*Guariglia et al*., 2006, *Nowroozi et al*., 1999). A layer saturated by brackish water or dissolved solids can have resistivity between 1 to 400 Ohm. m depending on the lithology of the layer (*Zohdy and Jackson*., 1969, *Worthington et al*., 1974, *Nowroozi et al*., 1999, *Satriani et al*., 2011). Based on these values of the resistivity of layers saturated by saline, brackish, and freshwater, qualification of observed values can be made and mixing of fresh and seawater be inferred. For comparison, **Table 2** and **Figure 5** are referenced

to validate calculated obtained values. These validated values are used as observed salinity values to recalibrate the groundwater flow model previously developed by *Ellis et al*. (in prep.) for the study area.

**Table 2** Typical resistivity values in different substrates (from *Zohdy and Jackson* (1969); *Dimova et al.*, 2012)

| Rock or Sediment Type | Resistivity (Ωm) |
|---|---|
| Clay saturated with brackish to saline water | < 3 |
| Clay saturated with brackish to fresh water | 5-8 |
| Clay, silty sand, and some gravel Saturated with fresh water | 11-25 |
| Sand and coral (*with brackish water*) | 40-400 |

In addition to the values presented in Table 2, to identify the substrate in our ERT images we used an empirically developed graph (**Figure 5**) by *Worthington et al.* (1974).The *Worthington et al.* (1974) graph is valid for cleansand and salinity less than 1ppt. This graph expresses the range of salinity (NaCl) in relation to formation factor, porosity, $\rho_w$, and $\rho_o$, therefore allowing quick comparison of calculated values.

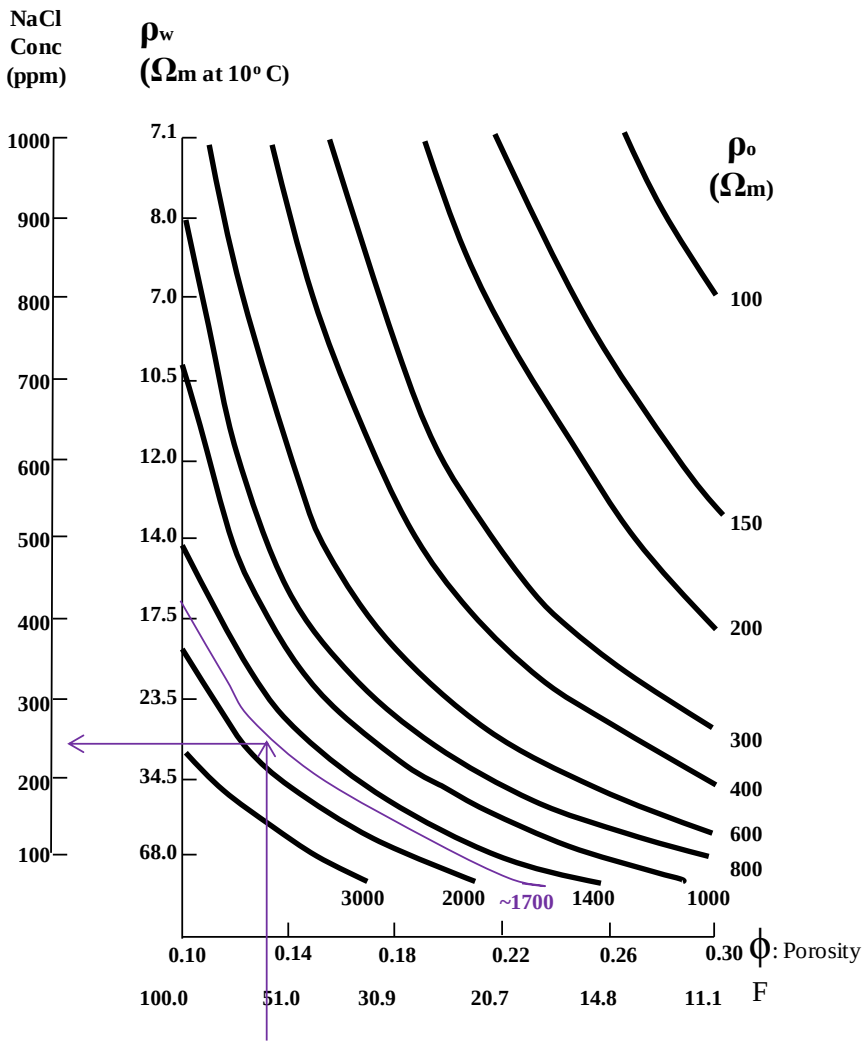


**Figure 5** Plot shows hydrogeophysical equivalence of $\rho_w$ (y-axis) versus F (x-axis) in isopleth form of $\rho_o$ for effectively clean sandy aquifers with low salinity pore-water.

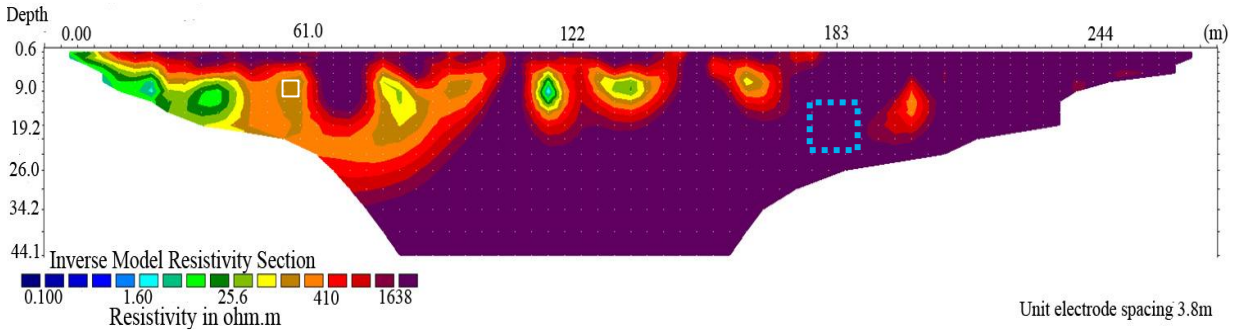


**Figure 6** ERT profile "a" taken near the beach perpendicular to the shore. The pore-water sample that correlates to the apparent resistivity in the "white square" is used to calculate the formation factor for the profile. Using the isopleth, **Figure 5**, the formation factor is checked to validate the calculated value where high resistivity (1700ohm.m) is observed, the "blue square".

For example: Using the profile in **Figure 6** (this profile is described in greater detail later in the paper) a $\rho_w$ sample from the borehole near the profile (which correlates to the "white square" in **Figure 6**) is taken and the formation factor (*F*) is calculated to be 65.7 Ohm.m. The $\rho_o$ of the highest resistivity within the profile (1700 Ohm.m- the "blue square" in **Figure 6**) is checked against the isopleth form to ensure first that $\rho_o$ (purple curve in the isopleth, **Figure 5**) are within experimentally excepted values. Then the calculated *F* (purple arrow pointing from the x-axis, **Figure 5**) is used to calculate the $\rho_w$ and salinity value and then the values are checked against the experimentally excepted values to ensure validity (purple arrow pointing from the purple $\rho_o$ isopleth line to $\rho_w$ and NaCl concentration values). The calculated $\rho_w$ and salinity value for this region of the example profile is 24.9 Ohm.m and 0.21 ppt respectively (the graph values are comparable at 28 Ohm.m and 0.24ppt)

In addition to validating the resistivity values (both observed and calculated) the formation factor calculated for salinity conversion must be validated. One calculated formation factor must be used for the entire profile, when the exact formation factor values in each of the layers are not experimentally determined. However, each calculated formation factor must be

validated to be within the acceptable range for the given lithology. The acceptable formation factor range is developed using Archie's Law Formation Factor Equation (**Equation 3**), the effective porosities (φ)from *McWorter and Sunada*, (1977) (**Table 3**) and cementation factor (*m*) from *Bateman*, (1985) (**Table 4**) and tortuosity "a" is considered to be 1. Ranges were developed per sandy sedimentary material type (**Table 5**). Borehole logs were used to determine lithological properties from which the pore-water samples were collected and the **Table 5** range was compared to the formation factor determined with equation 4 to validate the formation factor used for each profile.

**Table 3** Effective porosities for sedimentary material *McWorter and Sunada* (1977)

| **Sedimentary material** | **Effective porosity (range)** |
|---|---|
| Sandstone (fine) | 0.02-0.40 |
| Sandstone (medium) | 0.12-0.41 |
| Sand (fine) | 0.01-0.46 |
| Sand (medium) | 0.16-0.46 |
| Sand (coarse) | 0.18-0.43 |
| Gravel (fine) | 0.13-0.40 |
| Gravel (medium) | 0.17-0.44 |
| Gravel (coarse) | 0.13-0.25 |
| Silt | 0.01-0.39 |
| Clay | 0.01-0.18 |

**Table 4** Cementation factors for sand to sandstone *Bateman.* (1985)

| **Degree of Consolidation** | **Cementation Factor (*in situ*)** |
|---|---|
| shallow, very unconsolidated sands | 1.2 |
| unconsolidated sands | 1.6 |
| unconsolidated to friable sands | 1.7 |
| friable sandstone | 1.8 |
| hard to friable sandstone | 1.9 |

**Table 5** Formation factors (*F*) for sand to sandstone calculated using *McWorter and Sunada*, (1977) and *Bateman* (1985)

| **Sedimentary material** | **Formation Factor (*F*) (range)** |
|---|---|
| Sandstone (fine) | 5.2-1690.6 |
| Sandstone (medium) | 5.0-56.2 |
| Sand (fine) | 2.5-2511.9 |
| Sand (medium) | 2.5-23 |
| Sand (coarse) | 2.8-18.5 |

Archies' law and Worthington's finding, used previously, are requisite for clean sands only but, records from borehole logs indicate that the examined aquifer layers in our study area are composed of clay layers and clay intermixed with the sand. Although, the exact volume of clay intermixed in the sand layers is unknown, hydrological data indicates that the aquifers have potential yields > 5,451.0 $m^3$ /day per well. These yields suggest high permeability and thus relatively low content of clays within the aquifers. For layers (ie confining layers such as C1, **Figure 3**-the Fence Diagram) with higher clay content we used an alternative equation developed for shale-bearing sand aquifer systems by *Waxman and Smit* (1968).

$$1/\rho_O = \frac{1}{F*}\left(1/\rho_w + BQ_v\right) \tag{8}$$

$$B = \left[1 - 0.8e^{-50/\rho_w}\right]3.83 \tag{9}$$

$$Q_v = CEC/S_w \tag{10}$$

Where:

CEC is the cation-exchange capacity
$Q_v$is the CEC per unit pore volume of the shale/clay (meq/g) an electrical measure of clayiness or shaliness.

B is the equivalent conductance of (sodium) clay-exchange cations expressed (*Waxman and Thomas.,* 1974) as a function of $\rho_w$ by the Equation: so that the product has units of conductivity.
$S_w$is the pore-water saturation percentage of the media where 1 = 100%.

The ionic equivalent conductance of the exchange cation (*B*) and the Cation Exchange Capacity (*CEC*) of the clays are determined in laboratory experiments. Because we did not have access to clay core samples for this study, the established relationship from experimental data by *Waxman and Smit* (1968) is used as it relates to media with different shale/clay and sand contents for level of saturation and salinity (**Figure 7**).

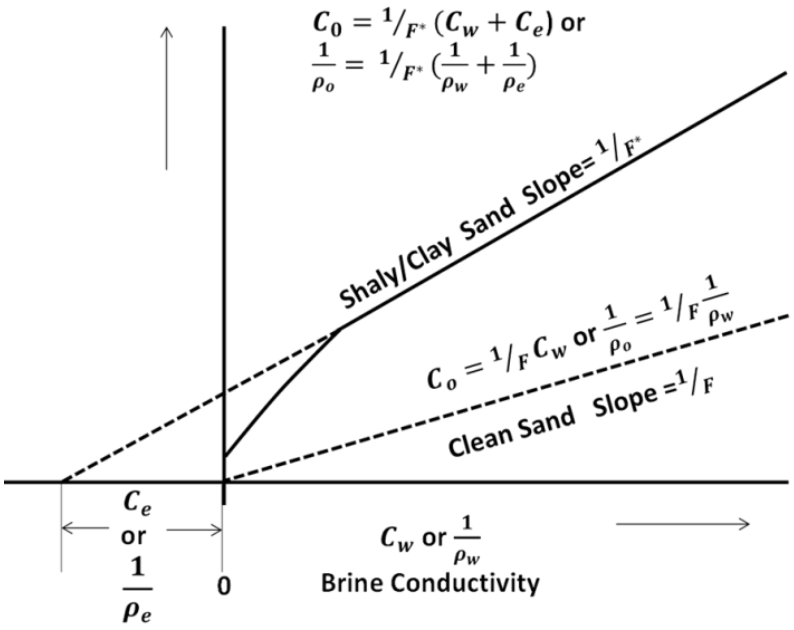


**Figure 7** Shaly/Clay sand core conductivity behavior, after Waxman and Smits (1968). The dotted line, labeled "Clean Sand" shows the behavior for rock with no extra conductivity paths that obeys Archie's Law. All the conductivity of the rock is due to the conductivity of the hydrated ions in the brine, thus when $C_w$ goes to zero, $C_0$ also approaches to zero. The solid line, labeled "Shaly/Clay Sand" shows higher core conductivity at any given value of brine conductivity than the "Clean Sand" due to another mechanism causing increased conductivity other than hydrated ions in the brine. The "Shaly/Clay Sand" line has a linear portion at high values of brine conductivity, the saltier part, but exhibits non-linear behavior in the low values of brine conductivity, the fresher part, so when the $C_w$ goes to zero, the $C_0$ still has measurable conductivity (*Thomas et al.,* (2010), *Jin et al.,* (2007))

Based on the data in **Figure 7** *Waxman and Smit* (1968) developed a linear equation relationship (**Equation 13**):

$$C_0 = {}^{1}/_{F^*}\,(C_w + C_e) \tag{13}$$

$$\frac{1}{\rho_o} = {}^{1}/_{F^*}\,(\frac{1}{\rho_w} + \frac{1}{\rho_e}) \tag{14}$$

Where:

$C_w$ is the conductivity of the pore-water ($\rho_w$ is the resistivity of the pore-water also related to the conductivity through ohm's law)

$C_e$ is the molar counterion conductivity of the equivalent NaCl solution and is equal to $BQ_v$ ($\rho_e$ is the molar counterion resistivity of the equivalent NaCl solution also related to the conductivity through ohm's law).

F is the formation factor as discussed with equation 1

F* is the formation factor for the shaly/clays sands.

The *Waxman and Smit* (1968) shaly/clay sand core behavior as compared clean sand behavior as developed by *Archie* (1942) (**Equation 3** )(related to resistivity by *Worthington et al*., (1974) in **Equation 4**) is illustrated in **Figure 7**. For both the clean sand and the shaly/clay sand $C_0$ is the conductivity of the sample core ($\rho_o$ is the resistivity of the sample core related to the conductivity through ohm's law). Both *Waxman and Smit.,*(1968) and *Archie* (1942) relationships indicate that a shale/clay layer (such as a confining layer) will have lower resistivity (or higher conductivity) than the sand layer provided the pore-water is the same salinity in both layers. As pore-water/brine increases in salinity the conductivity increases (resistivity decreases) as expected, but for shaly/sand or clay/sand the rate at which conductivity increases (resistivity decreases) is greater than conductivity increases in clean sand. This relationship allows a qualitative differentiation between the low resistivity cause by saturated clay and saturated sand in close proximity. Additional understanding of this relationship would indicate that when a formation factor is calculated for a sandy aquifer layer and used at the formation factor for the entirety of the profile, resistivity conversion to salinity, clay will exhibit greater salinity value

than the actual salinity value of the pore water. Where the pore-water salinity is high, clay saturated with 20ppt Saline water or greater could exhibit calculated salinities greater than 35ppt the base salinity of seawater. When these excessive calculated values arise it is a clear indication of clay.

### iii. MODFLOW/SEAWAT calibration procedure

Calibration of a MODFLOW/MT3DMS/SEAWAT model (referred to as SEAWAT herein) can be performed using two approaches: (i) conducting a trial and error process; or/and (ii) optimizing the model parameters using parameter estimation software such as PEST (Model-Independent Parameter Estimation and Uncertainty Analysis) or UCODE (Computer Code for Universal Inverse Modeling). PEST is nonlinear parameter estimation, parameter optimization, and uncertainty analysis software that operates independent of computer model used. UCODE is computer code that performs inverse modeling parameter estimation using nonlinear regression and is independent of computer model. For this study, the calibration procedure included the following steps:

*(i)* Developing a MODFLOW groundwater flow model based on hydrogeological data of the modeled region

*(ii)* Comparing model results to observed values of head data (typically from observations wells) and/or to groundwater flux assessments

*(iii)* Adjusting model parameter values (e.g. hydraulic conductivities) until a best fit between simulated and observed model outputs such as hydraulic heads or concentration is achieved (estimated by nonlinear regression)

To calculate the groundwater flow in coastal areas MODFLOW was combined with SEAWAT. SEAWAT is basically a code based on combining MODFLOW and MT3DMS to simulate variable-density groundwater flow and transport extending the two programs' capabilities to coastal aquifers and other environments where density dependent flow is important (*Guo and Langevin.*, 2002, *Langevin et al*., 2009). Note that because saltwater is treated as "*contaminant*" in SEAWAT modeling, the unit for salinity is expressed as concentration (mass/volume) not as the widely accepted unit "ppt" (parts per thousand).

The groundwater flow model in MODFLOW for this study was calibrated using PEST against observed well heads and observed groundwater flux. Changes within SEAWAT were calibrated using trial and error methodology until a best fit was achieved. The SEAWAT portion of the model is adjusted by varying the concentration at the constant concentration boundary. The salinity values (based on *Guo and Langevin*, 2002) at the constant concentration boundary are adjusted until the extent and magnitude of the SI closely fit the observed SI from the ERT

### iv. Calculating salinity from resistivity and location of "fresh water-seawater" interface

Using the Archie's Law via formation factors (*F*) the previously described the ERT profiles are converted to salinity profiles. To facilitate the conversion process, we assumed initially that: (*i*) each layer is homogenous, (*ii*) for the time of the measurements, the fresh-seawater interface is in a steady state condition and thus (*iii*) the formation factor is constant throughout each profile. In order to convert the ERT- profiles to salinity distribution, the resistivity values within each ERT profile (or the $\rho_o$ as described by *Worthington* (1974), **Equation 4**) are first converted to $\rho_w$ matrix profiles. The $\rho_o$ values are transferred to a

representative matrix that records the $\rho_o$ at the appropriate length and depth along each profile (**Appendix A**).

From field measurements of conductivity of pore-water from nearest located borehole the resistivity of these fluids is calculated using Ohm's Law and finally from the ratio of ERT resistivity and pore-water resistivity values, we calculated aquifer layer specific formation factor (**Equation 4**). To position the sample $\rho_w$ on the ERT profile the $\rho_w$ is projected in a linear method parallel to the shore (solid black arrows -**Figure 8**). In cases where the $\rho_w$ samples could not be projected linearly are extrapolated perpendicularly to the shore (dotted black arrows in **Figure 8)** using known, projected or calculated values of $\rho_w$ and extrapolated through another known, projected or calculated value of $\rho_w$.

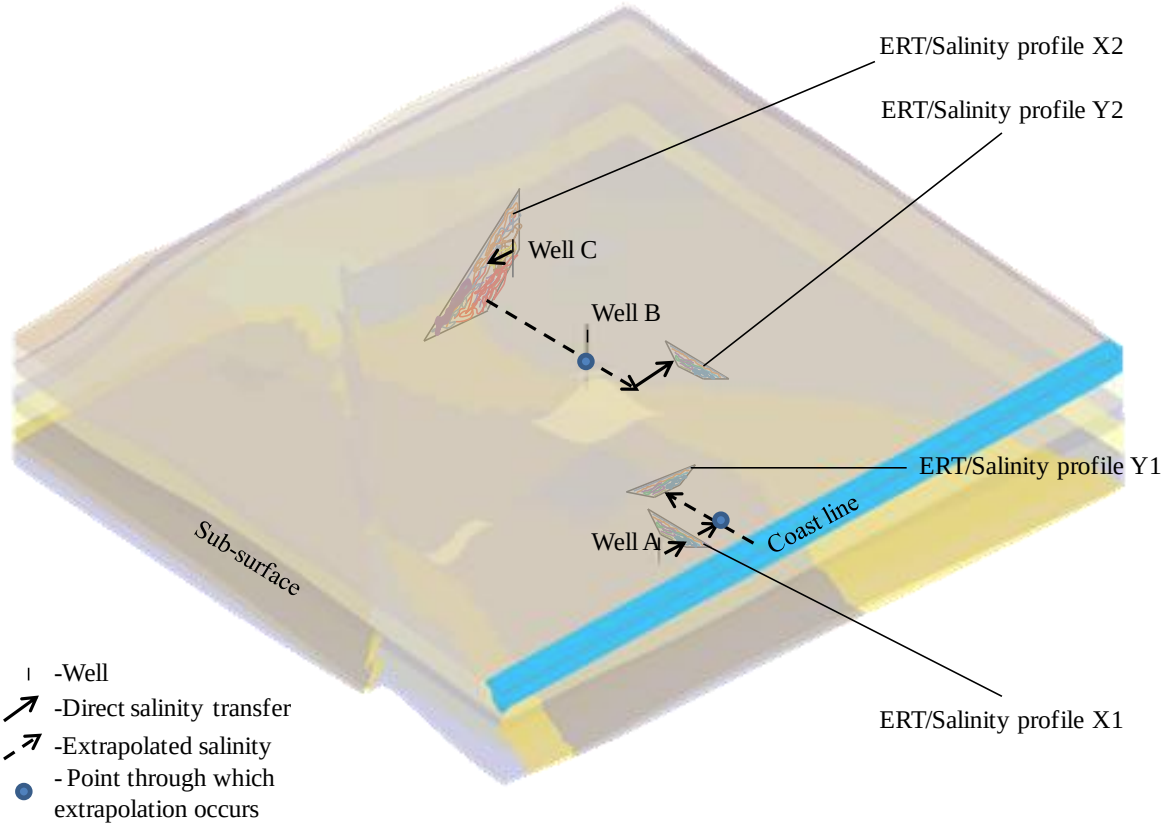


**Figure 8** Determination of profile salinity from nearby wells is accomplished using the two described methods. First the salinity of porewater (well sample) is transferred directly to a point on the ERT profile. The salinity is transferred along a line parallel to the coastline at the same depth as the well sampled (solid arrows). The second is determined through extrapolation. The salinity is extrapolated along a line perpendicular to the coastline from a determined salinity at a known depth through another known salinity at the same depth (solid arrows).

For example: starting with ERT/Salinity profile X1 (**Figure 8**)- the resistivity value from pore-water sample from well A, at known depth and location, is projected (solid arrow) parallel to the coastline onto the ERT/Salinity profile X1 at the same depth and distance from the coastline. Using the projected pore-water sample resistivity and the process described earlier the formation factor is calculated for the entire profile. For ERT/Salinity profile Y1 the process differs slightly- again, the pore-water sample resistivity value from well A (known depth and

location) is projected parallel (solid arrow) to the coastline until it crosses a line perpendicular to the coastline from another known pore-water sample resistivity value at the same depth as the well A sample. The resistivity value from sample nearest to the ocean is extrapolated through projected value at the corresponding depth to produce the resistivity value at ERT/Salinity profile Y1 (black dashed arrow) and allow the calculation of the formation factor. For the last profile described, ERT/Salinity profile Y2- ERT/Salinity profile X2 $\rho_w$ matrix profile is calculated first (in the same manner as ERT/Salinity profile X1 from well C (solid arrow)) and using the calculated $\rho_w$ (from ERT/Salinity profile X2) value that corresponds to the depth of well B along a line perpendicular to the coastline the resistivity is extrapolated through well B (black dashed arrow). The extrapolated value is then project onto ERT/Salinity profile Y2 (Solid black arrow).

Using the projected or extrapolated $\rho_w$ and the $\rho_o$ from the ERT profiles the formation factor is calculated for each profile. The newly calculated formation factor is then applied to each ERT profile in block matrix form to convert the $\rho_o$ in the ERT profile to its corresponding $\rho_w$ to create a $\rho_w$ matrix profile. The $\rho_w$ is finally converted to salinity using equations 5 and 6 to create each salinity profile in both a block matrix form and representative color form. The salinity values, separated by aquifer, are pinned to the same geographic location as the ERT profiles. Using ARCMAP 10.1 the ERT salinity values are combined with well sample salinity values from *Ellis et al.* (in prep.) as point values on a map. Using Empirical Bayesian Kriging, geostatistical tool from ARCMAP 10.1, the extent of salinity is interpolated in each observed aquifer. Kriging is a class of statistical techniques for optimal spatial prediction developed by *Gandin* (1959) and unlike classical Kriging, Empirical Bayesian Kriging, accounts for the error introduced by estimating the semivariogram model.

## 3. RESULTS AND DISCUSSION

### a. ERT imaging field results from Gulf State Park, Gulf Shore, AL

Six ERT arrays were collected in Gulf State Park (**Figure 9**). From south to north these are: (a) a shore-perpendicular array at the beach of Gulf Shore; (b) an east-west shore-parallel to a coastal lake (Lake Shelby); (c) one north-south shore-parallel traverse east of Shelby Lake; (d) and (e) two shore-perpendicular from piers on the north shore of Shelby Lake; and (f) one east-west oriented array on the Gulf State Park Golf Course, the farthest north ERT measurements. In order to verify previous assessments of SI [e.g., *Lin et al*., 2008, *Murgulet and Tick.,* 2008, and *Ellis et al*. (in prep.)], all ERT measurements were performed within the calculated and predicted SI lines. To eliminate seasonal influences on our results, ER measurements were carried during both dry and wet seasons. Specifically, the ERT array "a" (closest to the coastline) was performed early December 2012, while measurements for arrays "b", "c", "d", "e" and "f" were during mid-March 2013. The difference in measurement dates is significant only in that Fall (Sep 21 to Dec 21) monthly precipitation rates average 4.45 inches per month while winter months (Dec 21 to March 21) averages 6.05 inches of rain monthly (*NOAA NWS WFO*).

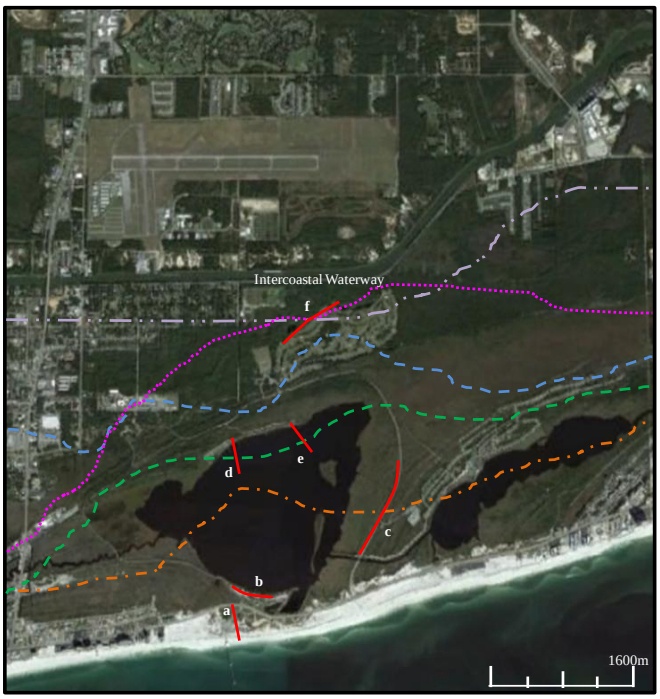


**Figure 9** Study site **(**Gulf State Park) with the location of the ERT arrays performed in December 2012 and March 2013 (red lines, "*a*" to "*f*"). The extent of SI in the A2a aquifer predicted by the *Lin et al*, 2008 for years: 1985 is presented by a dashed green line; 1996- dashed dark blue line, and 2036- dashed purple line. *Murgulet and Tick*, 2008 is the pink dotted line. The orange line is the *Ellis et al*., (in prep.) modeled SI line for 2013.

The resistivity profile presented in **Figure 10a** is of a 270-m ERT array deployed perpendicular (South-North) to the shoreline at Gulf Shores during the dry season in the area (December 2012) (**Figure 9**). The south side of the profile presents the end of the cable that was close to the shore and the right side the end that was farther on land. As one could expect, resistivity values decrease significantly (from 1700 to 2 Ohm.m) with approaching the shore line as a result of seawater intrusion in the aquifer (blue-green color areas in the image). The seawater- fresh water interface (white dashed line) is depicted between 60 and 100 m from the seaward side of the array at depth of 34 m. This depth is representative of the A1 and A2a top aquifer layers. The smooth interface indicates that the two aquifer layers are most likely connected which is to be expected: in typical coastal settings the coastal aquifer layers tend to become thinner and merge as they approach the shore line. Intermediate areas between the

"ocean" and "land" end of the array show indication of low resistivity (green features between 103 and 203 m). Probing the subsurface during our deployment indicates discontinuous distribution of clay layers that form more solid confining aquitard layers (C1) farther on land. However, because these are relatively shallow features (9 to 17m depth, Table 3), we suggest that the observed lower resistivity values could be as a result of seawater entrainment in the upper aquifer layers or of seawater absorption into the already identified discontinuous clay layer. Interspersed high resistivity area of 16 to1700 Ohm.m (the dark purple) shows higher values than *Zhody and Jackson*., (1969) and would indicate for typical resistivity values for coral and sand saturated with freshwater. However, the range falls within *Worthington et al.,* (1974) values for low salinity pore-water in clean sand (**Figure 5**) which is to be expected: tidally driven seawater intrusion on daily basis is common in such coastal settings. The profile resistivity values in the Aquifer Layer A1 increase as approaching Lake Shelby and the pore-water becomes fresher. At depth between 61 to 270 m areas of high resistive are attributed to clean sand saturated with fresh water from the lens. This freshwater is mixed with A2a lensed fresh water as well as aquitard clay layer C1 is discontinuous at this level. This is the reason we do not observe SI toward the back of the profile but it is evident in profile "*b*" at approximately 300 meters away where the C1 Aquitard is thin but intact. This led us to the following conclusions for the salinity distribution in the south portion of our study site: (*i*) from 0 to 103 m (S-N) we detect clear SI, blue to green areas reflect low resistivity area at areas where seawater is interacting with clay; and (*ii*) from 110 to 140 m the green and yellow areas are indication of preferential flow, residual seawater, or entrained seawater interacting with clay and beginning to intermix with freshwater, while the orange and red areas reflect brackish water in sand or/and

freshwater mixed with clay. We interpret the dark purple high resistivity areas as freshwater mixed with clean sand.

The resistivity profile presented in **Figure 10b** is of a 183-m ERT array deployed parallel (West-East) to the shoreline on the southern Lake Shelby shoreline during the wetter spring season (March 2013) (array "b" **Figure 10**). The resistivity is greatest at the top of the profile from 0 to 6 m in depth, ranging from 56 to 300 Ohm.m. During the fieldwork, the ground on the south shore of Shelby Lake was fully saturated by rain prior to the placement of ERT array "b". The infiltrated rainfall and an existing fresh to brackish water lens are the likely explanation for the high resistivity values in the first six meters of depth, the resistivity values are consistent for sand saturated with fresh to brackish water (*Zhody and Jackson*., (1969) and **Table 2**). As depth decreases from 6 to 9 m, the resistivity decreases as well from 76.1 to 3 Ohm.m which is likely caused by increasing salinity with depth. At resistivity values 3 Ohm.m at 8-9 m of depth, brackish to saline pore-water (**Table 2**) is likely interacting with a clay sand transition zone above the C1 clay aquitard (**Figure 3**). At depth between 9 and 23 m the resistivity ranges from less than 1 to 4.23 Ohm.m. Three zones have resistivity values less than 1 Ohm.m: the first is identified at depth 50 m (west to east) and 10 m depth the second at 135 m (west to east) and 20 m depth, and the third at 143 m laterally and 15m depth. These three zones distinctly agree with *Zhody and Jackson*., (1969) (**Table 2**) typical values for clay saturated with saline water. Below 23 m in depth, layer completely placed within the A2a Aquifer, the resistivity ranges from 2 to 4.5 Ohm.m which is an indication for high salinity pore-water.

The resistivity profile presented in **Figure 10c** is of a 717-m ERT array, (South-North) to the East of Lake Shelby parallel to State Road 2, (spring wet season-March 2013) (array "c" **Figure 9**) depicting depths up to 95 m and features aquifer A1 to confining layer C3 (**Figure 3-**

fence diagram). The resistivity generally increases, from 0.1 to 400 Ohm.m, as the distance from the shore (south to north) increases and decreases (from 400 to <1 Ohm.m) as depth from the surface increases. The exception to the above general statement is the zone from approximately 200 m to 380 m where the resistivity decreases significantly (< 1 to 3 Ohm.m) at depths from ~38 m to 95 m. The "dark blue" resistivity values (<1 Ohm.m) coupled with the downward intrusions of "light blue to bright green" (1 to 3 Ohm.m) from 80 to 380m (left to right) is likely vertical mixing of fresher water in the A2a aquifer though to the top of the A2c aquifer. The intrusion at 183 m from south descends from 19 m in depth to the bottom of the profile and remains contiguous and depicts a possible area of interconnectivity between all the A2 split layers. This possible interconnectivity effects what would be a brackish lens (3 to 9 Ohm.m) from 40 to 460m from at depths of 19 to 40m. The probable lens is split by SI upwelling from 150m to270m (depths of 19m to 40m). The split is clear because on both ends of the profile distinct layers can be delineated. The first layered area, from 0 to 170m (south to north), displays the following.

(i) 0 to 12 m A1 Aquifer (8 to 26 Ohm.m)

(ii) 12 to 19 m C1Clay Aquitard (0.1 to 1 Ohm.m)

(iii) 19 to 38 m A2a Aquifer (3 to 8 Ohm.m)

(iv) 38 to 40 m C2a Silty/Clay Aquitard (1 to 3 Ohm.m)

(v) 40 to 60 m A2b Aquifer (0.1 Ohm.m to 1 Ohm.m)

As the distance increases from shore (at 305 m from the south to north) a visible layer forms at the top (1-6m depth) of the array indicating that the pore-water is likely becoming less saline. From 427m to the end of the profile the second area of distinct layer delineation becomes apparent:

(vi) 0 to 12 m A1 Aquifer (83 to 400 Ohm.m)

(vii) 12 to 19 m C1Clay Aquitard (3 to 9 Ohm.m)

(viii) 19 to 38 m A2a Aquifer (27 to 83 Ohm.m)

(ix) 38 to 40 m C2a Silty/Clay Aquitard (3 to 27 Ohm.m)

(x) 40 to 60 m A2b Aquifer (1 to 3 Ohm.m)

(xi) 60 to 76 m C2b Clay Aquitard (3 to 9 Ohm.m)

(xii) 76 to 95 m A2c Aquifer (9 to 75 Ohm.m)

The last feature appears to be a Ghyben-Herzberg feature. Starting at 285m (south to north) and extending to 427m (white dotted line **Figure 10c**). While the measured resistivity along the line (3Ohm.m to 27Ohm.m) indicates saline to brackish water (**Table 2**) this is feature is likely the beginning of the zone of dispersion likely culminating at what appear to be a similar feature of fresh water from 370m to 610 from the left (the black dashed and dotted line **Figure 10c**)

The resistivity profile presented in **Figure 10d** is of a 230-m ERT array , (South-North) perpendicular to the north shore of Lake Shelby (spring wet season-March 2013) (Array "d" **Figure 9**) depicting depths up to 39.8 m and features aquifer A1 to the top of Aquifer A2b (**Figure 3**-fence diagram). The ERT profile depicted in **Figure 10d** is a mostly marine profile with all but the final 40m conducted on the bottom of Lake Shelby. From 0 m to ~122 m from the left the three distinct layered zones from top to bottom (7 to 4 Ohm.m) are visible. The top layer from 0 to~5m in depth has a resistivity of about 1 Ohm.m which is likely from the influence of Lake Shelby (a brackish lake) above this layer. It is possible this is the beginning of the C1 confining layer (**Figure 3**-the fence diagram) since the 1 Ohm.m resistivity is consistent

with clay saturated with brackish water (**Table 2**). The lower layer (depth between 4 and 10m) has a resistivity of 4 - 5 Ohm.m that is consistent with values for clay saturated with brackish to fresh water and suggesting that there is a contiguous clay layer and that most likely fresher water is lensing or saturating the clay layer at this depth. At depth between 10 and 39.8 m the resistivity is 2 Ohm.m suggesting consistent salinity (or SI) more than halfway through the profile. At depth larger than 122m from the left the resistivity values are more intermixed (ranging from 0.1 to 28.1 Ohm.m) with sharp increase (93 to 185 Ohm.m) in deeper layer (>146.3 m). This zone is most likely the dispersion zone composed of a layer incongruity of clay/silt from the C2a aquitard intruding into the A2a Aquifer. From 146.4 to 192 m (south to north) pore-water has composition that suggest some intermixing with fresh lake water as the observed resistivity increases steadily from 2 to 185 Ohm.m with depth. The last 40 meters (on the northern end) of the array are from measurements of the northern shore of Lake Shelby and the high resistivity values reflect fresh water saturation.

The resistivity profile presented in **Figure 10e** is of a 171-m ERT array,(South-North) perpendicular to the north shore of Lake Shelby (spring wet season-March 2013) (array "e" **Figure 9**) depicting depths up to 35.2 m and features aquifer A1 to the top of Aquifer A2b (**Figure 3-**fence diagram). During this deployment the resistivity cable was laying on the Lake bottom (i.e. was completely submerged). The top of the array (about 3m of depth) has low resistivity values (1 Ohm.m) most likely due to the brackish water in Lake Shelby, the average surface water salinity is about 3-4 ppt. This resistivity value is consistent with clay saturated with brackish water (**Table 2**). The maximum depth of Lake Shelby is 3 m at the southern end of the ERT Array "e" this could indicate that the C1 Aquitard is at the bottom of the lake and is only approximately 3 meters thick. This assessment is further supported by an immediate

increase in resistivity (3.5 to 8 Ohm.m) from depths between 3 and 9 m that is likely caused by freshwater lensing on the bottom of and absorbing into the C1 clay layer (**Table 2**). At depth between 9 and 28 m the resistivity decreases from 2.25 to 3 Ohm.m reflecting substrate of sand saturated with saline water. In the center of the profile (depth between 67 and 82 m) a low resistivity bulge (2.7 Ohm.m), a possible up welling protrudes through a higher resistivity layer (3.25 Ohm.m) and could indicate preferential flow within the freshwater/seawater mixing zone possibly caused by a change in transmissivity within the A2a Aquifer. If the previously described "protuberance" is considered an anomaly, then a possible zone of dispersion, as illustrated in **Figure 1,** becomes apparent (see the white dashed-dotted line **Figure 10e**). Below the ~28 m of depth the resistivity decreases again to between 1 Ohm.m and 2 Ohm.m, which is indication for brackish water in clay suggesting this is most likely the C2a Aquitard layer (**Figure 3**).

The last profile presented in **Figure 10f** is of a 717-m ERT array and it was deployed, west-east parallel to the northern edge of the Gulf State Park golf course (spring wet season-March 2013) (**Figure 10f**) depicting depths up to 95 m and features aquifer A1 to the top of Aquifer A3 (Figure 3). In this profile only two areas of observed resistivity (ranging from 15.7 to 68.5 Ohm.m) are lower than 181 Ohm.m. The first low resistivity area from 105 to 162 m at depth from 0 to 30 m is in the vicinity of an irrigation line (105 m and 1 m depth) and drainage pipe (155 and 2-3 m in depth). The lower resistivity area that joins between to these two water conveyances(from 105 to 162 m and below 3 to 30 m) is likely water leaking and being retarded at the above the C2a Aquitard layer. The second low resistivity zone, from 350 to 500m between 80 and 95 m of depth, has resistivity values between 15 and 42 Ohm.m and is most likely Aquitard C3 with the silty/clay composition (**Table 2** and **Figure 3**). The initial analysis of the

two low resistivity areas indicates that this is likely an indication that the lower resistivity values observed in the Figure 10f are not due to SI. Interpretations of this profile without conducting a salinity conversion indicate that no SI progressed past the 1996 line of Chandler et al., (1996) to the point indicated by Murgalet and Tick., (2009) or has significantly receded.

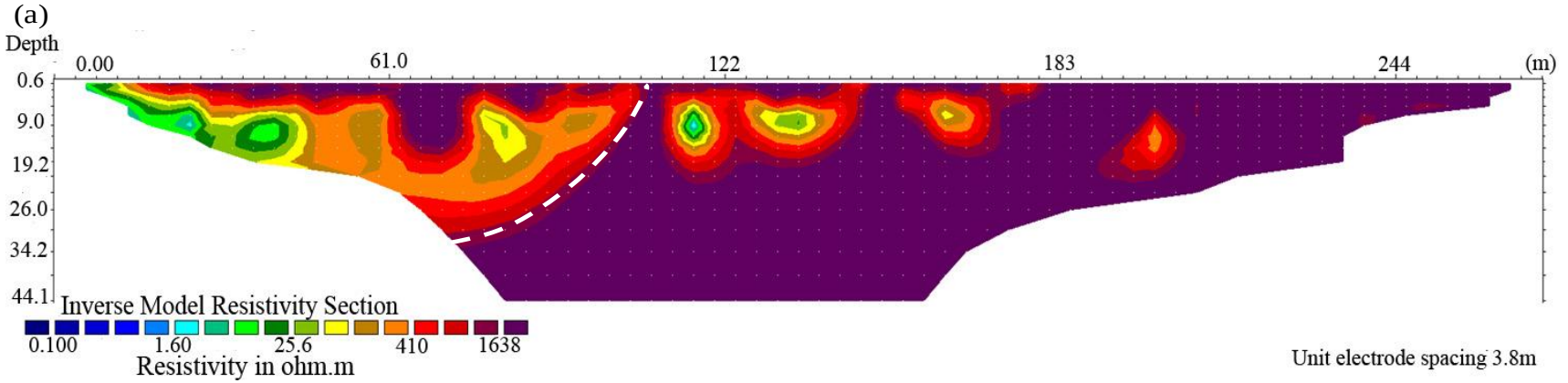
(a)
Depth
0.00
61.0
122
183
244
(m)
0.6
9.0
19.2
26.0
34.2
44.1
Inverse Model Resistivity Section
0.100
1.60
25.6
410
1638
Resistivity in ohm.m
Unit electrode spacing 3.8m

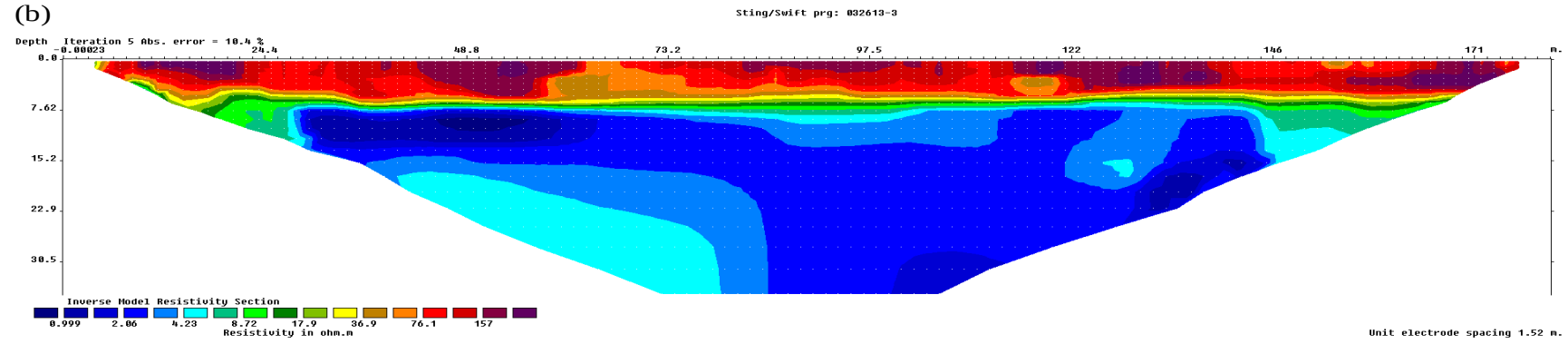
(b)
Sting/Swift prg: 032613-3
Depth
Iteration 5 Abs. error = 10.4 %
-0.00023
24.4
48.8
73.2
97.5
122
146
171
m.
0.0
7.62
15.2
22.9
30.5
Inverse Model Resistivity Section
0.999
2.06
4.23
8.72
17.9
36.9
76.1
157
Resistivity in ohm.m
Unit electrode spacing 1.52 m.

(c)

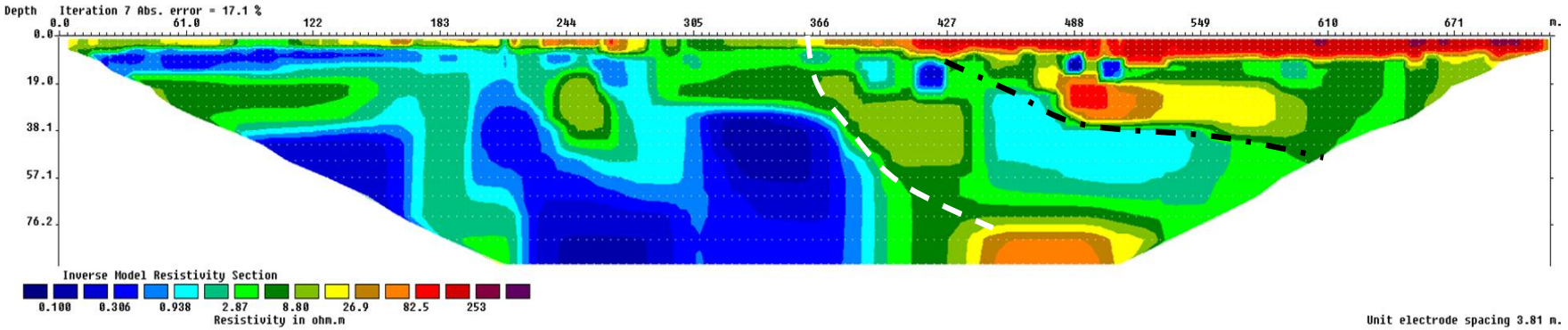
Depth Iteration 7 Abs. error = 17.1 %
0.0
61.0
122
183
244
305
366
427
488
549
610
671
m.
0.0
19.0
38.1
57.1
76.2
Inverse Model Resistivity Section
0.100
0.306
0.938
2.87
8.80
26.9
82.5
253
Resistivity in ohm.m
Unit electrode spacing 3.81 m.

(d)

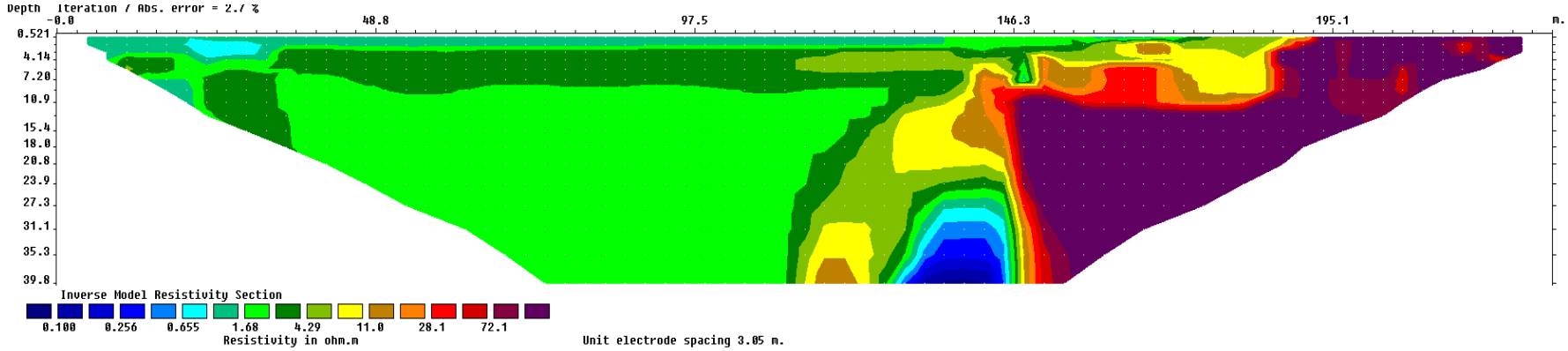
Depth Iteration 7 Abs. error = 2.7 %
-0.0
48.8
97.5
146.3
195.1
m.
0.521
4.14
7.20
10.9
15.4
18.0
20.8
23.9
27.3
31.1
35.3
39.8
Inverse Model Resistivity Section
0.100
0.256
0.655
1.68
4.29
11.0
28.1
72.1
Resistivity in ohm.m
Unit electrode spacing 3.05 m.

(e)

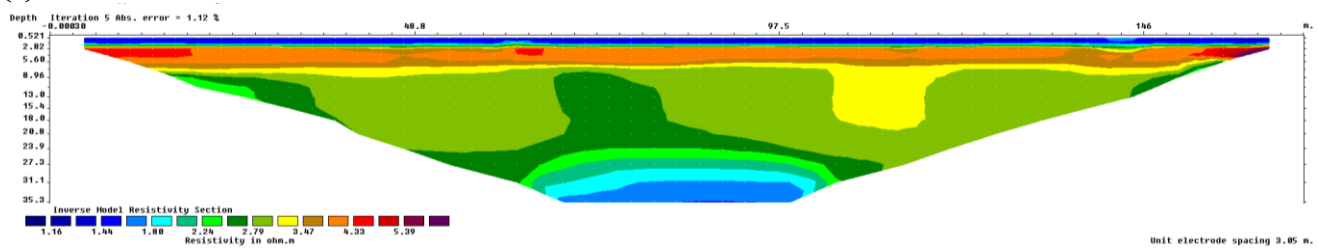
Depth Iteration 5 Abs. error = 1.12 %
-0.00830
48.8
97.5
146
m.
0.521
2.82
5.60
8.96
13.0
15.4
18.0
20.8
23.9
27.3
31.1
35.3
Inverse Model Resistivity Section
1.16 1.44 1.80 2.24 2.79 3.47 4.33 5.39
Resistivity in ohm.m
Unit electrode spacing 3.05 m.

(f)

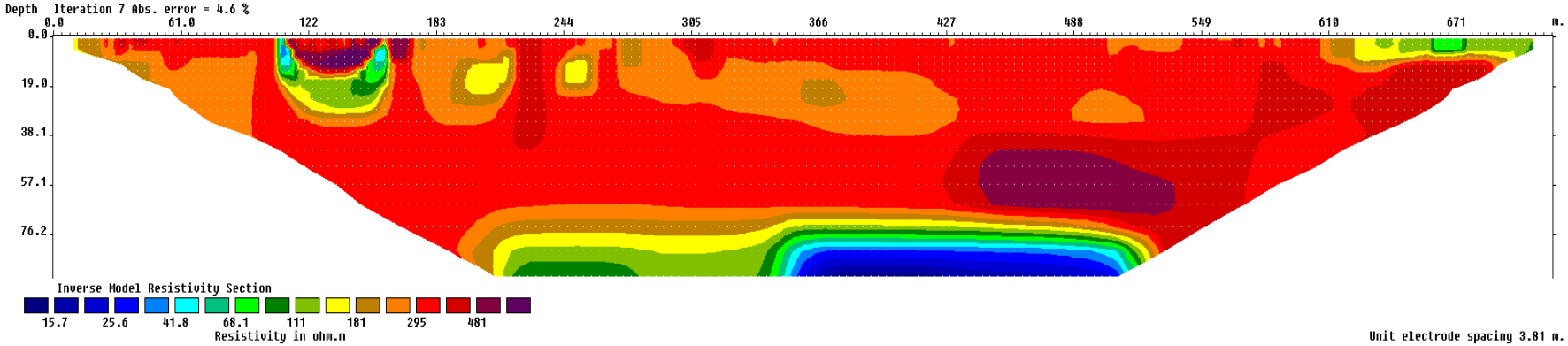
Depth Iteration 7 Abs. error = 4.6 %
0.0
61.0
122
183
244
305
366
427
488
549
610
671
m.
0.0
19.0
38.1
57.1
76.2
Inverse Model Resistivity Section
15.7 25.6 41.8 68.1 111 181 295 481
Resistivity in ohm.m
Unit electrode spacing 3.81 m.

**Figure 10. (previous three pages)** ERT mages of arrays carried within the study arera: (a) perpendicular to Beach; (b) South shore of Shelby Lake; (c) East Shore of Shelby Lake; (d) North East Pier Lake Shelby; (e) North West Pier Lake Shelby (f) Gulf State Park Golf Course. Lables (a-f) correspond with arrays depicted in Figure 4 and described in Table 3.

Each resistivity line was produced using different electrode configuration depending on the depth desired for particular area of investigation. Table 3 summarizes the parameters for each array:

**Table 6** ERT array characteristics and identified regional aquifer layers

| ERT line | GPS Coordinates (Center of Array) | | cable length (m) | electrode spacing (m) | depth below surface (m) | Regional aquifer layers | RMS error from inversion |
|---|---|---|---|---|---|---|---|
| | N | W | | | | | (%) |
| a | 30.250217 | -87.665589 | 270 | 3.80 | 34.2 | A1-A2a | 12.7 |
| b | 30.253019 | -87.664461 | 183 | 1.54 | 32.0 | A1-A2a | 10.4 |
| c | 30.259098 | -87.652098 | 717 | 3.81 | 95.0 | A1-C3 | 17.1 |
| d | 30.263795 | -87.667000 | 230 | 3.05 | 45.0 | A1-A2b | 1.12 |
| e | 30.265733 | -87.659413 | 171 | 3.05 | 40.0 | A1-A2a | 2.7 |
| f | 30.274717 | -87.660818 | 717 | 3.81 | 95.0 | A1-C3 | 4.6 |

### b. Converting ERT profiles to salinity profiles: uncertainties and assumptions

To convert the observed resistivity from the ERT profiles to salinity distribution, the pore-water resistivity across the entire profile must be determined. Using the method described in chapter 2 for projection and extrapolation the resistivity values ($\rho_o$) within each ERT profile are converted to $\rho_w$ matrix profiles. The $\rho_o$ values are transferred to a representative matrix that records the $\rho_o$ at the appropriate length and depth along each profile (**Appendix A**). Sample pore-water resistivity data ( $\rho_w$ ) corresponding to each ERT profile is gathered and then applied to each profile. Using the ascribed manner to position the sample $\rho_w$ on the ERT profile, the $\rho_w$ is projected in a linear method parallel to the shore (**Figure 11**). In cases where the $\rho_w$ samples

could not be projected linearly as with ERT profiles “b”, “d” and “e” the values were extrapolated using values of $\rho_w$ calculated from the other ERT profiles.

For ERT profile “b” the extrapolation is from a location at the shore where pore-water has a resistivity value of $0.207\ \mathrm{Ohm.m}$ and is extrapolated through the well A (**Figure 11**) with pore-water $\rho_w$ value of $4.77\ \mathrm{Ohm.m}$ at a depth of 2.4 meters from MSL (mean sea level). The well A depth is maintained along the extrapolation to the where it intersects ERT profile “b”. All extrapolation are resistivity per unit length from the start point of the line.

In extrapolating for ERT profiles “d” and “e” the corresponding calculated $\rho_w$ from ERT profile “f” is first projected to a point due north of well D at a depth of -45.5 meters from MSL. The resistivity is extrapolated from this northern point through well D to a point that corresponds with ERT profile “d”. The $\rho_w$values are then calculated throughout ERT profile “d” using the newly calculated formation factor to create the $\rho_w$matrix profile ‘d”. The calculated $\rho_w$ at 40 meter of depth from the now calculated $\rho_w$ matrix profile “d” is then projected onto ERT profile “e” to allow formation factor calculations and conversion to salinity.

The methodology of converting resistivity to salinity for this study is based on Archie’s Law and as described in chapter 2. However, Archie’s Equation is specifically designed for clean sands and carbonaceous rock without mixtures of clay or shale. To further verify the projected and obtained extrapolated resistivity values ($\rho_w$) and calculated salinity of the pore fluids in the different aquifer layer, we considered three approaches including:

1. Comparing ERT measured and extrapolated resistivity values to the true resistivity values of the local aquifer lithological make up obtained from borehole deep resistivity analyses (Appendix B).

2. Comparing resistivity of groundwater collected from a known depth or strata to calculated and interpolated resistivity of respective fluids.
3. Collecting cores along the traverse and to directly determine the core resistivity in a laboratory environment.

Therefore, it is critical to know the lithological composition when converting resistivity to salinity. For this study, the basic lithology is considered to match the nearby borehole lithology along the length of each respective ERT array. Pore-water samples were taken from four wells (boreholes) with known depths to determine the salinity along the ERT profiles pore-water samples were taken from four wells (known depth) were collected to determine the salinity along the ERT profiles. The locations of these four wells are depicted on the map presented on **Figure 11**; **Table 7** contains information about exact coordinates and pore-water depths. Well logs of each borehole (lithology) used to reference each of the ERT profiles can be found in Appendix B.

Ultimately, no cores were taken along the traverse of any of the ERT arrays. Extrapolated resistivity values were compared to true resistivity values from borehole deep resistivity analyses and the resistivity determined via deep resistivity analyses were in agreement with values detected using the ERT. None the less there were only four deep resistivity boreholes of limited quality (Appendix B), as a result the primary method of validation was comparing resistivity of groundwater collected from known depths.

**Figure 11** The stars present the locations of the boreholes sampled to pore-water for the salinity conversions. The solid yellow arrow illustrates the shore parallel projection of borehole pore-water sample to ERT profile. The dotted yellow lines illustrate where extrapolated salinity values were projected onto the ERT profile.

**Table 7** Depth, resistivity, and GPS coordinates of pore-water from sampled boreholes used for the calibration in this study.

| borehole ID | pore-water depth (m) | pore-water resistivity (Ohm · m) | GPS Coordinates | |
|---|---|---|---|---|
| | | | N | W |
| A | 3.40 | 4.77 | 30.249825 | -87.6673972 |
| B | 12.0 | 0.56 | 30.2580806 | -87.6515722 |
| C | 58.0 | 59.1 | 30.269820 | -87.662210 |
| D | 47.5 | 69.5 | 30.274830 | -87.657360 |

Using the lithology from the boreholes a simple evaluation was conducted of the different layers to ensure where and Archie's Equation applies and where the "*Waxman and Smit"*-relation applies. This evaluation enabled the identification of the layer depths where observed resistivity depths would differ widely despite the pore-water resistivity being the same. Because the use of a single formation factor (F) across the entirety of each profile will produce calculated $\rho_w$ values and associated calculated salinity values higher than the actual $\rho_w$ values and associated salinity values where the lithology is not clean sand, indentifying the each lithological layer (depth and thickness in each borehole is critical. Thus using a single value per pore-water per depth per respective borehole, assigning site-specific formation factor and identifying the lithology of each layer allows each profile to be qualitatively assessed, using the *Waxman and Smit* (1968) relation to *Archie* (1942), to determine where (location and depth) along the profile that observed resistivity is SI in clean sand.

Where the observed resistivity is determined to be in the clean sand all converted values using Archie's Law are considered usable for determining SI. As an example of qualitative comparison an ERT profile (**Figure 12)**, which is the non-combined second overlap of the profile "f" (**Figure 9** and **Figure 10f**), is used to explain the process. The pore-water sample near this profile is freshwater having a resistivity of 69.5 Ohm.m (**Table 7**), which converts to 0.08 ppt with the givens of this study. Given this fresh pore-water sample and resistivity values in excess of 400 Ohm.m (230 to 320 m at a depth of 40 m to 65 m) are clearly sand (**Table 2**). Again, considering the pore-water sample the apparent low resistivity zone below 82 m is examined. The relatively low resistivity values (15 Ohm.m to 25 Ohm.m) fall within clay/silt saturated in freshwater values of **Table 2**. Overlying interpolated lithology on apparent

resistivity values from ERT measurements, allows direct comparison and avoiding ambiguity of associated interpretations.

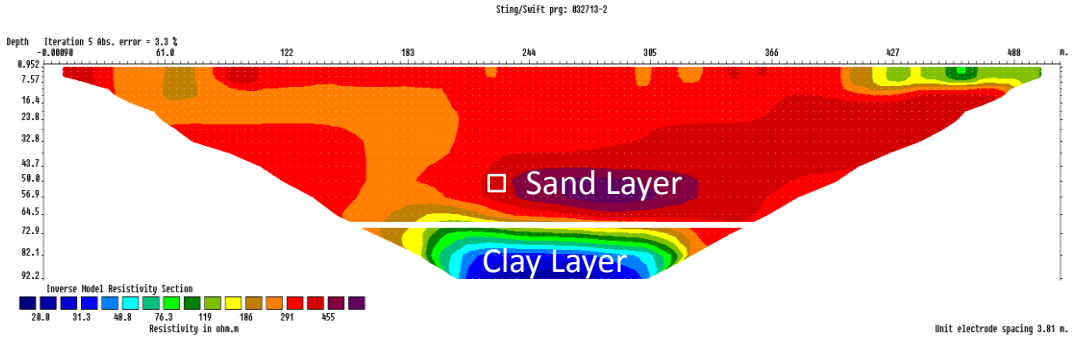


**Figure 12** The non-combined 2nd overlap profile of **Figure 10f** demonstrates clear delineation between a layer fully saturated with fresh pore water, i.e. salinity less than 0.25ppt. The pore-water sample (0.08 PPT) from the nearby well the correlates through direct transfer with the "maroon color", highlighted by the white square, which has a resistivity 400Ohm.m. The "purple colored" (labeled: sand layer) area of the profile, with resistivity values greater than 400Ohm.m, would therefore be freshwater because it is above the resistivity values for sand in brackish water (**Table 2**). Likewise, the "blue colored" (labeled: clay layer) area of the profile has resistivity values between 15Ohm.m and 25Ohm.m which aligns with clay/silt in freshwater from **Table 2**. Prior to converting apparent resistivity to salinity simple analysis of observed values to accepted resistivity values are used to remove ambiguity relating to the lithology and pore-water salinity.

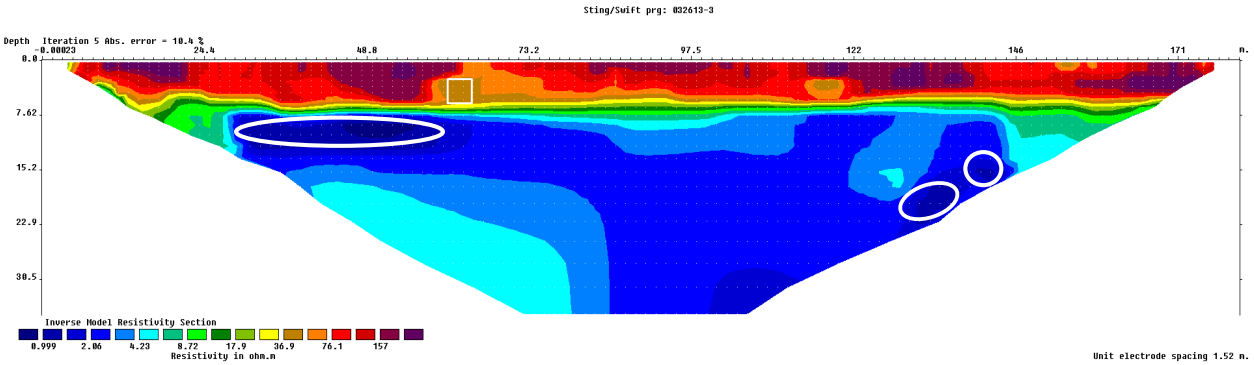


**Figure 13** From **Figure 10b** the above profile demonstrates low resistivity area saturated with high salinity pore-water, i.e. salinity greater than 25ppt. The pore-water sample (1.18 ppt) extrapolated from the nearby well correlates with the "brown color" area highlighted by the white square which has a resistivity 40Ohm.m. The "blue colored" (highlighted by 3 circles) areas of the profile has resistivity values less than 1Ohm.m which agrees with clay saturated in saline to brackish water from **Table 2**. Since all the resistivity values below ~8m are ~8Ohm.m or less it is likely that the pore-water is all highly saline. Comparison to interpolated lithology

indicates that the three circles are in or near the C1 Clay Aquitard (**Figure 3**). Once the resistivity profile was converted to salinity profiles the areas inside three circles converted to salinities higher than 35ppt as *Waxman and Smit,* (1968) relationship would predict. This is covered in further detail later in the paper.

Using the previously described approach, ERT profile "b" (from **Figure 9** and **Figure 10b**) is analyzed (**Figure 13**). Three areas of low resistivity deserve special attention. Due to the *Waxman and Smit.,* (1968) relationship to *Archie* (1942) as described in **Figure 7** a clay saturated in saline to brackish water will exhibit a lower resistivity than sand with the same salinity pore-water. As illustrated in **Figure 13** the three circles encompass low resistivity areas that are less than 1Ohm.m. Resistivity values less than 3Ohm.m are indicative of clay saturated with saline to brackish water according to **Table 2**. While apparent resistivity values < 3 Ohm.m are typical of clay with saline to brackish water, it is possible given high salinity pore-water (> 20ppt) in high effective porosity clean sands (>0.30) and low formation factors (< 11.1) can result in low apparent resistivity values of < 3 Ohm.m (Archie's Equation).

Starting with the ERT profiles (qualified using the just described process) and following the previously described methodology for conversion to salinity profiles, six salinity profiles were produced. The images (presented in **Figure 14a-f**) were imposed on interpolated lithological profiles for comparison. The *Waxman and Smit.,* (1968) relationship to Archie (1942) is utilized to identify clear indications of clay.

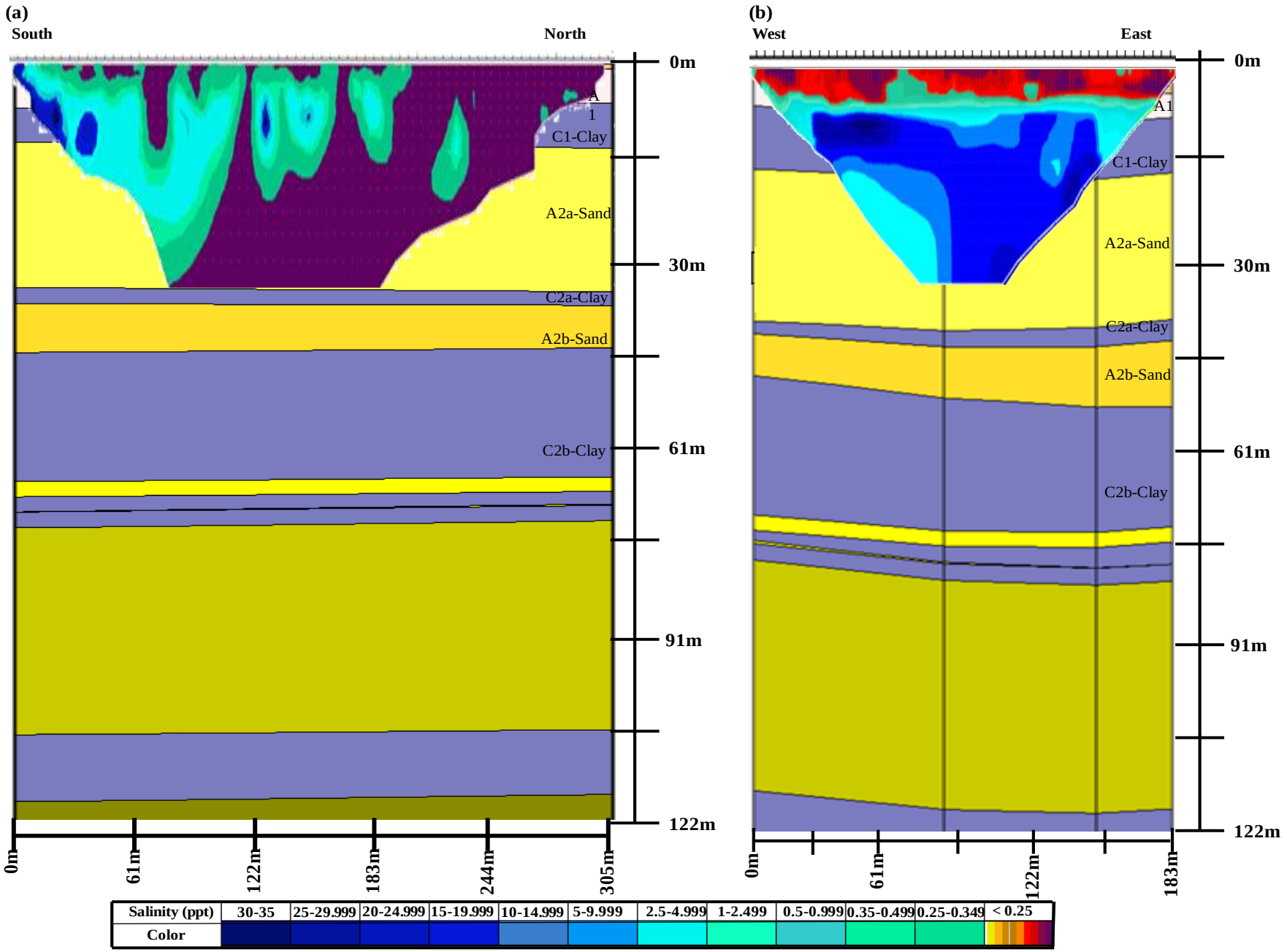
(a)
South
North
0m
30m
61m
91m
122m
A1
C1-Clay
A2a-Sand
C2a-Clay
A2b-Sand
C2b-Clay
0m
61m
122m
183m
244m
305m
(b)
West
East
0m
30m
61m
91m
122m
A1
C1-Clay
A2a-Sand
C2a-Clay
A2b-Sand
C2b-Clay
0m
61m
122m
183m
Salinity (ppt)
30-35
25-29.999
20-24.999
15-19.999
10-14.999
5-9.999
2.5-4.999
1-2.499
0.5-0.999
0.35-0.499
0.25-0.349
< 0.25
Color

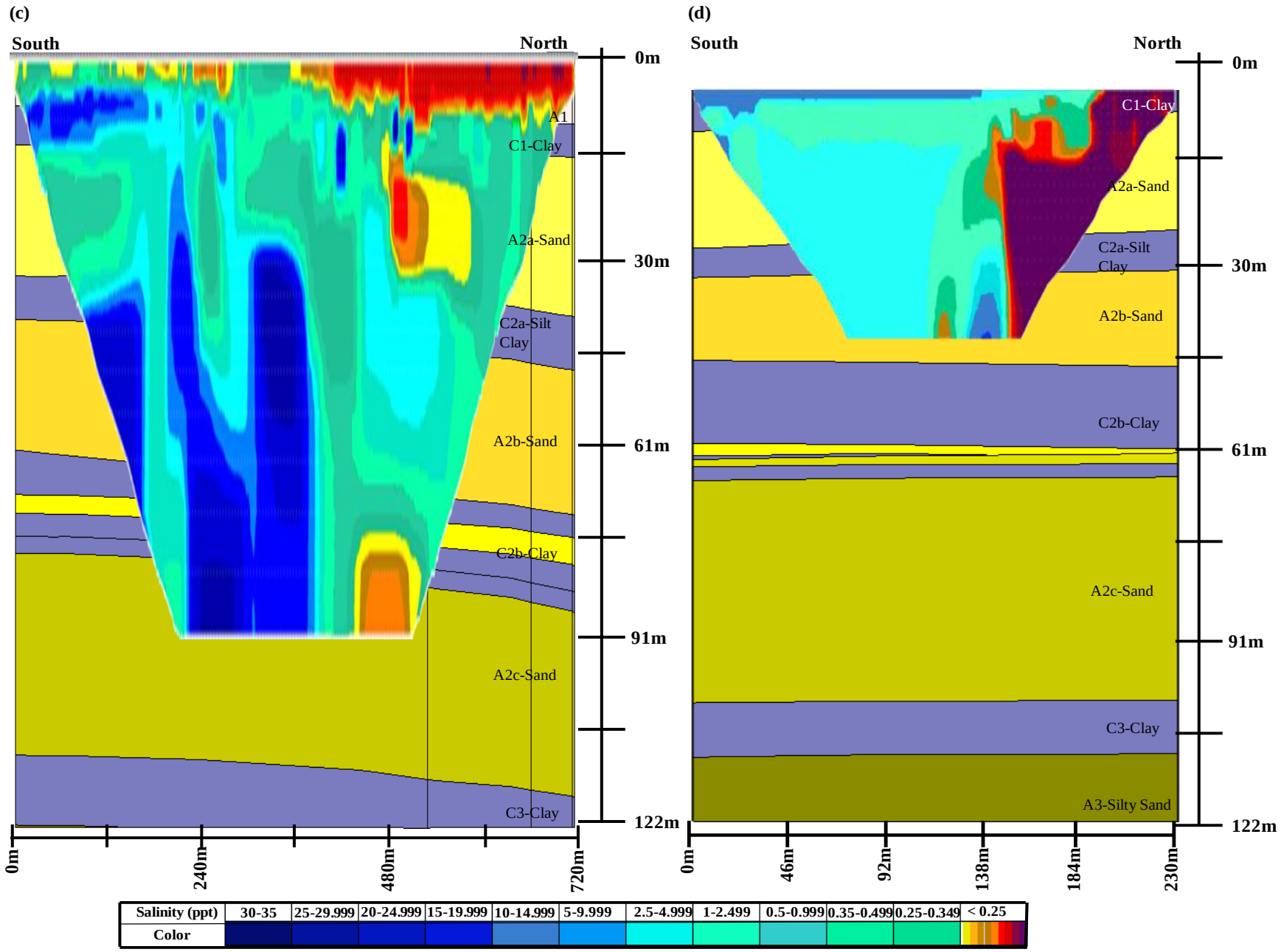
(c)
South
North
0m
30m
61m
91m
122m
A1
C1-Clay
A2a-Sand
C2a-Silt Clay
A2b-Sand
C2b-Clay
A2c-Sand
C3-Clay
0m
240m
480m
720m
(d)
South
North
0m
30m
61m
91m
122m
C1-Clay
A2a-Sand
C2a-Silt Clay
A2b-Sand
C2b-Clay
A2c-Sand
C3-Clay
A3-Silty Sand
0m
46m
92m
138m
184m
230m
Salinity (ppt)
30-35
25-29.999
20-24.999
15-19.999
10-14.999
5-9.999
2.5-4.999
1-2.499
0.5-0.999
0.35-0.499
0.25-0.349
< 0.25
Color

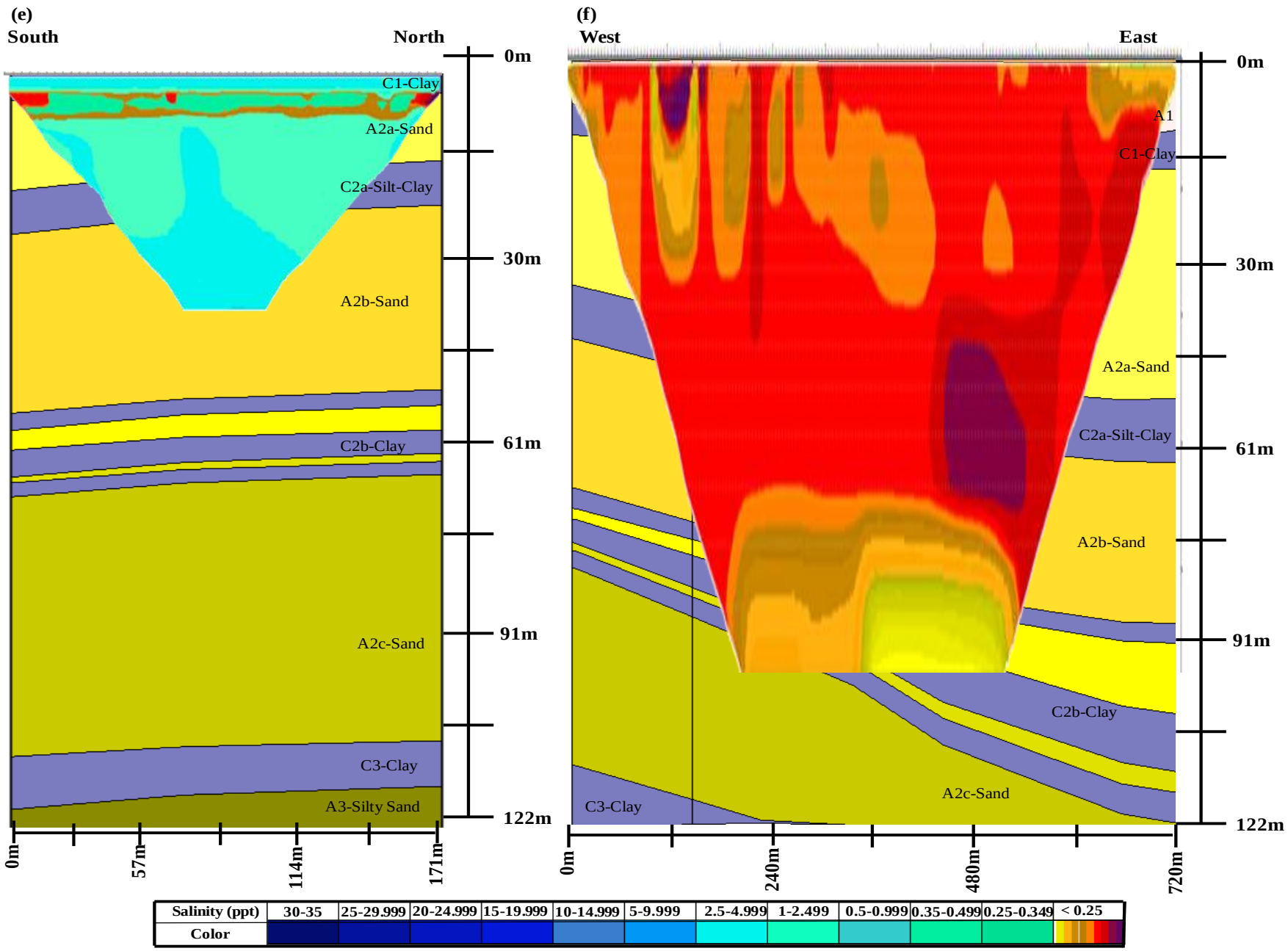
(e)
South
North
0m
30m
61m
91m
122m
C1-Clay
A2a-Sand
C2a-Silt-Clay
A2b-Sand
C2b-Clay
A2c-Sand
C3-Clay
A3-Silty Sand
0m
57m
114m
171m
(f)
West
East
0m
30m
61m
91m
122m
A1
C1-Clay
A2a-Sand
C2a-Silt-Clay
A2b-Sand
C2b-Clay
A2c-Sand
C3-Clay
0m
240m
480m
720m
Salinity (ppt)
30-35
25-29.999
20-24.999
15-19.999
10-14.999
5-9.999
2.5-4.999
1-2.499
0.5-0.999
0.35-0.499
0.25-0.349
< 0.25
Color

**Figure 14a-f**: (**Previous three pages**) Resistivity-derived salinity profiles superimposed on the lithological makeup of the aquifer system in the study area. The ERT profiles are converted to salinity and cross referenced with the stratagraphy interpolated from bore-holes using Aquaveo GMS. Imbedded in each of the figures is a table which correlates the salinity to colors observed in the profile. Red colors indicate freshwater saturated sand/rock.

The salinity profile presented in **Figure 14a** is the converted resistivity profile from **Figure 10a** which is perpendicular (South-North) to the shoreline (from ERT array "a" in **Figure 9**). Salinity is highest at the shoreline (30 - 35ppt) as expected decreasing as it distance from the shore increases (<0.25 ppt). Approximately 7-15 of depth there are five points of interests to be highlighted. The points, measered from the 0m point of the profile linearly, are at 15m, 30 m, 40 m, 115 m, and 135 m. Each of these locations have converted salinity values greater than 35 ppt, the excepted standard for seawater. As discussed ealier the *Waxman and Smits.*, (1968) relationship would highlight these zones distinctly as clays. The fact that the high salinity zone is not consistant across the length of the profile suggest that C1 ,the interpolated clay layer from near borehole data, is not consistant near shore (this is consistant with first assessment from the resistivity profile) . This also suggests that water from aquifers A1 and A2a intermix near shore. To further the assessment that clay at the 115 meter mark clay was observed at the surface at this point. Clay was also observed at the surface at the 170 meter mark. The sum of thes observations would indicated the following: (*i*) that intermixing is occuring between ~40 meter to ~150m in aquifers A1 and A2b; (*ii*) C1 and A1 are not consistant layers near shore and (*iii*) Water both fresh and seawater are mixing in both aquifiers near shore.

In **Figure 14b**, the south shore of Lake Shelby (from **Figure 9** array "b" and **Figure 10b**), the first seven meters of depth are saturated with freshwater (<0.25 ppt) with an exception in the vicinity of 60 m linearly. No clay was observed at the surface along the length of the ERT array used to create this profile. Three zones convert to salinity higher than than 35 ppt (these

are the same zones highlighted in **Figure 13**). The first zone is at 50 m from the west and 10 m of depth and the other two zones are at 157 m from the west and 19 m in depth. This suggests a dipping clay layer when traversing from west to east. The high salinity values between 7.5 meters in depth to 22 meters in depth are likely due to the influence of clay. Because of this suspected influence converted salinity, values retrieved from above 7.5 m in depth and below 22 m of depth are considered SI.

For the salinity profile for the east side of Lake Shelby (**Figure 14c**), which corresponds to ERT profile "c" (**Figure 9** and **Figure 10c**), freshwater lensing is observable as yellows and red color at depths above 15 meters. From the south side (shore side) to near the center of the profile linearly the freshwater layer ("yellows and reds") is not contiguous (depths above 15 m) and is likely due to two canals connected to Lake Shelby, a brackish lake; the first canal 15 m south of the beginning of the profile and the second canal crossing under the array at 340 m. From 12 m to 20 m in depth salinity values approach and in select thin layers exceed that of seawater (35 ppt) once again identifying clay (0m to 200 m, 450 m, and two at 480 m), which aligns with C1 from interpolated strata. Though as in **Figure 14a** the high salinity values is not consistent across the profile at that depth and suggests the clay layer C1 may not be contiguous. At depths larger than 300 m three freshwater layers (less than 0.25 ppt) are visible. The first layer is in Aquifer A1 (0 to 12 m in depth), the second layer is in the A2a Aquifer (at 480 to 600 m and 15 to 40 m depth), the third layer is in top A2c Aquifer (450 m from the south at 80 m to 95 m in depth). Using the first freshwater layer SI in Aquifer A1 is fully tapered by 380m. In Aquifer A2a the extent of SI is considered to end at 480 m. The calculated salinity never exceeds 0.5ppt at depth >600 m and is considered freshwater. Thus, the SI extent determined from the third freshwater layer in Aquifer A2c is considered to end at 450 m where the freshwater begins.

The western marine salinity profile (**Figure 14d**) crossing onto the northern shore of Lake Shelby, a distinct feature exists between 7 and 15 m depth which is between 33 m and 188 m displaying salinity from 0.7 to 1.62 ppt (this salinity is on the borderline fresh). This low salinity is significant to note because it aligns with the interpolated C1 Clay layer. Given that the salinity values both above and below this feature are higher (10-12 ppt above and 4.25 ppt below) it is likely that the C1 Clay layer is at the more shallow depth above 7m of depth from the surface of the lake. The higher calculated salinity values present near the top left of the profile are likely due to the influence of the Lake Shelby immediately above absorbing to a clay layer below it. The influence of the lake extends to its shore in the where salinity drops distinctly at 192m from the south (0.7 ppt to less than 0.25 ppt) and becomes freshwater. At approximately 143 m from the south and at 11 m depth a clear freshwater line rises at a sharp angle that starts at 150 m at a depth of 39.8 m. Two distinctive features arise from the bottom of the salinity profile; the first at 110 m is freshwater (<0.25 ppt), while the second is saline water (11-27 ppt) at 140 m. The saline feature (140 m) is distinctive and further inland than the freshwater feature (110 m). Two possible explanations can account for this occurrence; the first is preferential flow and the second is a decrease in effective porosity at the 110m located occurrence coupled with an intermixing of clay in the aquifer at the 140m with higher saline water at the bottom of the A2b Aquifer absorbing into this intermixed clay.

The salinity profile like the ERT profile is a 2D rendering of a 3D environment. The preferential flow explanation would suggest that one side of the profile has a greater extent of SI which crosses at 140 m while the other side of the profile has less SI and freshwater crosses through the cross section at 110 m. The effective porosity/clay explanation would suggest that the salinity of the water at 110 m did not change but that the effective porosity decreased which

would increase resistivity causing the calculated salinity to be low (**Figure 5**). Continuing the effective porosity/clay explanation at 140 m; because the salinity range is 11 ppt to 27 ppt denser saline water is likely intruding the aquifer from the bottom and absorbing into sands intermixed with low to moderate levels of clays. It is not likely that high salinity water (27 ppt) intruded this far into Aquifer A2a, but neither is it likely that 0.7 ppt salinity water would convert to 27 ppt salinity water with presence of clay. It is not possible to ascertain the true salinity in either of these features and are not considered for the model. As discussed earlier the conditions at the center (300 m to 450 m) of the resistivity profile and the salinity profile exhibit unconfined behavior. Between these two positions the *Ghyben-Herzberg (G-H) relation* is also exhibited further suggesting this area is unconfined. Following equation 1 at 360m (south to north) the depth of observed "h" is ~1m the observed "Z" is ~30m. This compares to a calculated "Z" of 37m for an "h" of one meter. At 450m (south to north) the depth of observed "h" is ~2m the observed "Z" is ~75m. The calculated "Z" for 2 meters is 74m. Comparison between calculated Z and the observed Z suggest that the observed SI line at from 360 to 450m is exhibiting *Ghyben-Herzberg* characteristic and further substantiates that the A2 Aquifer is unconfined within this region of the profile.

For **Figure 14e** (eastern marine profile near the northern shore of Lake Shelby) there is not the distinct break between freshwater and brackish water as in **Figure 14d** but there is evidence of lensing in Aquifer A2a (7 m to 11 m). The top layer (above 7 m) of the salinity profile (3-4 ppt) is likely the clay layer C1, infiltrated with water (1.7 ppt) from the brackish Lake Shelby, leaving a much lower salinity zone (<0.5 ppt) beneath it (7 m to 11 m). This is most likely due to lensing of freshwater above denser brackish water (2-4 ppt) below 11 m. Upwelling of higher salinity water (2.5 to 4ppt) is visible (67 m to 82 m) in the middle of the

salinity profile passing into lower salinity brackish water (~2 ppt). On the northern edge of the profile (at depths 7 m to 11 m) a "red and purple" zone (<0.25ppt) is the only indication of freshwater entering the profile. The *Ghyben-Herzberg (G-H) relation* applies primarily for unconfined aquifer systems but that does not invalidate the relationship in confined aquifers. The relation is a function of hydraulic head and density of the fluid. Equation 1 is a function the height of the water table (h) and the density of both the freshwater ($\rho_f$) and the density of the seawater ($\rho_s$). The relation defined that the height of the freshwater above sea level determined the depth to seawater below sea level. Therefore the *G-H relation* would still valid but as a function of hydraulic head (which determine the effective height water above sea level) within the aquifer not the actual height of the water above the sea level. In Figure 12e the east marine profile from Lake Shelby the depths (10 m to 22 m) of the top of observed SI (4-5 ppt) exhibits behavior similar to the *G-H relation.* From 15 m to 65 m from south to north following the bottom of the freshwater area (brown color) and the top of the SI (light blue) Z follows a steady curve that follow equation 1(**Table 8**). The curve approximately follows what the *G-H relation* would indicate and likely indicates the beginning of the zone of dispersion as the *G-H relation* would predict.

**Table 8** Position of *G-H relation* depth of Z to observed h and calculated h. All depths are approximate.

| **Position (m)** | **Observed Z (m)** | **Observed h (m)** | **Calculated h (m)** |
|---|---|---|---|
| 15 | 2-3 | >0.5 | 0.08 |
| 20 | 6 | >0.5 | 0.16 |
| 30 | 12 | >0.5 | 0.32 |
| 35 | 16 | ~0.5 | 0.43 |
| 65 | 20 | ~0.75 to ~1 | 0.55 |

The last converted salinity profile, **Figure 14f**, the northern most profile, shows no evidence of SI (from **Figure 10f** and ERT array "f" from **Figure 9**). Salinity conversions reveal definable features all the saturated pore-water is less than 0.25ppt. The definable features include clean sands that are "red to purple" and clays that are "yellow to orange-brown". Using this converted salinity profile to interpret the stratagraphy of this location suggests that the A1 aquifer and the C1 confining layer are tapering off. It is also likely that A2a and A2b are a single unconfined aquifer at this location. The C2b confining layer is distinct and identifiable under-laying the A2a/b Aquifer.

Using the salinity profiles just discussed in conjunction with chemical analysis of well water samples the observable extent of the SI is re-established (from previous studies). As stated earlier, when SI is determined with chemical analysis alone the interpolation and extrapolation from the known points used to check the results of the numerical groundwater/SI model is limited for multiple reasons. One reason the results are limited is typical sample wells are not established for scientific or engineering study but for private use, irrigation, or utility, therefore wells are not established in pattern that would inform linear interpolation and reduce error. Another reason the results are limited is that substrates are often heterogeneous, as seen in the salinity profiles, therefore SI derived from linear interpolation or extrapolation contains error. There for to improve accuracy and reduce error the salinity profiles inform the interpolation/extrapolation that was lacking from only chemical analysis input.

By using the salinity profiles an additional set of observed linear values can be input into the interpolation. While the results are subject to interpretation, as discussed, the information gathered is both understandable and relevant to the condition of the subsurface. The relationship of Archie's Equation to Waxman and Smits' Equation qualifies the values used to interpolate SI

in each layer. Qualifying the values increases the confidence that calculated pore-water salinity values approach the true salinity of the pore-water and therefore validating the additional data sets for interpolation that achieve more precise SI results.

With the validated salinity profiles complete, each profile's start and ends were "pinned" to their geographic coordinates on the map. The extent of SI was mapped in each observed layer (**Figure 15**). The validated observed salinities locations were inputted into ARCMAP 10.1. Utilizing the Imperial Bayesian Kriging Method of interpolating and extrapolating, the extent of SI was mapped in each layer A1 through A2c. **Figure 15a-d** displays the extent of SI into the A1and A2 Aquifer.

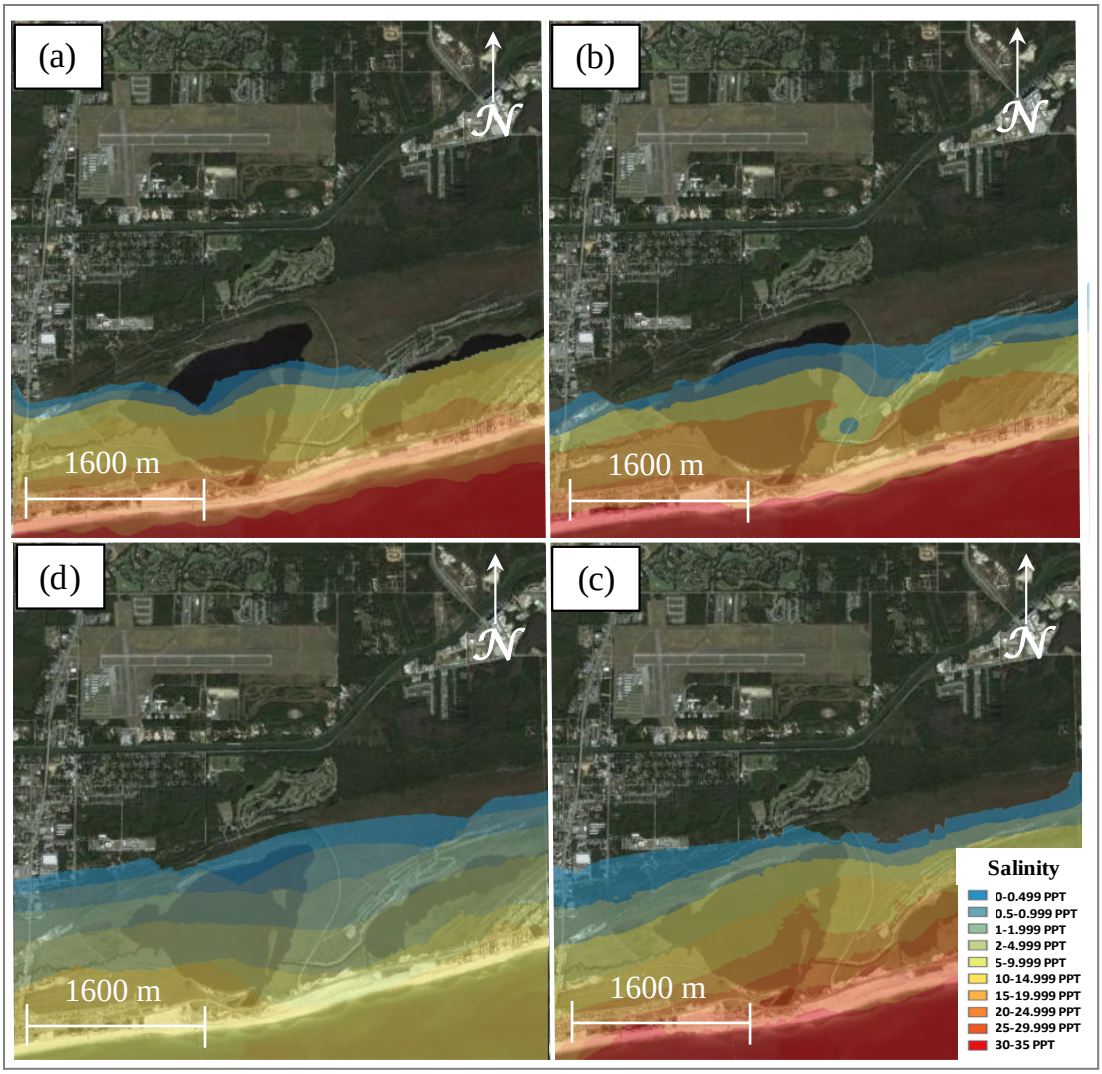


**Figure 15** Interpolated extent of SI (ppt) in Aquifer A1(13a) and Aquifer A2a-c (moving clockwise from 13b to 13d) as determined through Imperial Bayesian Kriging on ARCMAP 10.1 using salinity samples from sample wells and as determined through the ERT profile conversions to salinity profiles. Salinity level is represented by color with from highest to lowest salinity where red is the highest (30-35 ppt) and blue is the lowest (0 to 0.499 ppt).

Referring back to the *Murgulet and Tick*, (2008) SI line (**Figure 9**) and comparing it to the extent of SI in **Figure 15b** it is clear this study and *Murgulet and Tick* (2008) do not conclude the same extent for SI from interpolated results. The likely reason for the different conclusion is the consideration of the Intercoastal Waterway (**Figure 9**). The *Murgulet and Tick*, (2008) study considered this a contributing source of SI (Intercoastal Waterway salinity is ~18 ppt at depths

approaching 4m), while no evidence of contribution to SI by the Intercoastal Waterway was observed in this study (no salinity observed in salinity profile **Figure 14f [**from ERT Array "f" **Figure 9]** which was less than 200 m South of the Intercoastal Waterway at the eastern end of the array).

### c. MODFLOW/SEAWAT: groundwater flow model

Calculated and verified salinity values (as described above) are used as observed concentrations to calibrate a previously developed MODFLOW/SEAWAT model. The SEAWAT code, utilized in the *Ellis et al. (in prep.)* model, simulates three-dimensional variable-density groundwater flow in porous media and was used to simulate SI into coastal aquifers in the Gulf Shores area. SEAWAT works by combining both MODFLOW (*Harbaugh et al.,* 2000) and MT3DMS (*Zheng and Wang*., 1999). This single program resolves the density-dependent groundwater flow and solute-transport equations. The equation for density-dependent groundwater flow in terms of head, solved by MODFLOW routines in SEAWAT, is as follows:

$$\frac{\partial}{\partial\alpha}\left\{\rho \times K_{f\alpha}\left[\frac{\partial h_f}{\partial\alpha}+\frac{\rho-\rho_f\partial Z}{\rho_f\partial\alpha}\right]\right\}+\frac{\partial}{\partial\beta}\left\{\rho \times K_{f\beta}\left[\frac{\partial h_f}{\partial\beta}+\frac{\rho-\rho_f\partial Z}{\rho_f\partial\beta}\right]\right\}+\frac{\partial}{\partial\gamma}\left\{\rho \times K_{f\gamma}\left[\frac{\partial h_f}{\partial\gamma}+\frac{\rho-\rho_f\partial Z}{\rho_f\partial\gamma}\right]\right\}=\rho \times$$

$$S_f \times \frac{\partial h_f}{\partial t}+\theta \times \frac{\partial\rho\partial C}{\partial C\partial t}-\bar{\rho} \times q_s \qquad (13)$$

Where:

α, β, and γ are orthogonal coordinate axes, aligned with permeability
$K_{f\alpha}$, $K_{f\beta}$, $K_{f\gamma}$, are equivalent freshwater hydraulic conductivities in x, y, and z directions [$L\times T^{-1}$]
$\rho$ is the fluid density [$M\times L^{-3}$]
$\rho_f$ is the density of freshwater [$M\times L^{-3}$]
$h_f$ is the freshwater head [L];
$Z$ is the elevation above datum of the center of a model cell [L]
$S_f$ is the freshwater specific storage [$L^{-1}$]
$\theta$ is effective porosity [dimensionless]

$C$ is the solute concentration [M×L$^{-3}$]
$\bar{\rho}$ is the density of water entering from a source or leaving through a sink [M×L$^{-3}$]
$q_s$ is the volumetric flow rate of sources or sinks per unit volume of aquifer [T$^{-1}$]
$t$ is time [T].

As stated earlier, SEAWAT also uses MT3DMS routines to solve the solute-transport governing equation (*Zheng and Bennett*, 2002):

$$\frac{\partial C}{\partial t} = \nabla \cdot (D \times \nabla C) - \nabla \cdot (\bar{v} C) - \frac{q_s}{\theta} \times C_s + \sum_{k=1}^{N} R_k \quad (14)$$

With the following parameters:

D is the hydrodynamic dispersion coefficient [L$^2$×T$^{-1}$]
$\bar{v}$ is the fluid velocity [L×T$^{-1}$]
$C_s$ is the solute concentration of water entering from sources or leaving through sinks [M×L$^{-3}$]
$R_k$ (k = 1,…,N) is the rate of solute production or decay in reaction k of N different reactions [ML$^{-3}$T$^{-1}$]

A linear equation of state is used by SEAWAT to convert concentration of the solute to fluid density:

$$\rho = \rho_f + \frac{\partial \rho}{\partial C} \times C \quad (15)$$

Where $\frac{\partial \rho}{\partial C}$, the slope of the equation, reflects the relationship of the change in density of saltwater per change in salinity at a given temperature, in this study it was changed to 20.5$^o$ C. For example at 20.5$^o$ C the density of freshwater ($\rho_f$) is 998.20 kg/m$^3$ (0ppt/0ppm) while seawater (35ppt/35000ppm) density is 1024.88 kg/m$^3$ and the change in density per ppm is 0.00076 kg/m$^3$ (the slope) which is multiplied by concentration of the solute (NaCl). As stated earlier equivalent NaCl concentration in the model is then translated to salinity regarding SI.

The calculated and verified salinity values now considered observed concentrations are used to calibrate MODFLOW/SEAWAT model developed by *Ellis et al*. (*in prep.).* The SI model parameters (salinity, i.e. constant concentration boundary at the source, density of fluids, layer dimensions and hydraulic conductivity) were adjusted until the predicted intrusion matches

the observed intrusion. The calibrated SI model was then run forward to 2036 to predict future SI and compared with *Lin et al.* (2008) prediction of SI in 2036.

### d. Validating or refuting the existing SI models

The main difference between the previously developed models (by Lin and Ellis) and this model is the addition of another calibration SI line. While Ellis and Lin used as their only reference line the observed SI conditions as stated by *Chandler et al.*, (1996) in this study we additionally calibrated to the SI results interpolated from our ERT field observations (**Figure 15**). As a result, the SI boundary as determined by *Lin et al.*, (2008) is located farther on land compared to findings in our study. We suggest that there are at least two reasons for the large differences in evaluation of SI extent between *Lin*'s study and our study. One reason for the larger extent of SI in *Lin et al*, (2008) is that the salinity at the Gulf coastal boundary through all aquifer layers (regardless of depth) was set at 35 ppt. However, our field observations show that salinity in pore-water/groundwater (*i*) decreases with depth and (*ii*) increases in all aquifer layers as approaching the coast. Another reason for the differences in the extent of predicted SI in the *Lin et al.*, (2008) model is changes to the pumping rates for wells within his model. For the 40-year forecasting SI values, the pumping rates used by *Lin et al.*, (2008) were set at the 1996 level though well pumping rates changed after 1996 (Appendix E). In addition, *Lin et al*., (2008) used average precipitation for the previous ten years (from 1998 to 2008), which includes several years of drought in the area. In contrast, both this study and *Ellis et al*. (in prep) flow models updated the pumping conditions to reflect where new pumping rates, closed wells, and different precipitation data.

Like the Lin model that was only calibrated to the SI conditions as stated by *Chandler et al.,* (1996), the *Ellis et al*., (in prep.) model differed by introducing known changes to the pumping rates within the bounds of the model. The Ellis et al., (in prep.) modeled SI extent was compared to chemically analyzed well samples in the same manner as *Murgalet and Tick*., (2009), *Chandler et al.,* (1996) and *Chandler et al.,* (1985). However, the Chandler studies had access to additional sample locations unavailable for *Murgalet and Tick*.,(2009) and *Ellis et al*., (in prep.). As a result both *Murgalet and Tick*.,(2008) and *Ellis et al*.,(in prep.) contained less data than either chandler study and consequently introduced a greater margin of error and reduced precision for interpolated SI. The lack of sample sources likely accounts for most of the disparity between *Murgalet and Tick*.,(2008) and *Ellis et al*.,(in prep.) SI interpretations.

The *Ellis et al*., (in prep.) study focused on assessing submarine groundwater discharge (SGD) fluxes and characterizing contaminant and nutrient transport through the aquifer system to the Alabama Gulf Coast. To assess and characterize this, the density-dependent groundwater flow and transport model (SEAWAT) or the SI model, utilized in this study, was used to simulate the transport of nitrate and sulfate through the groundwater system to the coast. The model was refined and calibrated using independently determined field-based radon ($^{222}$Rn, $t_{1/2}$=3.82 d) isotopic tracer time-series surveys across a portion of the model area to enhance estimates of nearshore SGD. Thirty-two groundwater wells within the study area were sampled to constrain the groundwater $^{222}$Rn end-member in the model and characterize the extent of nutrient contamination and SI.

To further illustrate the differences between SI extent of *Ellis et al.,* (in prep.), *Murgalet and Tick*.,(2008), *Lin et al*.,(2008), *Chandler et al.,* (1996), and *Chandler et al.,* (1985) profiled SI extents are lain on a north to south cut of a stylized oblique view of study area (**Figure 16a**).

These differences illustrate the necessity for extensive input to precisely determine SI in order to properly calibrate groundwater/SI models. Both the *Lin et al*.,(2008) and *Ellis et al*., (in prep.) models initial condition is extent of SI established by *Chandler et al*., (1985) and calibrated to *Chandler et al*., (1996) but from that initial calibration the *Lin et al*.,(2008) model concludes further SI will occur in the future while *Ellis et al*., (in prep.) model concludes that SI has receded and will likely continue to recede. The ERT derived salinity profile observations (yellow) confirm that the SI does recede but not to the extent that the Ellis model has predicted (orange) (**Figure 16b**).

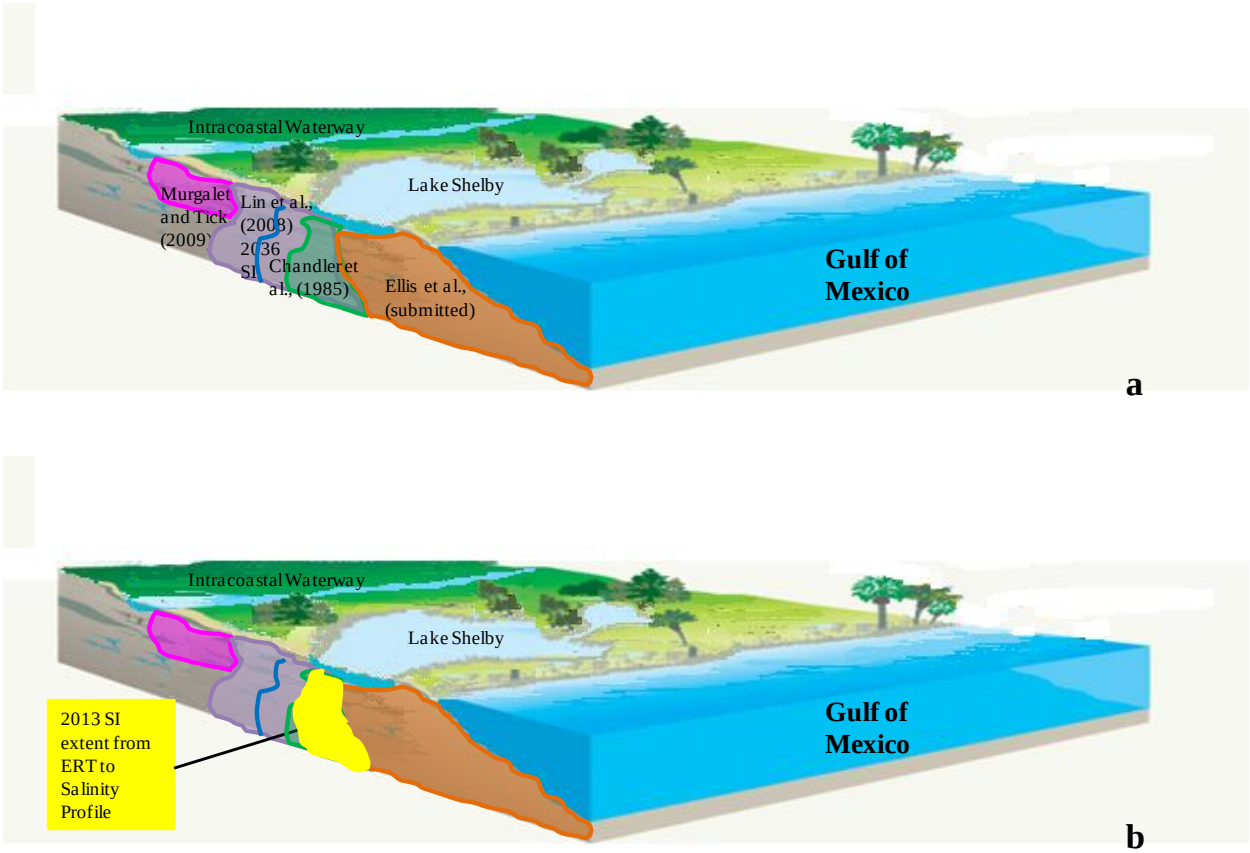


**Figure 16** (a) Illustrated: 2008 extent as determined by *Murgalet and Tick*.,2009 (dark pink), 2036 extent as modeled in *Lin et al.*, 2008(purple) and *Ellis et al.*, (in prep.) 2013 extent (orange) and the *Chandler et al.*, 1985 determined SI determined SI extent (green) and the *Chandler et al.*, 1996 (blue line (b) in yellow the extent of SI as observed by the ERT derived salinity profile.

Further analyses of the two models (Lin's and this study) indicate that the large difference in results stems from the differences in the scale and precision between of the modeled areas. The SI model developed by *Lin et al*., 2008 encompasses the entire Baldwin County Gulf Coast (534 $km^2$ and 24km of coastline) whereas in our study we focus on a much smaller region (45.5 $km^2$ and <7km of coastline) along the Baldwin County Gulf Coast using previously calibrated the density-dependent groundwater flow and transport model by Ellis et al (in prep.). Additionally, precision differs between the two models; the larger regional Lin model has a 51x61 matrix (17000 $m^2$ per model cell) while the smaller Ellis model has an 81x88 matrix (600 $m^2$ per model cell). Stated otherwise, 28 cells within the Ellis model fit within a single cell of the Lin model. Therefore, the Lin model is particularly useful for observing or predicting a regional trend but has limited use in determining the precise extent of SI. Likewise, the Ellis model was suitable for detailed calibration provided by the ERT to salinity observations in this study.

The initial SI model used in this study, the density-dependent groundwater flow and transport model by Ellis et al (in prep.), provides an additional advantage from initial calibration by field data ($^{222}Rn$ tracer approach) for flow dynamics of the upper two aquifers (A1 and A2). These two layers were observed through every ERT array. As a result the first two aquifer of the model are calibrated to two sets of data (Salinity via ERT and Groundwater flux via radon ($^{222}Rn$, $t_{1/2}$=3.8 d) isotopic tracer) in addition to data that is typically ascertained from wells (Groundwater head, pumping rates, Salinity via geochemical analysis, and transmissivity). Calibration of the deeper aquifer (aquifer A3) is therefore limited as compared to the upper two aquifers.

Calibration using PEST within the deeper aquifer allows for greater subjectivity when adjusting the K. However, the K adjustments are still constrained well determined transmissivity

(slug and pump test) by the drillers at the individual wells. The subjectivity in K within the aquifer applies as the distance increases from the wells. Other parameters that affect flow model as well include: (i) thickness of aquifer/aquitard layers, (ii) hydraulic conductivity (K) of the confining layer (aquitard) particularly in the vertical direction and (iii) the density of the water within the model.

Groundwater volumetric flow rate *Q* as defined in Darcy's Law (**Equation 16**) is a function of hydraulic conductivity (*K*), the hydraulic gradient (*i*) and the cross-sectional area (*A* is layer width X layer thickness). Changes to the thickness of an aquifer will affect the groundwater flow rate (horizontal direction).

$$Q = K \times i \times A \tag{16}$$

If groundwater flow rate and head loss are held constant and the aquifer thickness is changed (aquifer width also held constant) then hydraulic conductivity must change. An aquitard restricts or retards groundwater flow from one aquifer to another. The groundwater flow between aquifers is generally in the vertical direction where **i** is the head difference between the two aquifers. Assuming that the only factor changing between is the distance between the two aquifers (ie the thickness) then the residence time of water aquitard changes (i.e. the water between aquifers is exchanged more quickly or slowly due to the change in distance being traveled within the aquitard).

Another parameter that affects the resident time of water within any layer is the hydraulic conductivity (*K*). As stated *Q* is affected by *K, i,* and *A* so if *i* and *A* are held constant then a change in *K* will change *Q* proportionally. By changing the *K* in an aquitard between aquifers the *Q* between those layers changes as well as the residence time of the water within the aquitard.

Fluid density affects two parameters: hydraulic head (*h*) and hydraulic conductivity (*K*). Based on Bernoulli's Principle (**Equation 17**), the hydraulic head (*h* ) is a function of density:

$$h = z + \frac{p}{\rho \times g} \tag{17}$$

Where **z** is the elevation of the point above a reference plane, *p* is the pressure at the chosen point, $\rho$ is the density of the fluid at all points in the fluid, and *g* is the acceleration due to gravity. Changes to density of the fluid changes the hydraulic gradient *i* (head loss). Hydraulic conductivity (*K*) is a function density of the fluid as well, hydraulic conductivity from Darcy's Law (**Equation 18**):

$$K = \frac{\rho \times g \times k}{\mu} \tag{18}$$

Where: $\rho$ is the density of the fluid at all points in the fluid, *g* is the acceleration due to gravity, *k* a measure of the ability of a material to transmit fluids (permeability), $\mu$ is the viscosity of the fluid. Changing the density gradient (as density relates to concentration, discussed earlier) within the model therefore changes the groundwater flow characteristics.

In this study, we use SEAWAT code for density dependent flow that is coupling MODFLOW to MT3DMS (the contaminant transport model). Briefly, the changes in the density of the fluid are handled as salinity changes and salinity is expressed as NaCl concentration and treated as contaminant in MT3DMS within the groundwater flow model to indicate the extent of SI under the provided conditions. Each of the previously discussed the parameters (e.g., layer thickness, layer vertical and horizontal hydraulic conductivity, and head at the constant concentration boundary parallel to the ocean) affect the groundwater flow characteristics to different magnitudes. The greater the magnitude per degree of change the more sensitive the

model is to that particular parameter. Sensitivity analyses of the model showed that the model is most sensitive to the parameter "constant concentration boundaries values" (e.g.,salinity at the source). To understand how the concentration values at the ocean-side boundary affect the model, the concentration value at the boundary was initially adjusted to align closely with the beach salinity profile shown on **Figure 14a**. Because the beach salinity profile did not intercepts the constant concentration boundary, an iterative process occurred with concentration values at the boundary to properly adjust the magnitude of the SI (**Table 9**).

**Table 9** Comparing of constant concentration boundary *Ellis et al,* (in prep.) model to the model parameters used in this study

| **Model layer** | **Starta** | **Salinity (ppt)** | |
|---|---|---|---|
| | | *Ellis et al* | *This study* |
| 1 | Surface | 35 | 35 |
| 2 | Aquifer A1 | 10 | 17 |
| 3 | C1 confining | 10 | 17 |
| 4 | Aquifer A2a | 5 | 14.3 |
| 5 | C2a confining | 5 | 14.3 |
| 6 | Aquifer A2b | 5 | 5 |
| 7 | C2b confining | 0 | 5 |
| 8 | Aquifer A2c | 0 | 5 |
| 9 | C2c confining | 0 | 1 |
| 10 | Aquifer A3 | 0 | 1 |
| 11 | C3 confining | 0 | 1 |

Further refining of the model of the concentration (salinity) required manual adjustment to the horizontal conductivity by decreasing it from 26.5 m/day to 22.25 m/day within southeastern corner of layer 2 (Aquifer A2a). Finally, the C1 confining layer was thinned (effectively halved) in southern center of the model (Eastern half of Lake Shelby) and vertical conductivity increased from 0.03 cm/day to 1.52 cm/day. Once the manual adjustments were

complete, these parameters were fixed in the discussed location while the parameters elsewhere were estimated using PEST.

Using observed hydraulic heads, PEST software adjusted the hydraulic conductivity. These adjustments were only constrained where the K was not fixed from the manual process. This was process repeated until model results closely compared to the observed values of SI (**Figure 15**) and Darcy flux (between 6.41 cm/day and 8.62 cm/day in both Aquifer A1 and A2a-c (*Ellis et al*., (in prep.).

PEST software optimized model calibration head had a residual value of 0.04 m and a Root Mean Squared Error (RMSE) between the observed and simulated heads of 0.2m. The scatter diagram (**Figure 17**) illustrates the difference between calculated heads (calculated from the change to hydraulic conductivity using Darcy's Law) and observed heads (Appendix C and D contains the PEST optimization results and the PEST parameter values). The average Darcy flux for the refined and calibrated for the model developed in this study was 7.41 cm/day which was determined by Ellis from the radon ($^{222}$Rn) isotopic tracer field experiments.

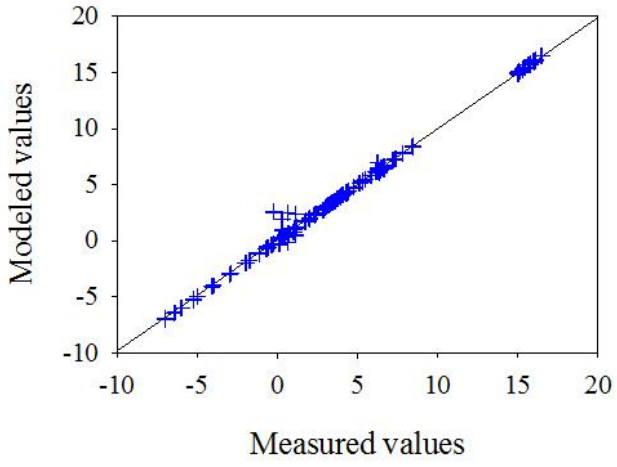


**Figure 17** Scatter diagram showing the goodness of fit between the measured and modeled heads for 2013 produced by the model developed in this study. Calculated (modeled) heads (y-axis) are plotted versus the observed (measured) heads (x-axis). Line shows the better the fit. The plotted values are used to determine the residual and root mean square error.

Comparing the SI between *Ellis et al.* (in prep.) model and this study (**Figure 18a-b**), a cross-section view of SI (white line on imbedded aerial view), the SI extent is farther inland in the model in this study (**Figure 18b**) and more closely resembling the observed SI from the geophysical investigation. Further comparison between *Ellis et al*, (in prep.) (**Figure19a-d**) and the model in this study (**Figure 20a-d**) illustrates the utility of ERT to calibrate the extent of SI as the model in this study close resembles the results from **Figure 15**. Though this study's modeled SI extent does not match exactly to the interpolated SI extent this does not discount the validity of the model. First the interpolated SI extent was determined from two snap shots in time. The interpolated SI extent captures the SI at the moment and does not account for tidal ebbs and flows or differences due seasonal changes. The modeled SI extent is an average of expected SI under averaged annual conditions. The intent of the model is to capture whether SI further intrudes or recedes over time due to long term changes not the changes due to daily or seasonal oscillation.

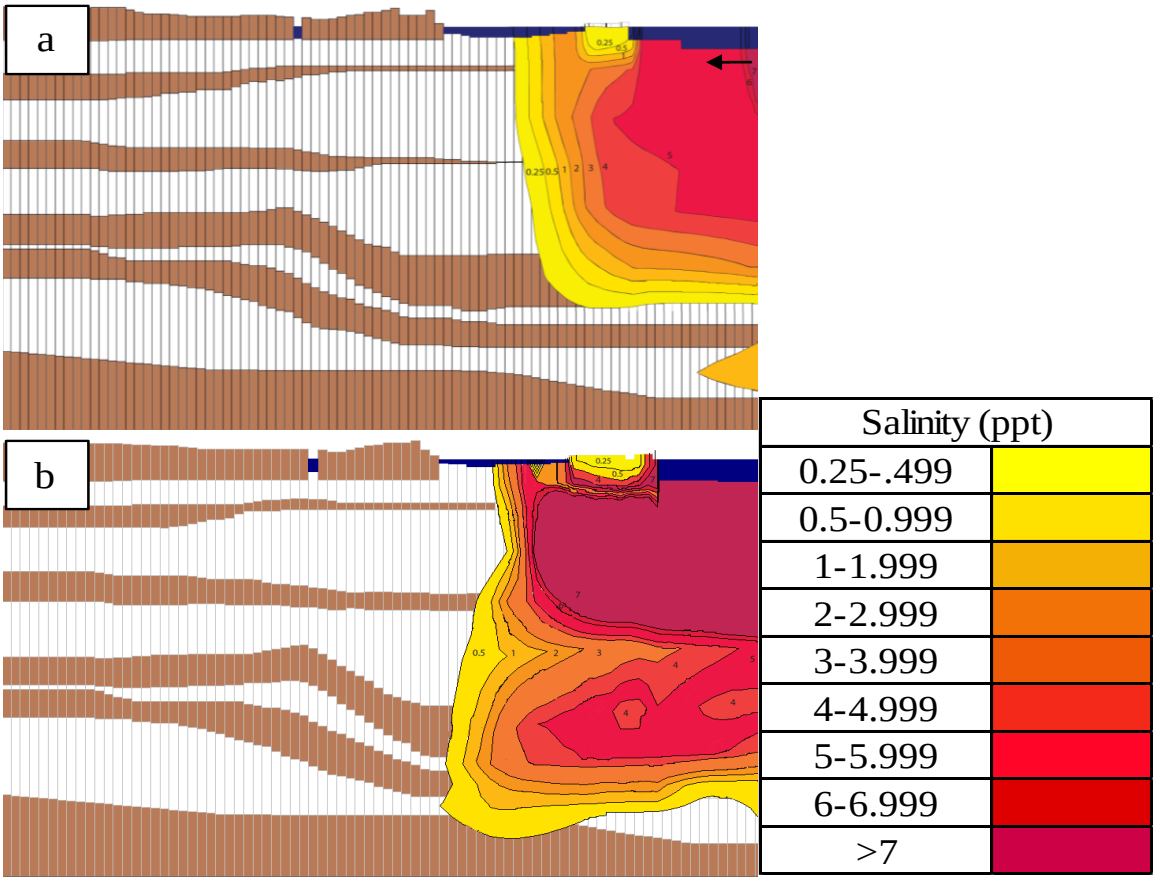


**Figure 18** Comparison of the seawater extent between (**a**) *Ellis et al.*(in prep.) and (**b**) this study. This illustration demonstrates the difference in the extent and concentration through all the aquifers between the two models.

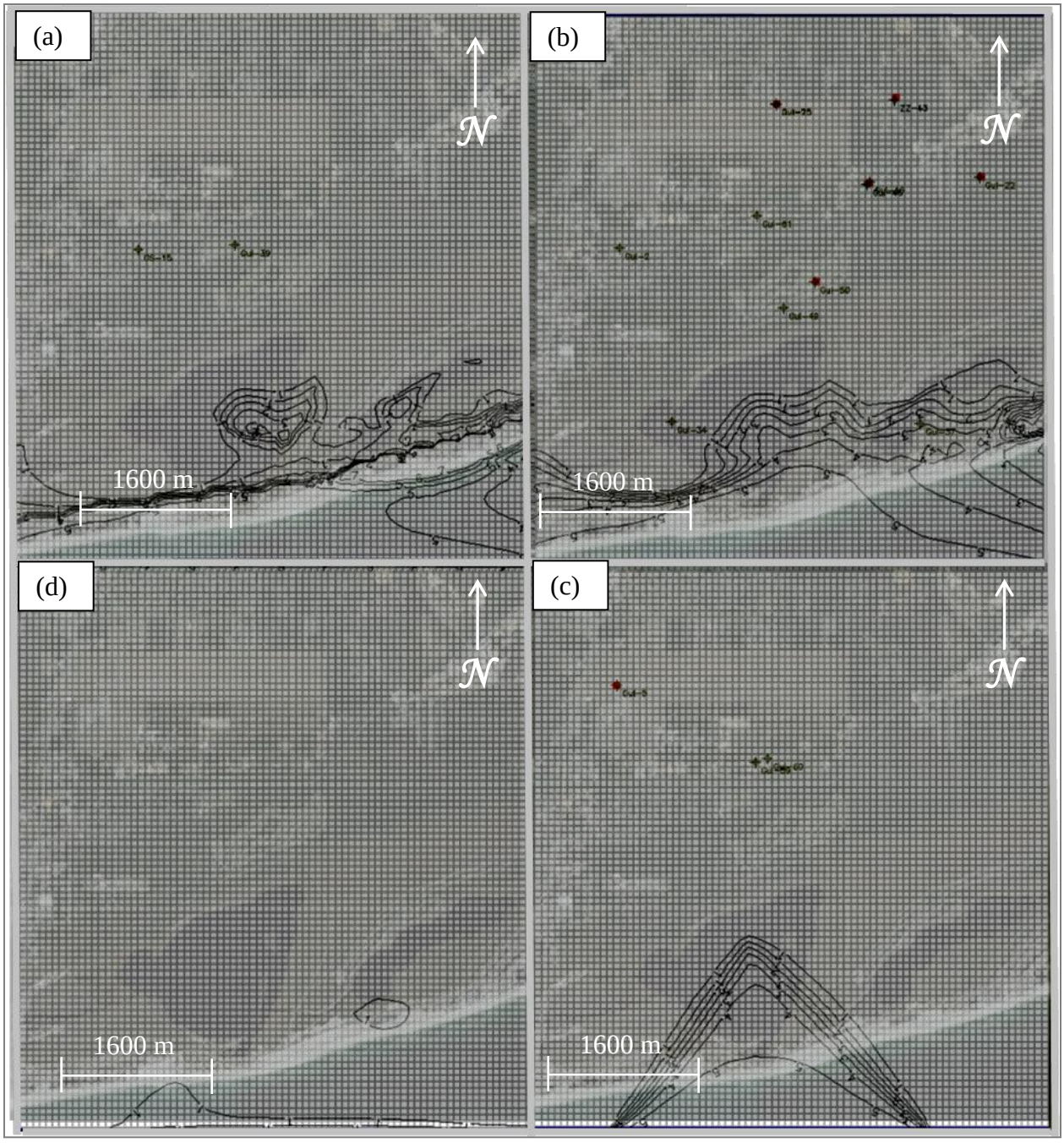


**Figure 19** Current (year 2013) seawater intrusion extent for aquifers (**a**) Aquifer A1; (**b**) Aquifer A2a; (**c**) aquifer A2b and (**d**) Aquifer A2c as determined by *Ellis et al*, (in prep.).

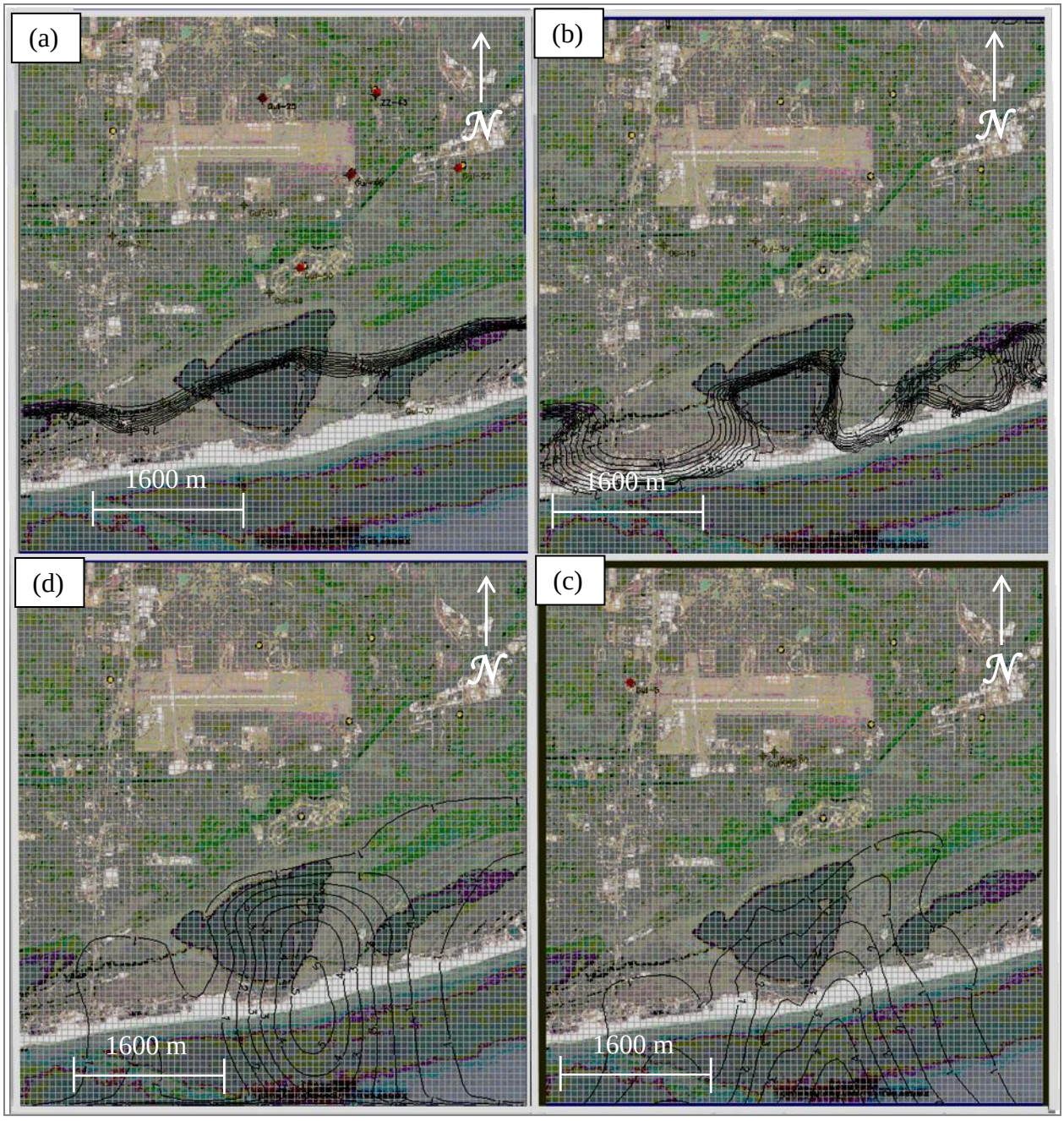


**Figure 20** Seawater intrusion extent for aquifers (**a**) Aquifer A1; (**b**) Aquifer A2a; (**c**) aquifer A2b and (**d**) Aquifer A2c as determined by this study (equivalent to *Ellis et al (*in prep.*)* that is presented in **Figure 12).**

### e. Predictions Based on SI Model developed by this Study

The developed model in this study is used to forecast future SI extent under different scenarios. Five predictions were conducted. The first prediction was for the average of the well

pumping rates from 1996 to 2013 with average recharge for the period (Appendix E). This is to understand that if conditions remain relatively unchanged how SI would change, if any. The second prediction was for the maximum well pumping rate from between 1996 to 2013 with average recharge for the period. The year 2000 pump rates were chosen for the maximum pumping scenario (Appendix E). The third prediction was for the minimum well pumping rate from between 1996 to 2013 with average recharge rate for the period. For the minimum pumping rate scenario the lowest pumping rates for each well were selected from different years to achieve the most distinct minimum from actual pumping rates (Appendix E). The fourth and fifth predictions were no pumping scenarios. The fourth prediction is no pumping until 2036 and the fifth prediction is for 100 years until the year 2113. Aquifer A2a is used to illustrate the changes that occur given the four different scenarios (**Figure 21a-d**) (model result of the additional aquifer is in Appendix D).

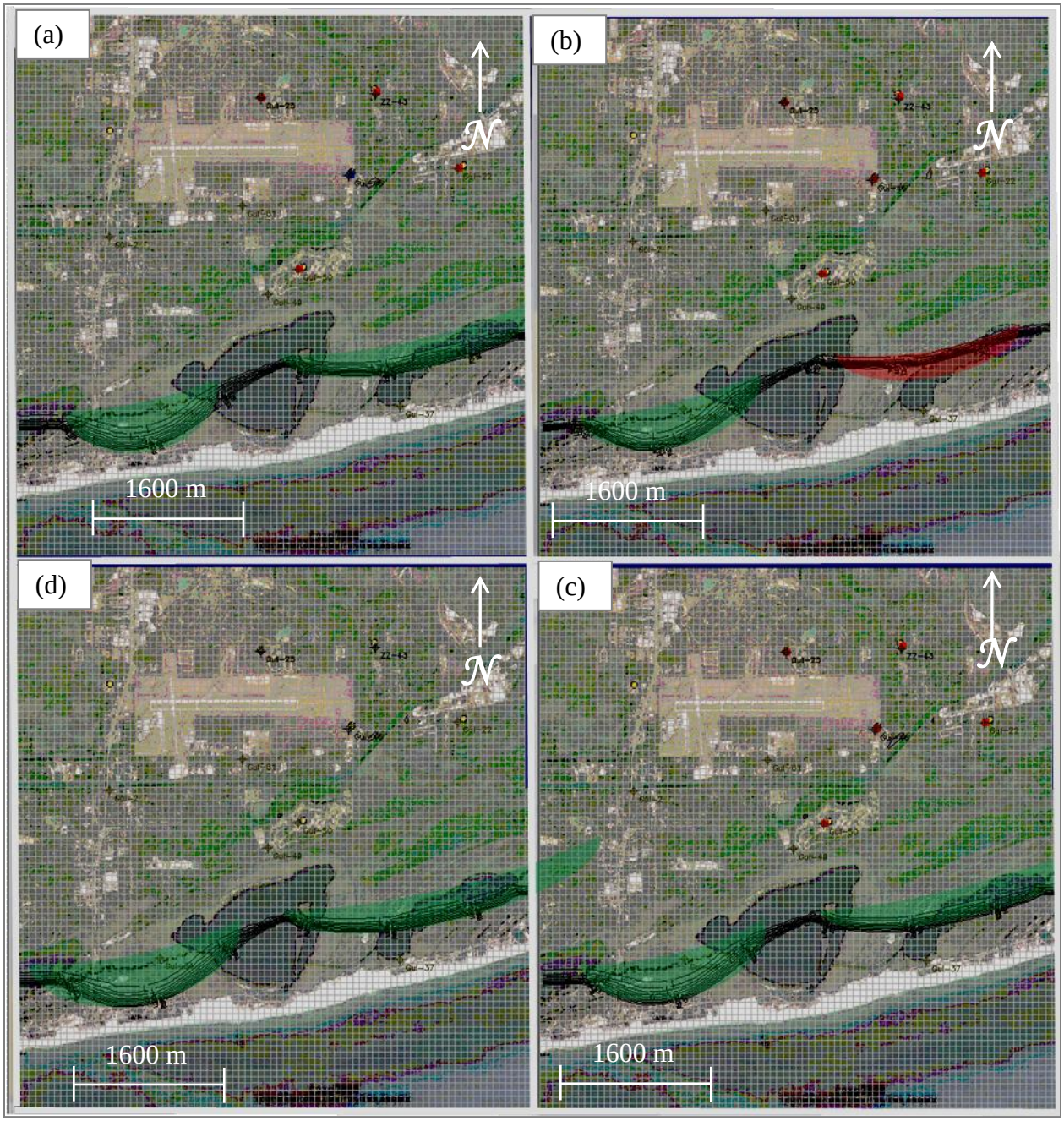


**Figure 21** Predicted extent of seawater intrusion by this study for Aquifer A2a for year 2036 under different conditions: (**a**) average pumping rate; (**b**) maximum pumping rate; (**c**) minimum pumping rate; and (**d**) "zero" pumping. Red color indicates areas where seawater intrusion would potentially advance, whereas green color illustrates where extend would recede.

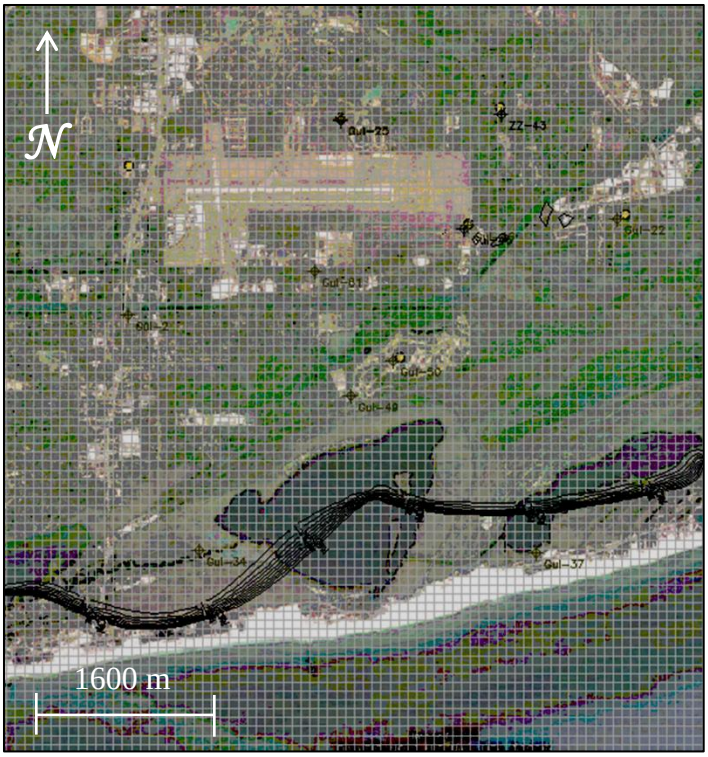


**Figure 22** Predicted extent of SI in Aquifer A2a for 2113 for 100 years of "zero" pumping. This figure illustrates that near natural equilibrium SI is a natural occurrence and other factors other than pumping effect extent of SI in the near-shore aquifers to near the same magnitude of the average pumping rate.

Comparing the SI in **Figure 20b** to the **Figures 21a-d** demonstrates that only the maximum pumping rate (**Figure 21b)** continued to advance SI further inland while the average and minimum pumping rates caused the SI to recede. However, the maximum pumping rate advanced SI less than 100 meters the zone of dispersion narrowed significantly increasing the salinity (from 1ppt to 5ppt). The average pumping rate receded but was less than 100 meters and the minimum pumping rate receded less than 200 meters. This should give confidence to the utility companies in the area that they have made good adjustments for the increasing tourist population every summer. When the new position of the SI-line is compared to the no pumping rate scenarios the maximum pumping rate extends only 300 meters from what is likely near the natural equilibrium SI state of 100 years of no pumping (**Figure 22**).

When compared to the model developed by *Lin et al*., 2008 ( as illustrated in **Figure 9**) SI extent and understanding that wells were shut down and moved by Gulf Shores utilities it is obvious that conditions changed. The SI extent, as predicted and modeled in *Lin et al*., 2008 for 2036, have been avoided for now. Nonetheless, SI continues even in the current conditions. Should pumping rates increase from increasing tourist population or recharge decrease such as from a drought or climate change, it is safe to predict a further advance of SI from the observed state of SI in 2013.

## 4. CONCLUSIONS

Coastal communities' water resource managers must account for seawater intrusion into local aquifers, as population growth increases the demand for groundwater, the only affordable coastal source of fresh water. MODFLOW/SEAWAT is often used to support management of coastal aquifers, but as seen in this study these models tend to be limited spatially for calibration. Therefore, to ensure that water managers continue to make the proper decisions with available groundwater resources, updated calibration is necessary to adjust SI models to reflect the changing conditions. This study used ERT, with the aim of calibrating an existing SI model, to an extent previously not researched.

This ERT utilization yielded very useful results for quantifying the extent of SI in four near-shore aquifer layers. Using the ERT to determine magnitude of the SI and the salinity within the A1 and A2 aquifers (a-c) allowed for the proper adjustment to the "constant concentration boundary" in the *Ellis et al*, (in prep) Model. Additionally, the fact that the *Ellis et al*, (in prep) flow model had been calibrated using the radon tracer method increased the confidence in the groundwater flow model. This confidence encouraged adjustments toward increasing salinity at the "constant concentration boundary" and not large adjustments in other parameters of the model.

Ultimately, this study lends credence not only to using ERT to calibrate SI modeling but to employing a coupled approach toward SI determination and modeling. Since the *Ellis et al.,* (in prep) verified the ground water flow model with the $^{222}$Radon tracer and ERT was used to determine the salinity in the subsurface the groundwater conditions could be observed in situ. As a result both sets of data provided a measure to constrain the model and increase confidence in

the results.

It is inevitable that conditions will change in the future. The tourist population has increased every year for the last 30 years and shows no sign of abating. Climate change predictions forecast rising sea levels and changes in regional rain fall amounts. It is in light of these changes that this study will prove the most useful. It provides a means to verify and calibrate SI models that will surely be needed and used for the expansion and management of groundwater resources in coastal regions worldwide.

# REFERENCES


Alabama Gulf Coast Region Chamber of Commerce, Area Information & Demographics. Coast Living (2010), pg 39

Archie, G.E. (1942). The electrical resistivity log as an aid in determining some reservoir characteristics. Petroleum Transactions of AIME 146: 54–62.

Auken, E., L. Pellerin, A.V. Christiansen, and K. Sorensen. (2006). A survey of current trends in near-surface electrical and electro-magnetic methods. Geophysics 71, no. 5:G249–G260.

Bateman, R.M. (1985) Cased-Hole Log Analysis and Reservoir Performance Monitoring Published by Prentice Hall Printing

Barlow, Paul M. (2003). Ground Water in Freshwater-Saltwater Environments of the Atlantic Coast, USGS.

Chandler RV, Moore JD, Gillett B (1985) Ground-water chemistry and salt-water encroachment, southern Baldwin County, Alabama.Ala Geol Surv Bull 126:166

Chandler RV, Gillett B, DeJarnette SS (1996) Hydrogeologic and water-use data for southern Baldwin County, Alabama. Ala Geol Surv Circ 188:124

Cooper, H. H., (1964), A hypothesis concerning the dynamic balance of fresh water and salt water in a coastal aquifer: U.S. Geological Survey Water-Supply Paper 1613-C, p. 1-12

Davis ME (1987) Stratigraphic and hydrogeologic framework of the Alabama coastal plain. U. S. Geological Survey Water-Resources Investigations Report 87-4112

Dimova,Natasha T., Peter W. Swarzenski, Henrieta Dulaiova, and Craig R. Glenn, (2012) Utilizing multichannel electrical resistivity methods to examine the dynamics of the fresh water–seawater interface in two Hawaiian groundwater systems, Journal Of Geophysical Research, Vol. 117, C02012 .

Ellis, J , Dimova, N, (in prep)

EPA, Ecosystem Research, Athens, GA, http://www.epa.gov/athens/learn2model/part-two/onsite/ex/jne_henrys_map.html

Fofonoff, N. P., and R. C. Millard Jr. (1983), Algorithms for computation of fundamental properties of seawater, UNESCO Tech. Pap. Mar. Sci., 44.

Guariglia, A., Buonamassa, A., Losurdo, A., Saladino, R., Trivigno, M.L. Zaccagnino, A. and Colangelo, A.,(2006) A multisource approach for coastline mapping and identification of shoreline changes, Annals of Geophysics, Vol. 49, 297-306.

Guo W, Langevin CD (2002) User's guide to SEAWAT: a computer program for the simulation of three-dimensional variable-density ground-water flow. USGS Techniques of Water Resources Investigations, Book 6, chap A7

Harbaugh, A.W., E.R. Banta, M.C. Hill, and M.G. McDonald. (2000). MODFLOW-2000, the U.S. Geological Survey modular ground-water model—User guide to modularization concepts and the Ground-Water Flow Process. USGS Open-File Report 00-92. Reston, Virginia: U.S. Geological Survey.

Herckenrath, D., Odlum, N., Nenna, V., Knight, R., Auken, E. and Bauer-Gottwein, P. (2012), Calibrating a Salt Water Intrusion Model with Time-Domain Electromagnetic Data. Ground Water. doi: 10.1111/j.1745-6584.2012.00974.x

Igroufa, S., Hashim, R., Taib, S., (2010) Mapping of salt-water intrusion by geoelectrical imaging in Carey Island. 5th International Symposium on Hydrocarbons & Chemistry (ISHC5), Sidi Fredj, Algiers, May the 23rd to 25th.

Jin, G., Torres-Verdin, C., Devarajan, S, Toumelin, E., and Thomas, E.C. (2007) "Pore-Scale Analysis of the Waxman-Smits Shaly-Sand Conductivity Model," ***Petrophysics***, 48; 2, P 104-120

Langevin, C.D., (2009) SEAWAT: A Computer Program for Simulation of Variable-Density Groundwater Flow and Multi-Species Solute and Heat Transport: U.S. Geological Survey Fact Sheet 2009-3047, 2 p.

Lin,L., Snodsmith J.B., Zheng, C.,Wu, J. (2008) A modeling study of seawater intrusion in Alabama Gulf Coast, USA Journal: Environmental Earth Sciences - ENVIRON EARTH SCI , vol. 57, no. 1, pp. 119-130, 2009

Loke, M.H. and Barker, R.D., (1996) Rapid least-squares inversion of apparent resistivity pseudosections by a quasi-Newton method, Geophysical Prospecting, Vol. 44, pp.131-155.

McWorter, D.B. and D.K. Sunada. (1977) Groundwater and Hydraulics, Water Resources Publications, Fort Collins, CO.

Murgulet, D., Tick, G.R. (2013). Characterization of Flow Dynamics and Vulnerability in a Coastal Aquifer System, *Ground Water*, doi: 10.1111/gwat.12020

Murgulet, D., Tick G.R. (2007). The extent of saltwater intrusion in southern Baldwin County, Alabama. *Environmental Geology*, doi 10.1007/s00254-007-1068-0

National Oceanic and Atmospheric Administration, Nation Weather Service, Weather Forecasting Office, Archives: Monthly Rainfall Averages for Baldwin County, AL

Nowroozi, A.A., Horrocks, S.B. and Henderson, P., (1999) Saltwater intrusion into the freshwater aquifer in the eastern shore of Virginia: a reconnaissance electrical resistivity survey, J. of Applied Geophysics, Vol. 42, pp. 1–22.

Robinson, J. (1996). Ground-Water Resources Data for Baldwin County, Alabama: *U.S. Geological Survey Open File Report 96-487.*

Sasaki, Y., (1992) Resolution of resistivity tomography inferred from numerical simulation, Geophysical Prospecting, Vol.40, pp. 453- 464.

Satriani, A, Loperto, A. Proto, M, (2011) Electrical resistivity tomography for coastal salt water intrusion characterization along the Ionian coast of Basilicata region (Southern Italy), Fifteenth International Water Technology Conference, IWTC-15 2011, Alexandria, Egypt.

Snodsmith, JB, (1998) Simulation of Seawater Intrusion in Southern Baldwin County, Alabama, A Thesis

Thomas, E. C., (2010) Understanding the Waxman-Smits Equations, Schlumberger-Techsia , Techlog 2010.1 User Manual Supplemental, March.

United States Census Bureau, 2010 Census, http://www.census.gov/2010census/popmap/ipmtext.php?fl=01

Walter G.R., Kidd R.E. (1979) Ground-water management techniques for the control of salt-water encroachment in Gulf Coast aquifers, a summary report. *Alabama Geological Survey Open File Report, 84p*

Waxman, M. H. and Smits, L. J. M.(1968):"Electrical Conductivities in Oil-Bearing Shaly Sands," Soc. Pet. Eng. J. (June) 107-22; Trans., AIME, 243.

Waxman, M. H. and Thomas, E. C. (1974):"Electrical Conductivities in Shaly Sands - I. The Relation Between Hydrocarbon Saturation and Resistivity Index; II. The Temperature Coefficient of Electrical Conductivity," J. Pet. Tech. (Feb.) 213-23; Trans., AIME, 257.

Worthington, P.F. (1976) Hydrogeophysical equivalence of water salinity, porosity and matrix conduction in areanaceous aquifers, Groundwater, Vol. 14, No. 4, July-August, 224-232.

Zheng, Chunmiao, (2010) *MT3DMS v5.3 Supplemental User's Guide*, Technical Report to the U.S. Army Engineer Research and Development Center, Department of Geological Sciences, University of Alabama, 51 p.

Zheng, C., and G.D. Bennett, (2002) Applied Contaminant Transport Modeling, Second Edition, Wiley, New York, 621 pp.

Zheng, C., Wang, P.P. (1999). MT3DMS: a modular three-dimensional multispecies model for simulation of advection, dispersion and chemical reactions of contaminants in groundwater

systems; Documentation and User's Guide. Contract Report SERDP-99-1. U.S. Army Engineer Research and Development Center, Vicksburg, MS.

Zohdy, A. A. R., and D. B. Jackson (1969), Application of deep electrical soundings for groundwater exploration in Hawaii, Geophysics, 34(4), 584–600, doi:10.1190/1.1440033

Verrjuit, Arnold (1968), A note on the Ghyben-Herzberg formula, *Bulletin of the International Association of Scientific Hydrology* (Delft, Netherlands: Technological University) **13** (4): pp. 43–46. Retrieved 2009-03-21

# APPENDIX A: ρo and ρw and Salinity Matrix profiles

Beach $\rho_o$ and $\rho_w$ and Salinity Matrix profile "a"

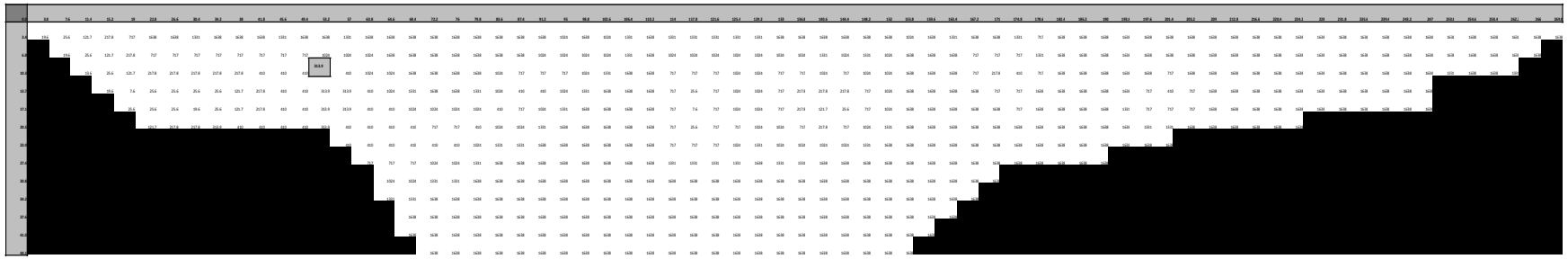

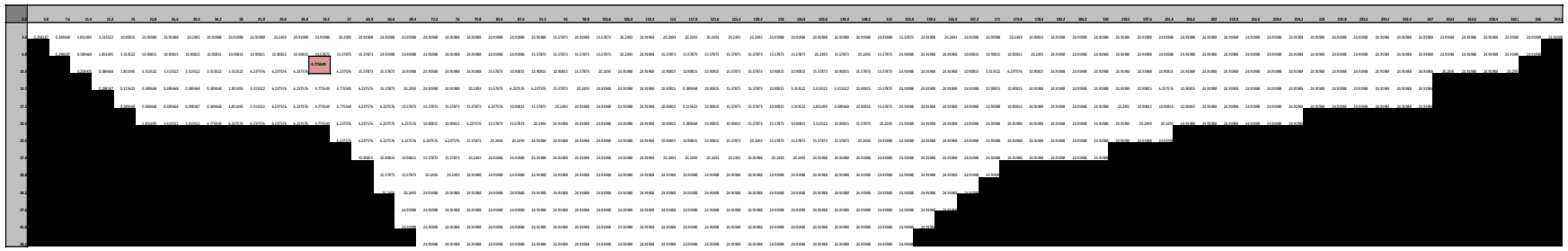

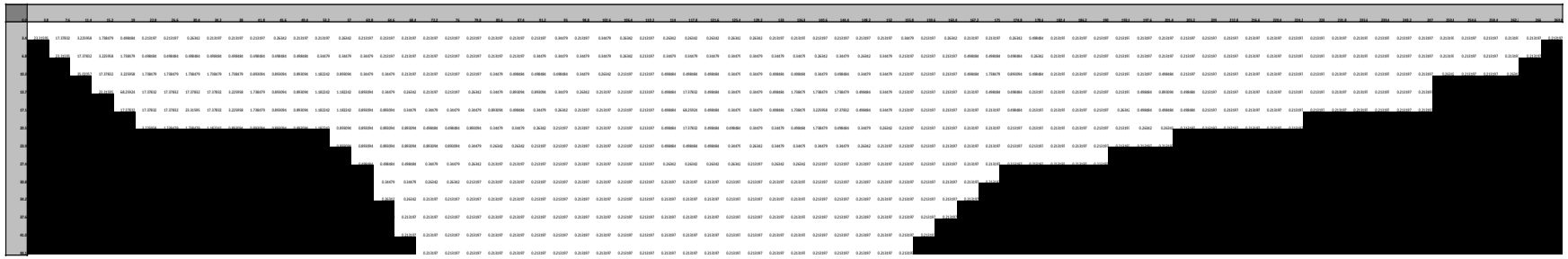

South Shelby $\rho_o$ and $\rho_w$ and Salinity Matrix profile

"b"

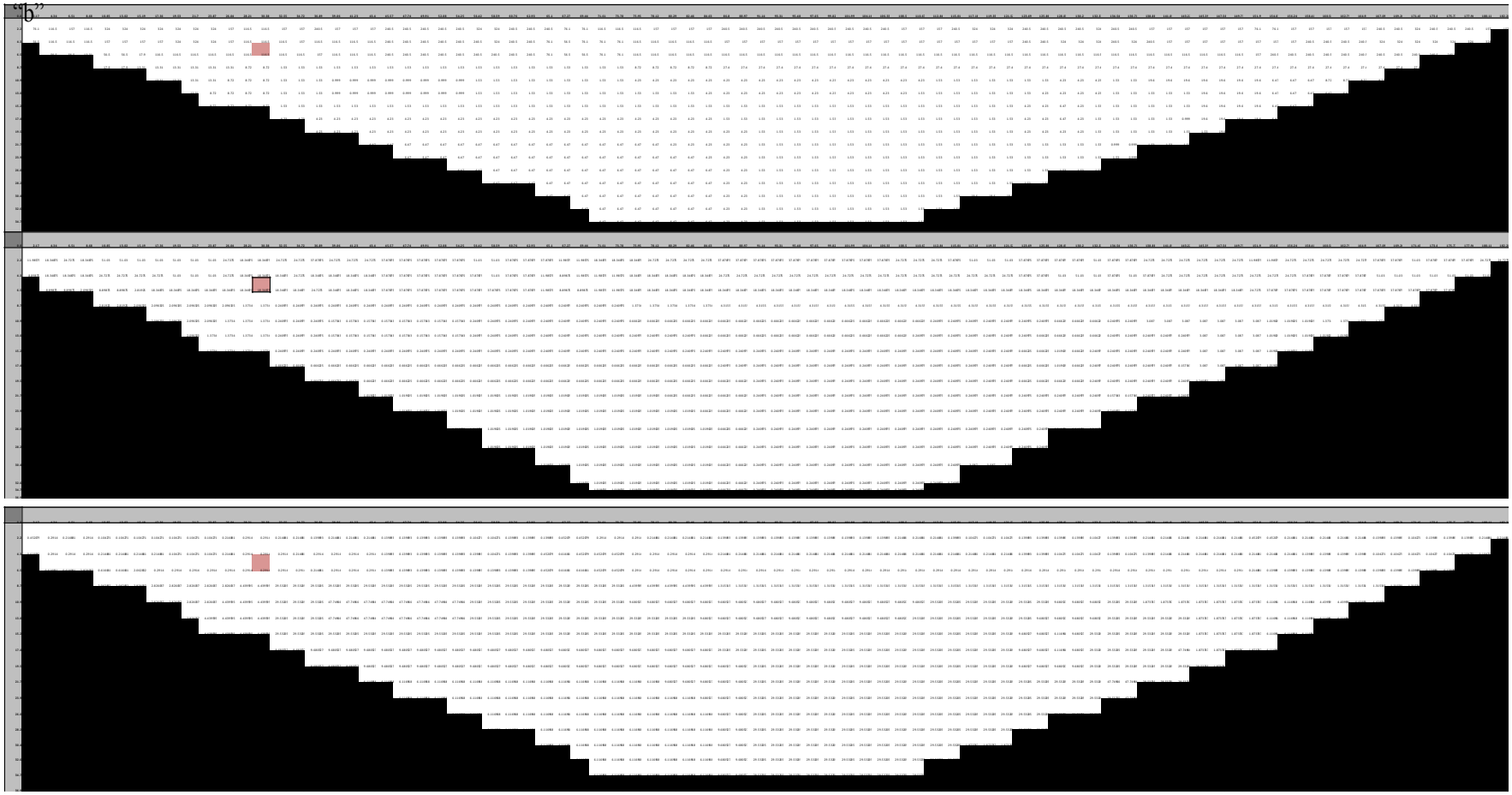

East Shelby $\rho_o$ and $\rho_w$ and Salinity Matrix profile "c"

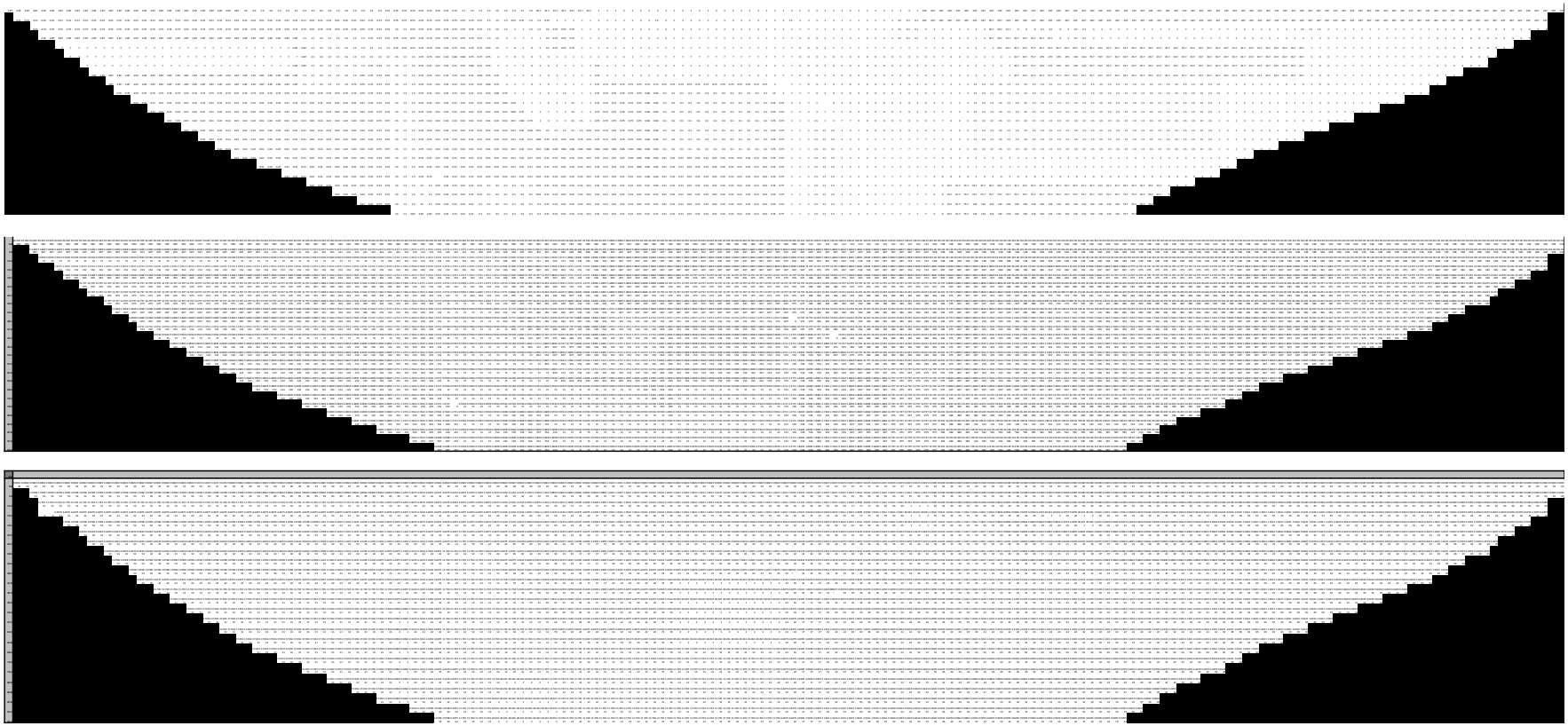

West Marine Shelby $\rho_o$ and $\rho_w$ and Salinity Matrix profile “d”

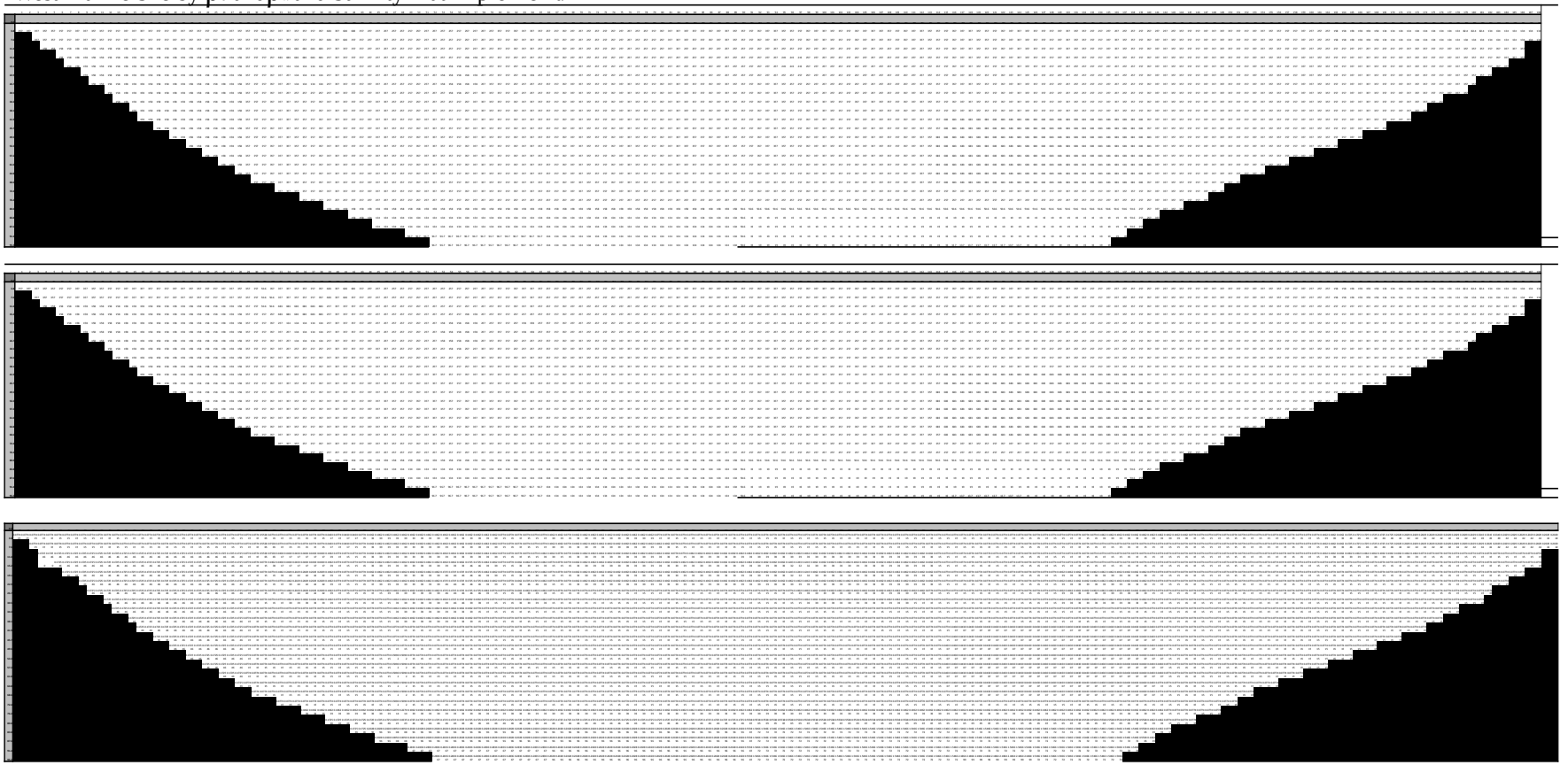

East Marine Shelby $\rho_o$ and $\rho_w$ and Salinity Matrix profile "e"

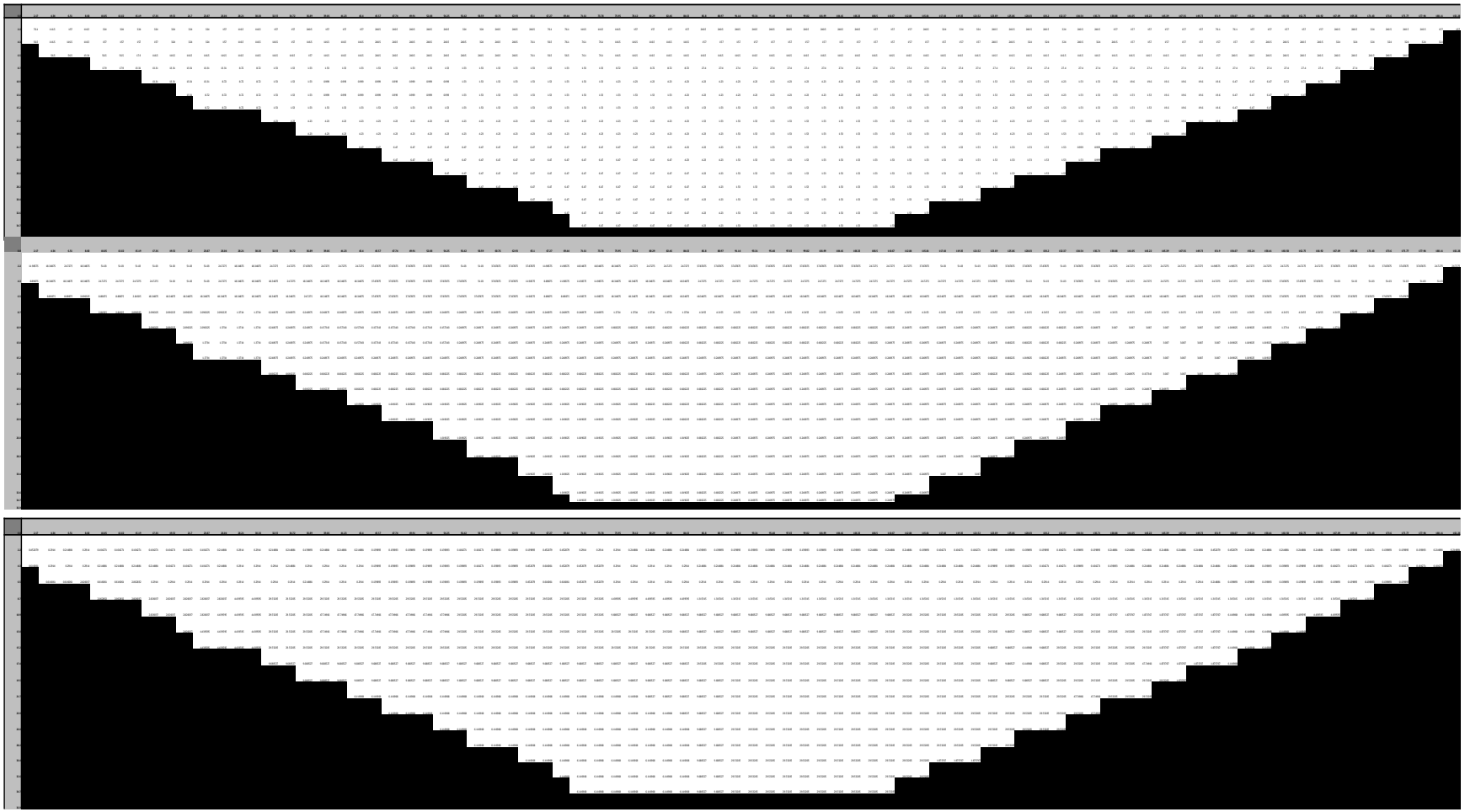

Northern Gulf State park (Golf Course) $\rho_o$ and $\rho_w$ and Salinity Matrix profile "f"

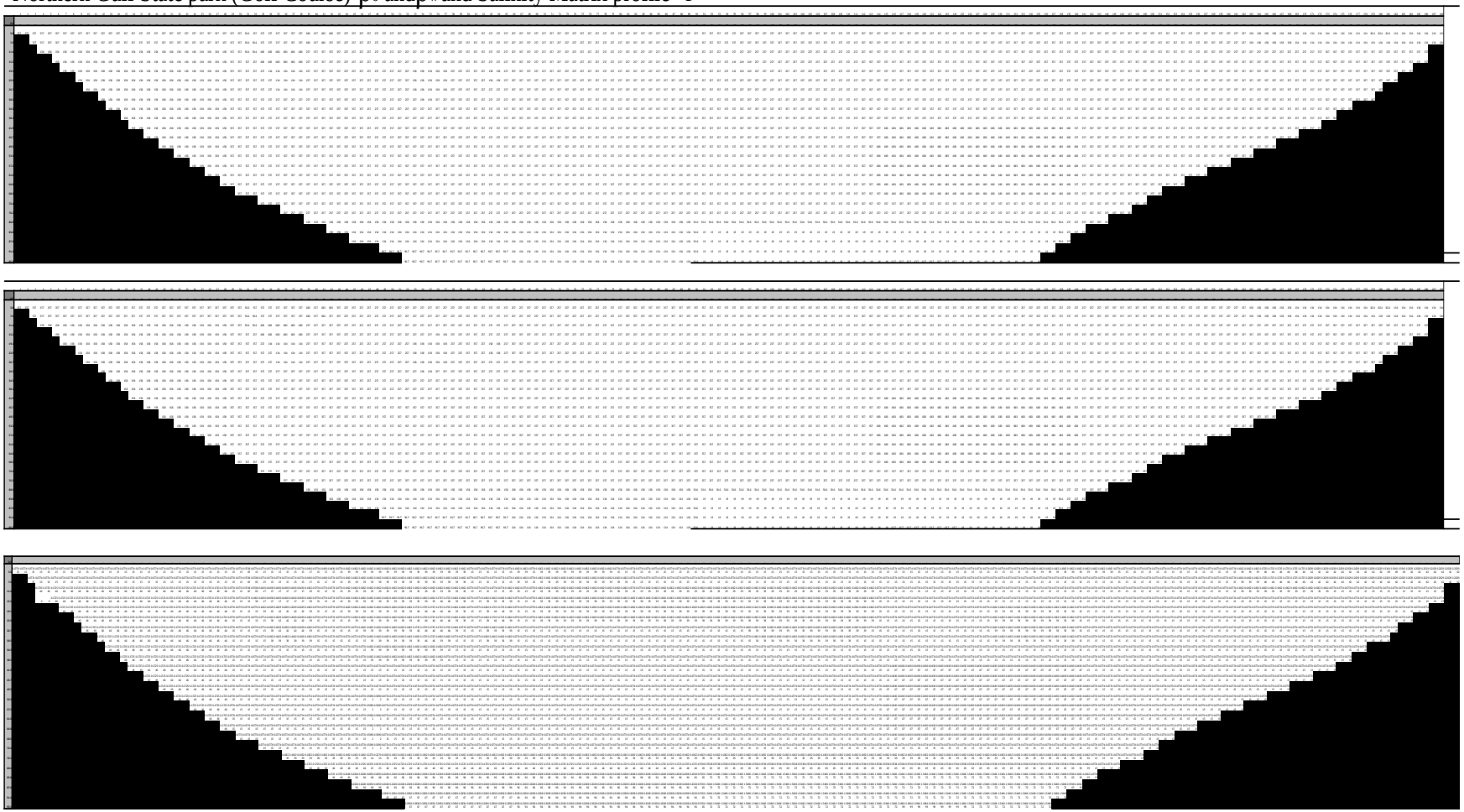

**Young's by the Sea (Just west of Well A)**

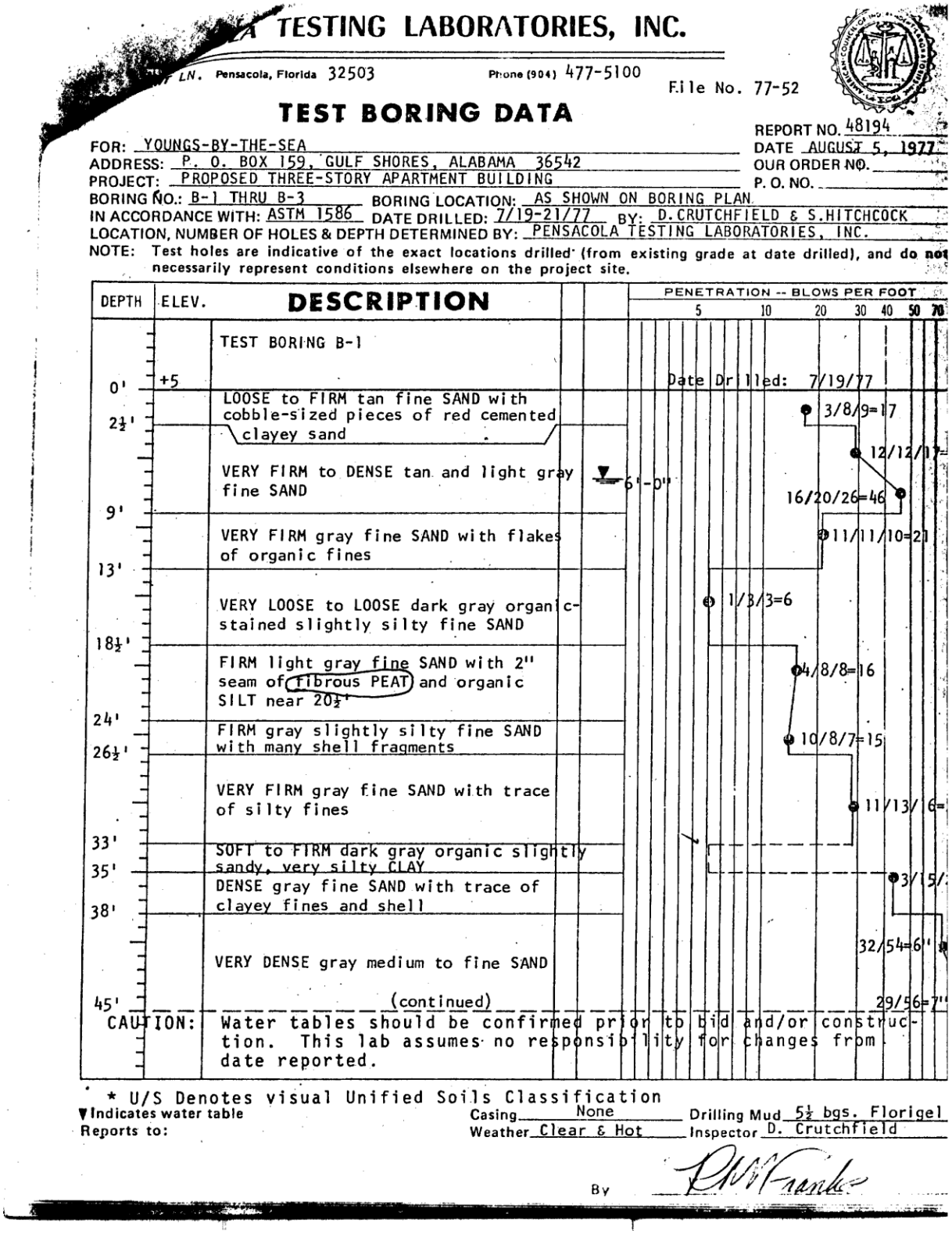

TESTING LABORATORIES, INC.

LN. Pensacola, Florida 32503 Phone (904) 477-5100 File No. 77-52

TEST BORING DATA

REPORT NO. 48194
DATE AUGUST 5, 1977
OUR ORDER NO.
P. O. NO.

FOR: YOUNGS-BY-THE-SEA
ADDRESS: P. O. BOX 159, GULF SHORES, ALABAMA 36542
PROJECT: PROPOSED THREE-STORY APARTMENT BUILDING
BORING NO.: B-1 THRU B-3 BORING LOCATION: AS SHOWN ON BORING PLAN
IN ACCORDANCE WITH: ASTM 1586 DATE DRILLED: 7/19-21/77 BY: D. CRUTCHFIELD & S. HITCHCOCK
LOCATION, NUMBER OF HOLES & DEPTH DETERMINED BY: PENSACOLA TESTING LABORATORIES, INC.
NOTE: Test holes are indicative of the exact locations drilled (from existing grade at date drilled), and do not necessarily represent conditions elsewhere on the project site.

| DEPTH | ELEV. | DESCRIPTION | PENETRATION -- BLOWS PER FOOT (5 10 20 30 40 50 70) |
|---|---|---|---|
| | | TEST BORING B-1 | |
| 0' | +5 | | Date Drilled: 7/19/77 |
| 2½' | | LOOSE to FIRM tan fine SAND with cobble-sized pieces of red cemented clayey sand | 3/8/9=17 |
| | | VERY FIRM to DENSE tan and light gray fine SAND ▼6'-0" | 12/12/17= |
| 9' | | | 16/20/26=46 |
| | | VERY FIRM gray fine SAND with flakes of organic fines | 11/11/10=21 |
| 13' | | | |
| | | VERY LOOSE to LOOSE dark gray organic-stained slightly silty fine SAND | 1/3/3=6 |
| 18½' | | FIRM light gray fine SAND with 2" seam of fibrous PEAT and organic SILT near 20½' | 4/8/8=16 |
| 24' | | FIRM gray slightly silty fine SAND with many shell fragments | 10/8/7=15 |
| 26½' | | VERY FIRM gray fine SAND with trace of silty fines | 11/13/ 6= |
| 33' | | SOFT to FIRM dark gray organic slightly sandy, very silty CLAY | |
| 35' | | DENSE gray fine SAND with trace of clayey fines and shell | 3/15/ |
| 38' | | VERY DENSE gray medium to fine SAND | 32/54=6" |
| 45' | | (continued) | 29/56=7" |

CAUTION: Water tables should be confirmed prior to bid and/or construction. This lab assumes no responsibility for changes from date reported.

* U/S Denotes visual Unified Soils Classification
▼Indicates water table
Reports to:
Casing None Drilling Mud 5½ bgs. Florigel
Weather Clear & Hot Inspector D. Crutchfield

By

# PENSACOLA TESTING LABORATORIES, INC.

OR YOUNGS-BY-THE-SEA REPORT NO. 4819

## TEST BORING DATA (Continued)

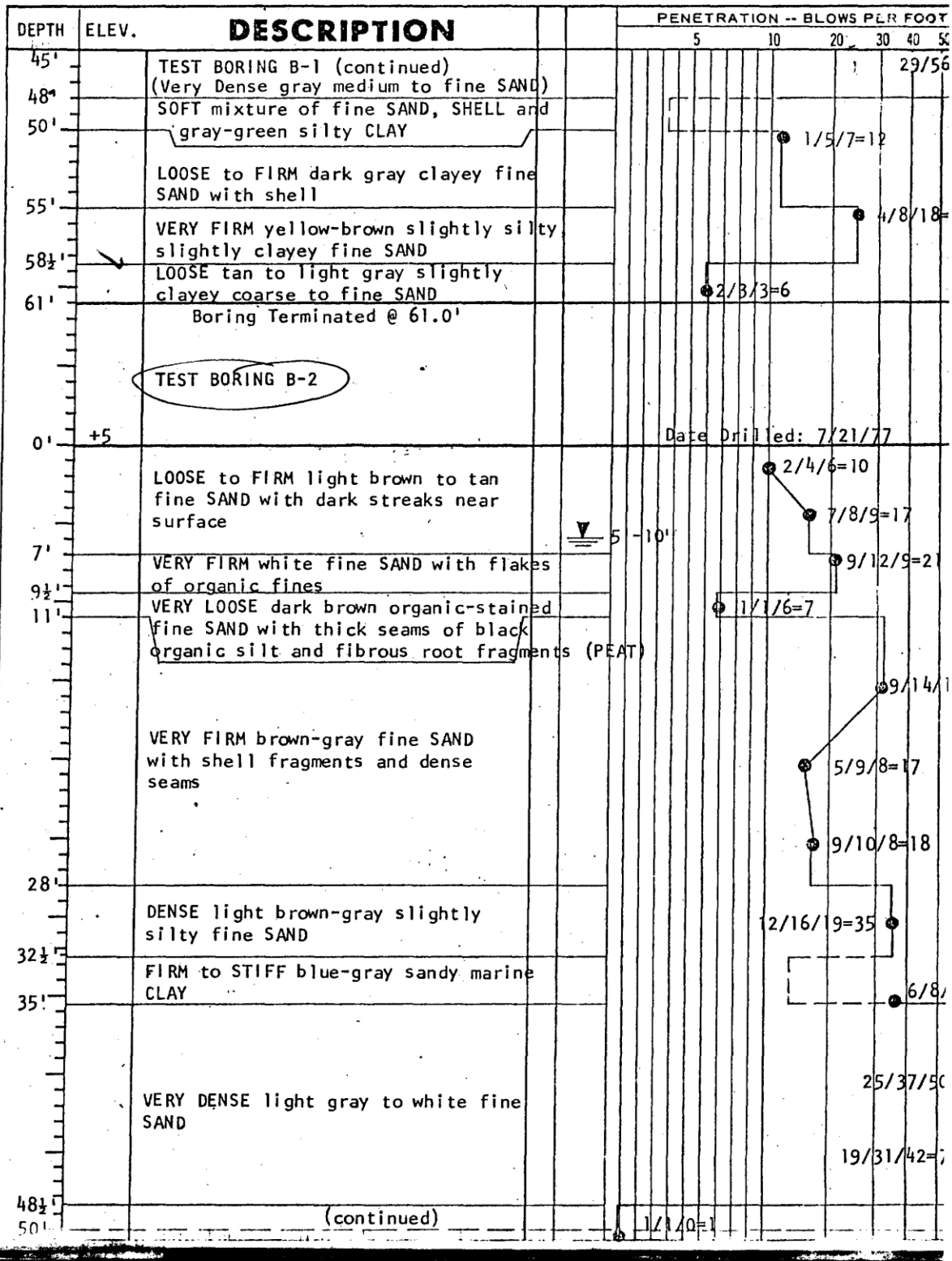

**Well B: DDD-17**

DDD-

# Geological Survey of Alabama
## WELL LOG

COMPANY ACME Drilling

AREA Gulf Shores and Orange Beach, together

WELL Gulf Coast Utilities Twp 1

COUNTY Baldwin STATE Alabama

COORDINATES: 1/4 SE Sec. 1
N
S
ELEVATION: 10 ft.
D.F.
K.B.
G.L. 10 ft.

LOCATION

WELL

| | Run No. 1 | Run No. 2 | MUD | Run No. 1 | Run No. 2 |
|---|---|---|---|---|---|
| Date | Sept. 7, 1983 | | Nature | | |
| First Reading | 227 | | Density | | |
| Last Reading | | | Viscosity | @ °F | @ |
| Footage Logged | 21y | | Resistivity | @ °F | @ |
| Bottom (Driller) | 225 | | Res. @ BHT | @ °F | @ |
| Casing (From Log) | 4 | | pH | | |
| Casing (Driller) | | | Circ. Temp. | | |
| Casing Size | 6" | | B.H. Temp. | | |
| Bit Size: | 5 7/8" | | | | |
| Bit Size: | | | | | |
| [illegible] | 8' | | Logged by | Phillip Dark | |
| | | | Witnessed by | Randall Gibson | |

REMARKS

SPONTANEOUS POTENTIAL
Millivolts

DEPTH

RESISTIVITY
Ohms m²/m

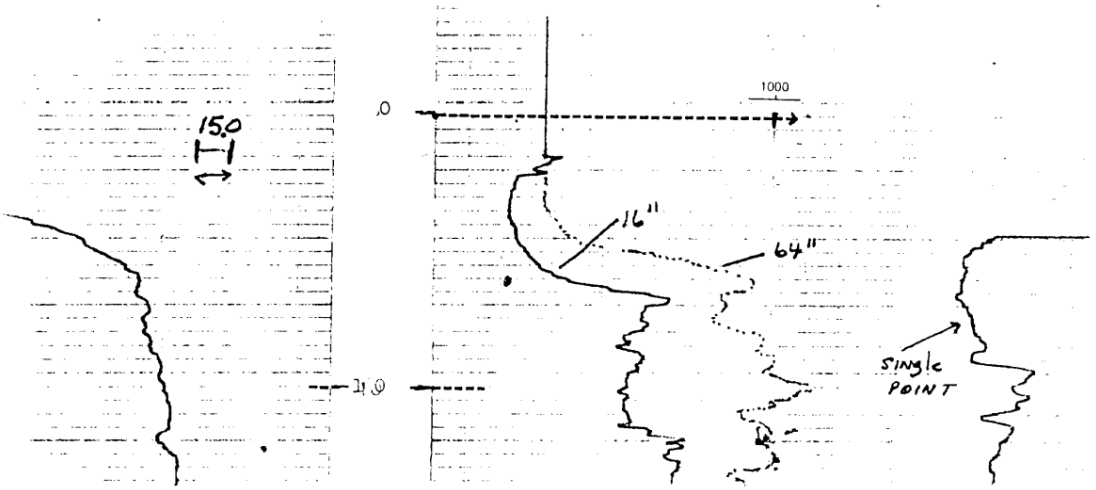

**Nearby borehole lithology: Well P-1**

TEST WELL NO. P-1

| Depth (feet) | Sample Description |
|---|---|
| 0 - 5 | Sand, quartz, clear to white and very pale-yellow, subangular to subrounded, medium- to coarse-grained, moderate to well sorted; trace of organics. |
| 5 - 10 | Clay, organic rich, dusky brown (5YR 2/2), slightly sandy. |
| 10 - 15 | Clay, same; shell fragments, oysters. |
| 15 - 20 | Clay, same with more sand; shells, coquina. |
| 20 - 25 | Sand, quartz, clear to white, subangular to subrounded, medium- to coarse-grained, moderately sorted; trace to 1% shell fragments; trace of heavy minerals; trace of clay, same. |
| 25 - 30 | Clay, same; shell fragments, oysters; sand, same, 5 to 10% of sample. |
| 30 - 35 | Sand, same; clay, same; shell fragments, abundant, some echinoid fragments. |
| 35 - 40 | Sand, same; 75% of sample; silt, quartz, clear to very pale-yellow; clay, light-brown (5YR 5/6), very soft; trace of shell fragments; trace of ironstone (ferruginous cemented sandstone). |
| 40 - 45 | Sand, quartz, clear, subangular to subrounded, medium- to very coarse-grained, moderately sorted, about 50% of sample; clay, organic rich, dusky-brown (5YR 2/2), very sandy, about 40% of sample; shell fragments, 10% of sample. |
| 45 - 50 | Clay, grayish-green (10G 4/2), dense and plastic; shell fragments, abundant; trace of sand, same. |
| 50 - 55 | Clay, same; shell fragments, same. |
| 55 - 60 | Clay, same; shell fragments, same; trace of sand. |
| 60 - 65 | Clay, same; shell fragments, same; trace of sand. |
| 65 - 70 | Clay, same; shell fragments; trace of sand, same. |

251

TEST WELL NO. P-1

| | |
|---|---|
| 70 - 75 | Clay, same; trace of shell fragments; trace of sand. |
| 75 - 80 | Clay, same, slight decrease in amount; shell fragments, abundant; sand very coarse to fine, increase in amount. |
| 80 - 85 | Clay, same; shell fragments, abundant; sand, quartz, very pale-orange (10YR 8/2), subangular to subrounded, fine-grained to silt; sand, quartz, clear, fine- to very coarse-grained, same. |
| 85 - 90 | Clay, same; shell fragments, same; sand, clear to white, fine to very coarse, same. |
| 90 - 95 | Sand, quartz, clear to white, subangular, coarse- to very coarse-grained, moderately well sorted; trace of quartz granules, white to grayish-orange-pink (5YR 7/2). |
| 95 - 100 | Sand, same; trace to 1% quartz granules, same; clay, grayish-green (5G 5/2); trace of shell fragments. |
| 100 - 105 | Granules, quartz, clear to white and dark greenish-yellow (10Y 6/6), subrounded; sand, same; clay, moderate greenish-yellow (10Y 7/4); trace of pebbles, quartz, color same as granules; trace of shell fragments. |
| 105 - 110 | Granules, same but slightly smaller; sand, same; clay, same; trace of shell fragments. |
| 110 - 115 | Sand, quartz, clear to white and moderate yellow (5Y 7/6), subrounded, medium- to very coarse-grained, poorly sorted; trace of ironstone. |
| 115 - 120 | Sand, same; silt, quartz, clear; trace of shell fragments; trace of igneous rock fragments. |
| 120 - 125 | Sand, quartz, clear to white and moderate yellow, subrounded, coarse- to very coarse-grained, moderately sorted; trace of silt. |
| 125 - 130 | Sand, same; trace of silt, same; trace of mica. |
| 130 - 135 | Sand, same; clay, light olive-gray (5Y 5/2) to olive-gray (5Y 3/2); granules, quartz, white to grayish-orange (10YR 7/4). |
| 135 - 140 | Sand, same; granules, same; trace of clay. |

TEST WELL NO. P-1

| | |
|---|---|
| 140 - 145 | Sand, same; granules, same; clay, same; more abundant. |
| 145 - 150 | Sand, same; granules, same; trace of clay, same. |
| 150 - 155 | Sand, same; trace of granules, same. |
| 155 - 160 | Sand, same; trace of granules, same. |
| 160 - 165 | Granules, same, very abundant; sand, same, approximately 25% of sample. |
| 165 - 170 | Sand, quartz, very pale-orange, subrounded to subangular, fine- to medium-grained, moderately sorted; silt, very pale-orange; clay, medium light-gray. |
| 170 - 175 | Sand, very fine- to very coarse-grained, poorly sorted, otherwise same; silt, same. |
| 175 - 180 | Sand, same; quartz granules, subrounded. |
| 180 - 185 | Quartz granules, same; clay, medium light-gray; sand, same. |
| 185 - 190 | Sand, same; clay, same; quartz granules, same. |
| 190 - 195 | Sand, quartz, very pale-orange to white and dark yellowish-orange (10YR 6/6), subrounded, very coarse-grained, moderately sorted; trace of clay, same. |
| 195 - 200 | Sand, same. |
| 200 - 205 | Sand, same. |
| 205 - 210 | Sand, quartz, clear to very pale-orange, subrounded, moderately well sorted, very fine to silt; trace of clay; mica, abundant. |
| 210 - 215 | Sand, very fine to silt, same; sand, quartz, white to very pale-orange, very coarse-grained; trace of clay, same; trace of mica. |
| 215 - 220 | Sand, very fine to silt, same; sand, quartz, very coarse- to medium-grained, poorly sorted, subrounded; trace of clay, same. |
| 220 - 225 | Sands, same; trace of clay, same. |
| 225 - 230 | Sands, same; trace of clay, same. |

TEST WELL NO. P-1

| | |
|---|---|
| 230 - 235 | Sand, very fine to silt, same; trace of very coarse to medium, same; trace of clay, same. |
| 235 - 240 | Sand, very fine to silt, same. |
| 240 - 245 | Sand, very fine to silt, same. |
| 245 - 250 | Sand, quartz, clear to white, fine- to very coarse-grained, moderately sorted, subangular; silt, quartz, very pale-orange; trace of clay, medium-gray. |
| 250 - 255 | Sand, same; silt, same; trace of clay. |
| 255 - 260 | Sand, same, with an increase in very coarse; silt, same; clay, same, more abundant. |
| 260 - 265 | Sand, same; silt, pale yellowish-orange; trace of clay, same. |
| 265 - 270 | Sand, same; silt, same; clay, grayish-olive (10Y 4/2), soft; trace of mica. |
| 270 - 275 | Sand, quartz, clear to moderate yellow, subangular to subrounded, medium- to coarse-grained, moderately sorted; silt, very pale-orange, abundant; trace of clay, grayish-green (10GY 5/2); trace of mica. |
| 275 - 280 | Sand, same but coarse- to very coarse-grained; silt, same, more abundant; clay, same, but more abundant. |
| 280 - 285 | Sand, quartz, clear to moderate-yellow, subangular to subrounded, coarse to very coarse-grained, moderately sorted; silt, same, but less abundant; trace of granules, white rock fragments; trace of clay, same. |
| 285 - 290 | Sand, quartz, clear to moderate-yellow, subangular to subrounded, medium-grained, well sorted; silt, same but more abundant; trace of mica; trace of shell fragments. |
| 290 - 295 | Sand, same with trace of very coarse-grained; silt, same. |
| 295 - 300 | Sand, quartz, clear to yellow and very dusky-red-purple (5RP 2/2), subangular to subrounded, medium- to very coarse-grained, poorly sorted; silt, same but less abundant; trace of clay, very pale-green (10G 8/2). |

TEST WELL NO. P-1

| | |
|---|---|
| 300 - 305 | Sand, quartz and chert, clear to light blue-green (5BG 6/6), subangular to subrounded, medium- to very coarse-grained; silt, same; clay, same; trace of pyrite; trace of mica. |
| 305 - 310 | Sand, quartz, clear to white, subangular to subrounded, medium- to very coarse-grained, poorly sorted; granules, quartz, white, subrounded; silt, same; trace of clay, light-green (5G 7/4). |
| 310 - 315 | Sand, quartz, clear, subangular, fine- to medium-grained with trace of coarse-grained, moderately sorted; silt, same, very abundant; clay, dark yellowish-green (10Y 6/6); trace of mica. |
| 315 - 320 | Sand, same; silt, same; clay, yellowish-gray (5Y 8/1); trace of mica. |
| 320 - 325 | Sand, quartz, clear to white, subangular, silt size to medium-grained with some very coarse, poorly sorted; silt, quartz, very light-gray, grades to very fine sand; clay, very light-gray to white, silty. |
| 325 - 330 | Sand, same with more very coarse present; silt, same; clay, same with increase in amount present. |
| 330 - 335 | Sand, quartz, clear to white, subangular to subrounded, predominantly medium-grained with some coarse- and fine-grained, moderately well sorted. |
| 335 - 340 | Sand, same; trace of white silt; trace of very light-gray clay. |
| 340 - 345 | Sand, same with an increase in amount of coarse-grained; silt, same; trace of very light-gray clay. |
| 345 - 350 | Sand, quartz, clear to white, subrounded, coarse-grained with some fine, medium, and very coarse-grained, moderately well sorted; silt, quartz, very light-gray, more abundant. |
| 350 - 355 | Sand, same; silt, same. |
| 355 - 360 | Sand, decrease in coarse-grained and increase in medium-grained, otherwise, same; silt, same with an increase in amount; clay, very light-gray, small amount. |
| 360 - 365 | Sand, same; silt, same; trace of clay, same; trace of mica. |

**Well C: T-3**

TEST WELL NO. T-3

| Depth (feet) | Sample Description |
|---|---|
| 0 - 5 | Organic material; sand, quartz, clear to light-olive-gray (5Y 6/1), subangular, medium- to coarse-grained, moderately sorted. |
| 5 - 10 | Sand, same; trace of organics. |
| 10 - 15 | Sand, same; trace of organics. |
| 15 - 20 | Sand, same; clay, white-(N 9) to bluish-white (5B 9/1), streaks or stringers mixed with sand. |
| 20 - 25 | Sand, same; clay, same, slight increase in amount, 10 percent of sample. |
| 25 - 30 | Sand, same; clay, white- to very pale-orange (10YR 8/2); 10 percent of sample. |
| 30 - 35 | Sand, fine- to medium-grained, same; clay, same. |
| 35 - 40 | Sand, quartz, clear to light-olive-gray, subangular to subrounded, medium-grained, moderately well sorted; clay, white streaks, same. |
| 40 - 45 | Sand, quartz, same, medium-grained; clay, same with increase in amount, 10 to 15 percent of sample. |
| 45 - 50 | Sand, same; clay, same; trace of glauconite; trace of mica. |
| 50 - 55 | Sand, same; clay, same; trace of glauconite. |
| 55 - 60 | Sand, same; clay, same; trace of glauconite. |
| 60 - 65 | Sand, same; clay, same; trace of glauconite. |
| 65 - 70 | Sand, coarse-grained with some medium grains, same; clay, small amount, same. |
| 70 - 75 | Sand, same; trace of white clay. |
| 75 - 80 | Sand, same; trace of clay, same. |

266

| | |
|---|---|
| 80 - 85 | Sand, same; trace of clay, same. |
| 85 - 90 | Sand, same; trace of clay, pale-yellowish-orange (10YR 8/6). |
| 90 - 95 | Sand, same; trace of clay, white; trace of siltstone, moderate olive-brown (5Y 4/4) thinly laminated, soft. |
| 95 - 100 | Sand, same; trace of white clay; trace of siltstone. |
| 100 - 105 | Sand, same; siltstone, same, increase in amount; trace of white clay. |
| 105 - 110 | Sand, quartz, clear; white- to pale-yellowish-orange, subangular to subrounded, coarse- and very coarse-grained with some medium grains, moderate to poorly sorted; pea gravel, white to pale-yellowish-orange, subangular. |
| 110 - 115 | Sand, very coarse, same; pea gravel, same. |
| 115 - 120 | Sand, very coarse with some coarse and medium grains, same; pea gravel, same; trace of clay. |
| 120 - 125 | Sand, same; pea gravel, same; clay, white, small amount. |
| 125 - 130 | Sand, same; pea gravel, same, less amount; clay, white, approximately 10 percent of sample, more abundant. |
| 130 - 135 | Sand, same; gravel, same; clay, same. |
| 135 - 140 | Sand, same; gravel, same; clay, white, 6-inch layer at 138 feet. |
| 140 - 145 | Sand, same; gravel, same; clay, white- to very pale-orange (10YR 8/2). |
| 145 - 150 | Sand, quartz, clear to light-olive-gray, subrounded, medium-grained, well sorted; clay, white- to very pale-orange, more abundant. |
| 150 - T.D. | Set 20 feet of slotted ABS at 90 to 110 feet. |

## Well D: GUL-50

Well DDD-22, Bull. 106, GSA

DDD-22

~~DDD-08~~

U.S. GEOLOGICAL SURVEY
Water Resources Division

WELL SCHEDULE

Date 4/13, 1984 Local No. GUL-50
Recorded by R.V. Chandler Site ID I-2 (well no 2)
Source of data Drillers' Record

1. Location: State Alabama County Baldwin
Map Gulf Shores, Al. quad. sheet
NW 1/4 SE 1/4 sec. 15 T 9 N/S R 4 E/W
2. Owner: Gulf State Park Address Rt 2 Box 7 Gulf Shores, Al. 36542
Tenant Address
Driller Carloss Well Co. Address Memphis, Tn.
3. Topography Coastal lowland - inland
4. Elevation 13 ft below
5. Type: Dug, drilled, bored, jetted 10/ 19 72
6. Depth: Rept. 153 ft. Meas. ft
7. Casing: Diam. 20 in., to 12 in., Type Steel
Depth 0-102 ft., to 0-120 ft.
8. Openings (screens): Diam. 10 in., Type louvered steel
Depth 120 ft., to 148 ft. 0.45" (Gravel pack)
9. Chief Aquifer Tm-As
10. Water level 26 ft. meas. 4/13 1984
above (27 ft. Meas 6/30/84) above
below air line which is 35 ft. below lsd
11. Pump: Type Turbine Capacity G.M.
Power: Kind Horsepower 75
12. Yield: Flow G.M., Pump G.M., Method
Drawdown ft. after hours pumping G.M.
13. Use: Dom., Stock, PS., RR., Ind., Irr., Obs.
Adequacy, permanence
14. Quality Temp. — °F.
Yes
Taste, odor, color Sample No
15. Remarks: (Log, Analyses, etc.) pH = 5.2 Bicarb = 1120 = 2.
SC = 180 Urban-fire color = 0 Turb = 0
Cl = 40 Air line length ~ 82'

see last page

16. Site Location Description in central part of golf course

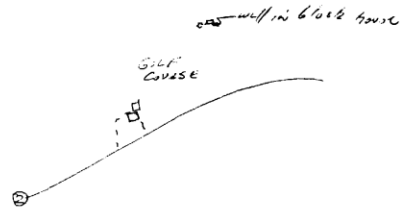

## DDD-05 Next to GUL-50

ALABAMA GEOLOGICAL SURVEY
Water Resources Division

DDD-05

WELL SCHEDULE

Date 03/11, 1987 Local No. Gul-100
Recorded by R.V. Chandler Site ID DDD-05
Source of data Driller's report

1. Location: State Alabama County Baldwin
Map Gulf Shores, A/2 quadrangle sheet
— 1/4 C. ~~1/4~~ sec. 10 T 9 N/S R 4 E/W
2. Owner: Gulf State Park Address Gulf Shores, Al.
Tenant Address
Driller Graves Well Drlg Co. Address Sylacauga, Al.
3. Topography low -- on golf green
4. Elevation 23 ft below
5. Type: Dug, drilled, bored, jetted 12/64 1985
6. Depth: Rept. ft. Meas. ft
7. Casing: Diam. in., to in., Type
Depth ft., to ft.
8. Openings (screens): Diam. in., Type
Depth ft., to ft.
9. Chief Aquifer Tmu - A3
10. Water level 16.5 ft. meas. 03/11 1987
above above
below base of pump which is 2.1 ft. below lsd
11. Pump: Type turbine Capacity G.M.
Power: Kind Horsepower 150
12. Yield: Flow G.M., Pump G.M., Method
Drawdown ft. after hours pumping G.M.
13. Use: Dom., Stock, PS., RR., Ind., Irr., Obs.
Adequacy, permanence
14. Quality Temp. °F.
Yes
Taste, odor, color Sample No
15. Remarks: (Log, Analyses, etc.)

16. Site Location Description 150' ± W-NW. of northern (old) golf-course well

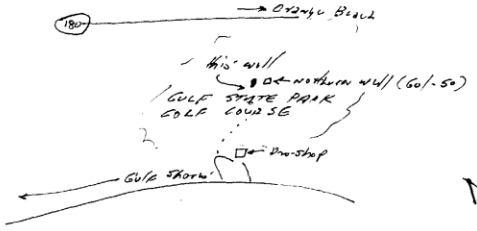


L-Bal-DDD-0005

DDD - 85

# REPORT OF DRILLED WELL

LARGE WELL DDD (5)

Graves Well Drilling Company, Inc. P.O. Drawer 168, Sylacauga,AL 35150

DRILLING CONTRACTOR | License Number | Address | Zip Code | Date

State of Alabama, Dept. of Conservation, 64 North Union St., Montgomery,AL 36130

PROPERTY OWNER | Address (mailing) | Zip Code

Gulf Shores State Park Golf Course

WELL LOCATION | County | Section | ¼ Section | Township | Range ---or:

Baldwin County,AL

Distance and direction from nearest town, community, road junction or other reference point

WELL WILL BE USED FOR: [ ] Private supply [ ] Public supply [ ] Industrial supply [X] Test well TW-1 1985 [ ] Irrigation Other:

12-2-85 Estimated starting date

Drilling method: (check) Cable tool Rotary X Jetted Bored Other:

6" Diameter of well

450' Estimated depth

Stanley H. Graves
SIGNATURE of Drilling Contractor

Total Depth 620'

Completion Date December 4, 1985

| Interval | Description of cuttings | Interval | Description of cuttings |
|---|---|---|---|
| 0-20' | medium white sand & streak gray clay | | |
| 20-40' | medium white sand | | |
| 40-100' | medium white sand and streak gray clay | | |
| 100-135' | white sandy clay | | |
| 135-178' | coarse white sand | | |
| 178-212' | coarse yellow sand | | |
| 212-220' | coarse yellow sand and streak gray clay | | |
| 220-274' | medium to coarse white sand and streak gray clay | | |
| 274-280' | gray clay | | |
| 280-320' | gray clay and streak white sand | | |
| 320-360' | medium to coarse white sand and streak gray clay | | |
| 360-380' | gray clay and streak white sand | | |
| 380-398' | fine to medium white sand and streak gray clay | | |
| 398-428' | gray sandy clay | | |
| 428-449' | coarse white sand and shells | | |
| 449-468' | gray clay and streak medium sand | | |
| 468-469' | white rock | | |
| 469-492' | fine white sand and shells | | |
| 492-492.5' | white rock | | |
| 492.5-520' | fine white sand and shells | | |
| 520-560' | gray clay and shells | | |
| 560-600' | fine white sand and streak gray clay | | |
| 600-620' | gray clay | | |
| | Total Depth: 620' | | |
| | Yield: Air Test 250-300 GPM | | |

Completion date: report depths below ground level

**Pump**

Type: [ ] Turb. [ ] Subm. [ ] Jet [ ] Cyl:; Other:

Intake depth ____ H.P. ____ Yield ____ gpm

**Capacity**

Tested by: [ ] pumping [ ] air lift [ ] bailer [ ] none

Measured Static Water Level ____ ft.

Measured pumping level ____ ft. after ____ hrs. pumping ____ gpm

Development time prior to testing ____ hrs.

**Finish**

[ ] Open hole [ ] Screened [ ] Slotted pipe [ ] Gravel pk.

Interval(s) screened: ____ to ____ ft; ____ to ____ ; ____ to ____ ft.

Packer(s) set at ____ and ____ ft.

Screen: diam. ____ ; Size openings ____

**Casing**

| Interval cased | Diam. (Inches) | *Type pipe | *Type couplings | Interval grouted |
|---|---|---|---|---|
| | | | | |
| | | | | |
| | | | | |
| | | | | |

*Couplings: Threaded & Coupled (T&C) Welded (W) Threaded & coupled & welded (TC&W)

Other:

*Pipe: Black; PVC; Galv.; Other:

**Quality**

Water analysis obtained? (check) [ ] No [ ] Bacteriological [ ] Chemical

Analysis by: [ ] Ala Geol. Surv. [ ] U.S. Geol. Surv. [ ] Ala Health Dept. [ ] Private lab.

Signed:

*For deeper well please attach continuation sheet.

Well reportedly Yields 700-1000 gpm

ADEM Form 60 1/83

DDD-85

**Deep Resistivity Logs:**
**Well DDD-17**

DDD-

# Geological Survey of Alabama
## WELL LOG

LOCATION ... WELL ...

COMPANY ACME Drilling

AREA Gulf Shores and Orange Beach, together

WELL Gulf Coast Utilities Twp 1

COUNTY Baldwin STATE Alabama

COORDINATES: 1/4 SE Sec. 3
N
S
ELEVATION: 10 ft.
D.F.
K.B.
G.L. 10 ft.

| | Run No. 1 | Run No. 2 | MUD | Run No. 1 | Run No. |
|---|---|---|---|---|---|
| Date | Oct. 7, 1955 | | Nature | | |
| First Reading | R-log | | Density | | |
| Last Reading | 227 | | Viscosity | @ °F | @ |
| Footage Logged | | | Resistivity | @ °F | @ |
| Bottom (Driller) | 224 | | Res. @ BHT | @ °F | @ |
| Casing (From Log) | 225 | | pH | | |
| Casing (Driller) | 4 | | Circ. Temp. | | |
| Casing Size | | | B.H. Temp. | | |
| Bit Size: | 6" | | | | |
| Bit Size: | 5 7/8" | | | | |
| | | | | | |
| | 8' | | Logged by | Phillip Dark | PD |
| | | | Witnessed by | Rundall Gibson | |

REMARKS

SPONTANEOUS POTENTIAL
Millivolts

DEPTH

RESISTIVITY
Ohms m²/m

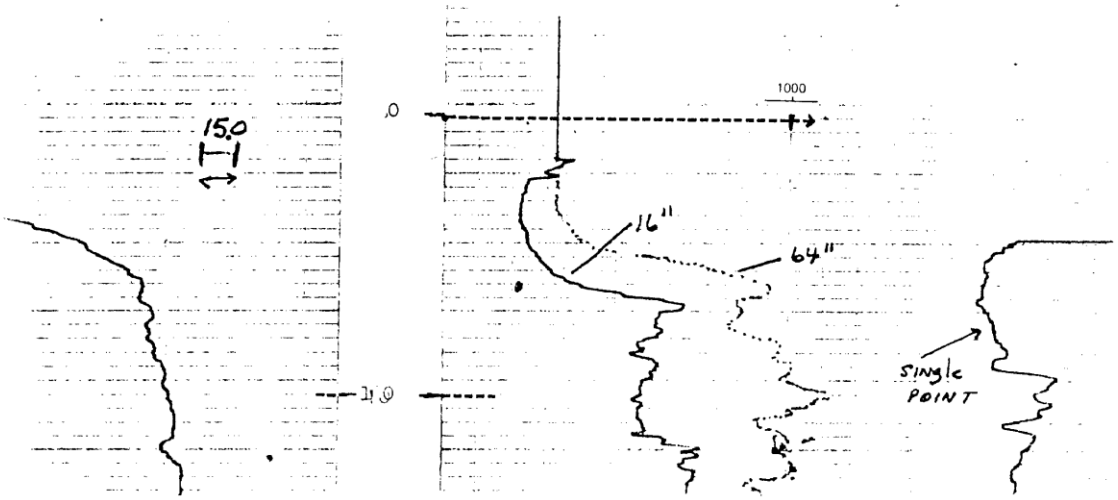

**Well T-3**

ELECTRIC LOG

DATE: 23 May 1977

State:_____ County:_____ Town:_____

LOGGING INFORMATION

_____

ddress:_____

:_____ No._____

_____

, cable head to measuring point:_____ft_____in

:_____

:ed:_____ft/min up down

:cale:_____ft/in

MODULE SETTINGS

SINGLE POINT RESISTANCE

:h (range):__50__ohms

)t. (base, zero, or suppression):_____Dial div.

/ Pot. (Span):_____Dial div.

le:__50__ohms } chart div (or) full scale (circle as applicable)

RESISTIVITY

inch normal

(other resistivity)

:h:_____ohm-meters

)t.:_____dial div.

/ Pot.:_____dial div.

le:_____ohm-m } chart div (or) full scale (circle as applicable)

_____inch normal

Scale switch:_____ohm-meters

Position Pot.:_____dial div.

Sensitivity Pot.:_____dial div.

Actual scale:_____ohm-m } chart div (or) full scale (circle as applicable)

SPONTANEOUS POTENTIAL

U.S. GEOLOGICAL SURVEY, WATER RESOURCES DIVISION

District or Project:_____

FILE LOCATION NO.:_____

WELL INFORMATION

Well No. (USGS): T-3

Other:_____

Map or Quad_____

Site description_____

_____

Agency or Owner:_____

Address:_____

Altitude of L.S._____

Log M.P._____

Btm log interval:_____ft

Top log interval:_____ft

Well TD:_____

Type of finish:_____

Casing: Elev. of top_____ft/in Above Below L.

I.D._____, from_____to_____, type

I.D._____, from_____to_____, type

I.D._____, from_____to_____, type

Cement: from_____to_____

Perf. interval(s) from_____to_____, type

Open hole diameter:_____from_____to_____

_____from_____to_____

Fluid level:_____ft/in Above At Below L.S., Top Csg

Fluid type:_____; temp_____

Fluid resist.:_____ohm-m

Driller:

[redacted]

ch: millivolts
ot.: dial div.
y Pot.: dial div.
le: Mv chart div (or)
full scale (circle as applicable)

RECORDER SETTINGS

| | Ch 1 | Ch 2 | Ch 3 |
|---|---|---|---|
| ot.: | | | |
| y Pot.: | | | |

of

Type of rig:
Date started: completed
Aquifer or formation:

NOTE: This log is not to be used to fulfill priva contractual obligations.

Other data and logs available for this well:

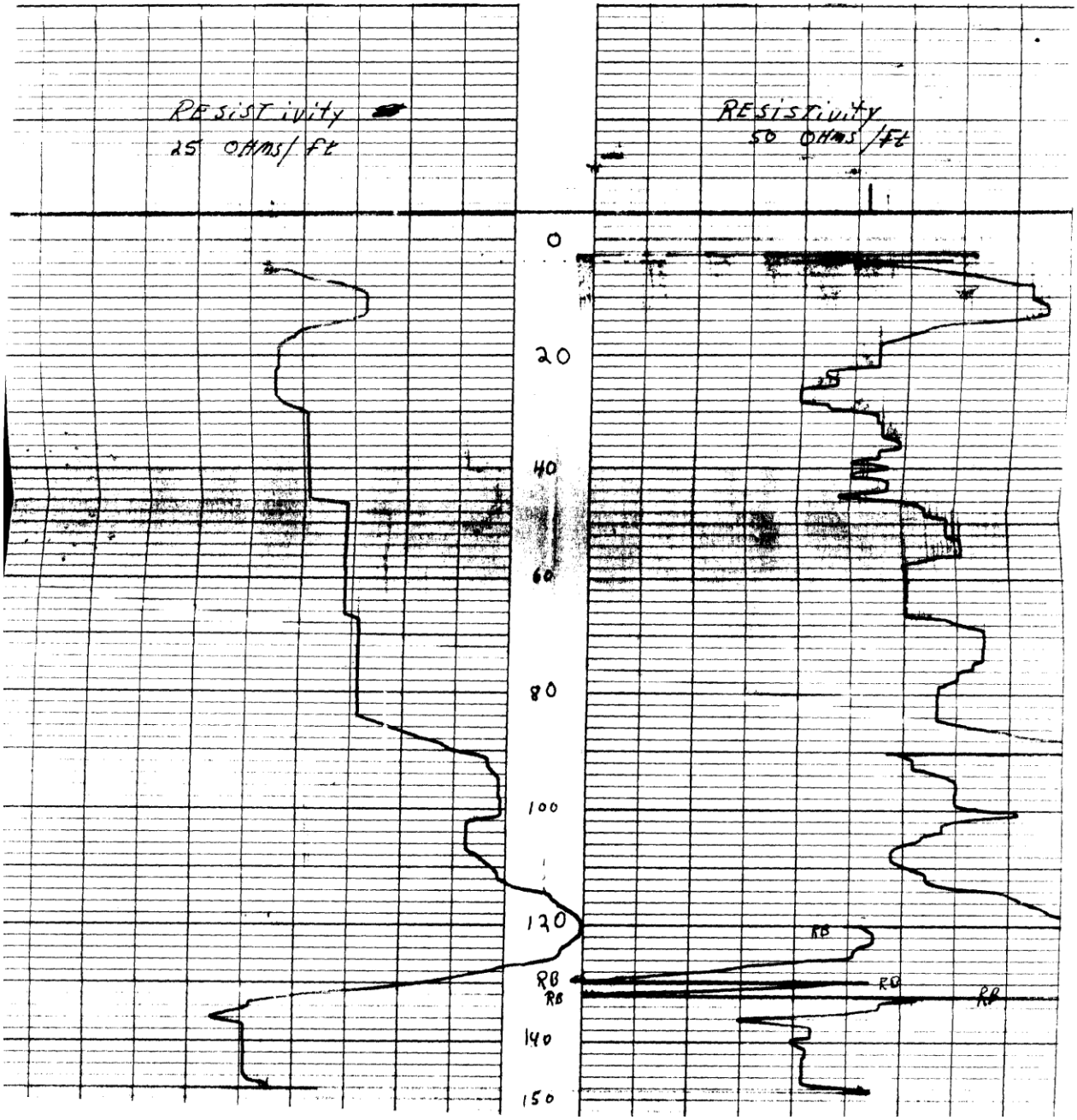

**Well P1:**

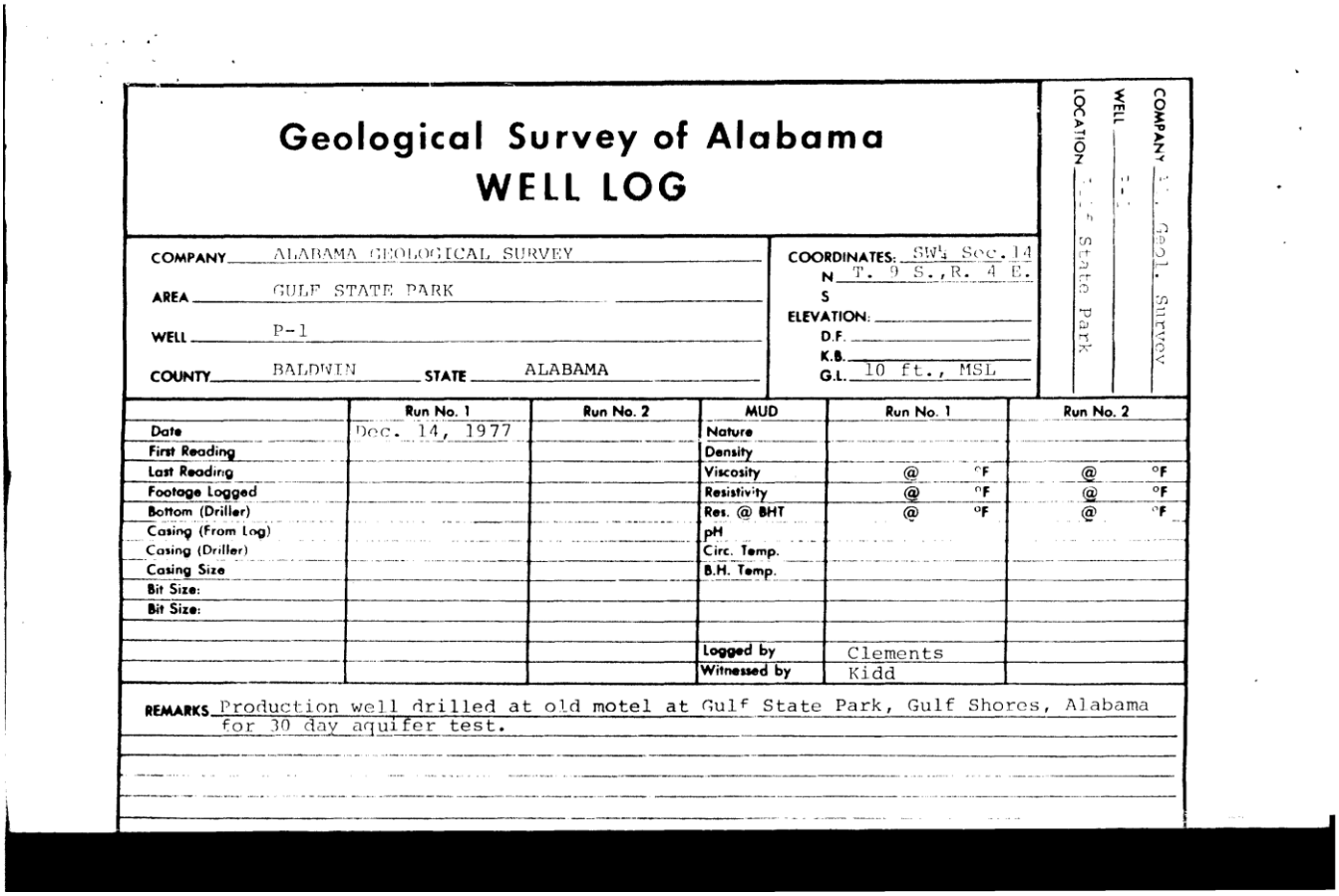

# Geological Survey of Alabama
# WELL LOG

COMPANY ALABAMA GEOLOGICAL SURVEY
AREA GULF STATE PARK
WELL P-1
COUNTY BALDWIN STATE ALABAMA

COORDINATES: SW¼ Sec. 14
N T. 9 S., R. 4 E.
S
ELEVATION:
D.F.
K.B.
G.L. 10 ft., MSL

COMPANY Ala. Geol. Survey
WELL P-1
LOCATION Gulf State Park

| | Run No. 1 | Run No. 2 | MUD | Run No. 1 | Run No. 2 |
|---|---|---|---|---|---|
| Date | Dec. 14, 1977 | | Nature | | |
| First Reading | | | Density | | |
| Last Reading | | | Viscosity | @ °F | @ °F |
| Footage Logged | | | Resistivity | @ °F | @ °F |
| Bottom (Driller) | | | Res. @ BHT | @ °F | @ °F |
| Casing (From Log) | | | pH | | |
| Casing (Driller) | | | Circ. Temp. | | |
| Casing Size | | | B.H. Temp. | | |
| Bit Size: | | | | | |
| Bit Size: | | | | | |
| | | | Logged by | Clements | |
| | | | Witnessed by | Kidd | |

REMARKS Production well drilled at old motel at Gulf State Park, Gulf Shores, Alabama for 30 day aquifer test.

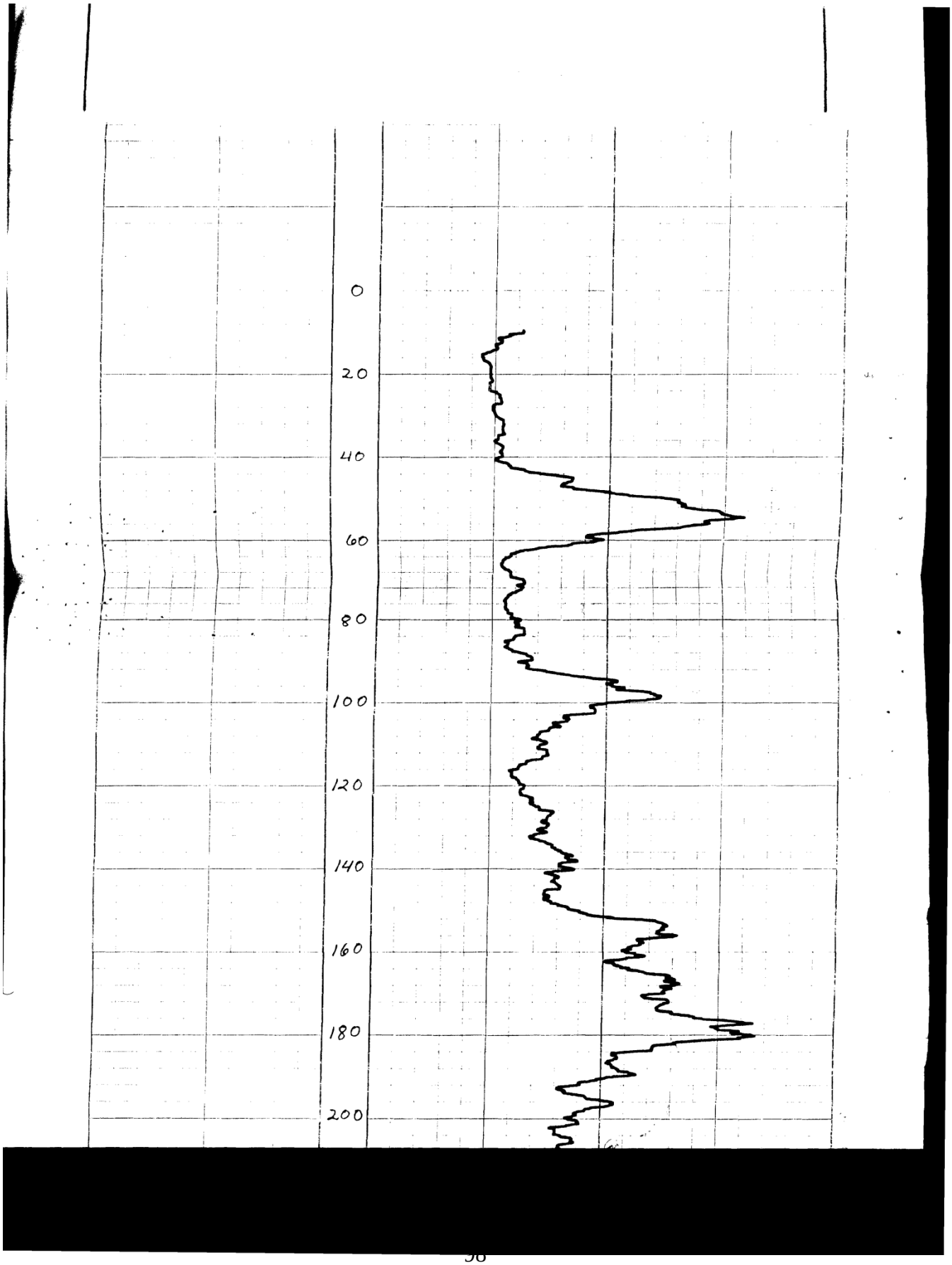
0
20
40
60
80
100
120
140
160
180
200

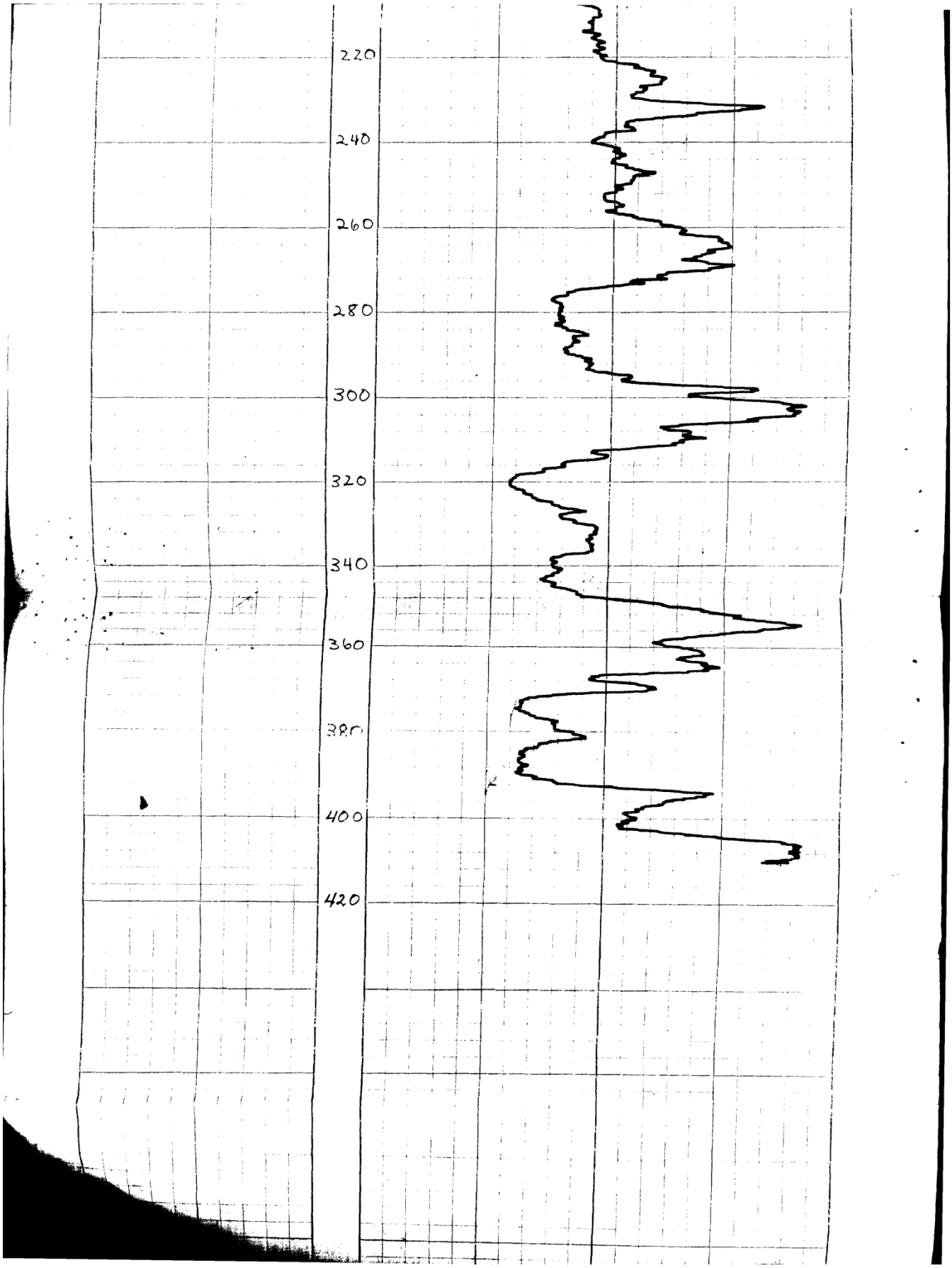
220
240
260
280
300
320
340
360
380
400
420

**Well T-8:**

ELECTRIC LOG

U.S. GEOLOGICAL SURVEY, WATER RESOURCES DIVISION

...ity - SP DATE: 23 June 1977

District or Project: _____

...e: _____ County: _____ Town: _____

FILE LOCATION NO.: _____

DDD-09

LOGGING INFORMATION

...lements

...ss: _____

_____ No. _____

...ble head to measuring point: _____ ft _____ in

_____ ft/min up down

: _____ ft/in

MODULE SETTINGS

SINGLE POINT RESISTANCE

...nge): 50 ohms

...ase, zero, or suppression): _____ Dial div.

(Span): _____ Dial div.

_____ ohms } chart div (or) full scale (circle as applicable)

RESISTIVITY

...ormal resistivity) _____ inch normal

___ ohm-meters

___ dial div.

: _____ dial div.

_____ ohm-m } chart div (or) full scale (circle as applicable)

Scale switch: _____ ohm-meters

Position Pot.: _____ dial div.

Sensitivity Pot.: _____ dial div.

Actual scale: _____ ohm-m } chart div (or) full scale (circle as applicable)

SPONTANEOUS POTENTIAL

WELL INFORMATION

Well No. (USGS): T-8

Other: _____

Map or Quad _____

Site description _____

Agency or Owner: _____

Address: _____

Altitude of L.S. _____

Log M.P. _____

Btm log interval: _____ ft

Top log interval: _____ ft

Well TD: _____

Type of finish: _____

Casing: Elev. of top _____ ft/in Abov... Belo...

I.D. _____, from _____ to _____,

I.D. _____, from _____ to _____,

I.D. _____, from _____ to _____,

Cement: from _____ to _____

Perf. interval(s) from _____ to _____,

Open hole diameter: _____ from _____ to _____

_____ from _____ to _____

Fluid level: _____ ft/in Above At Below L.S., To...

Fluid type: _____; temp...

Fluid resist.: _____ ohm-m

Driller: _____

Address: _____

RECORDER SETTINGS

| Ch 1 | Ch 2 | Ch 3 |
|---|---|---|
| | | |

NOTE: This log is not ... contractual obligations.

Other data and logs available for this well:

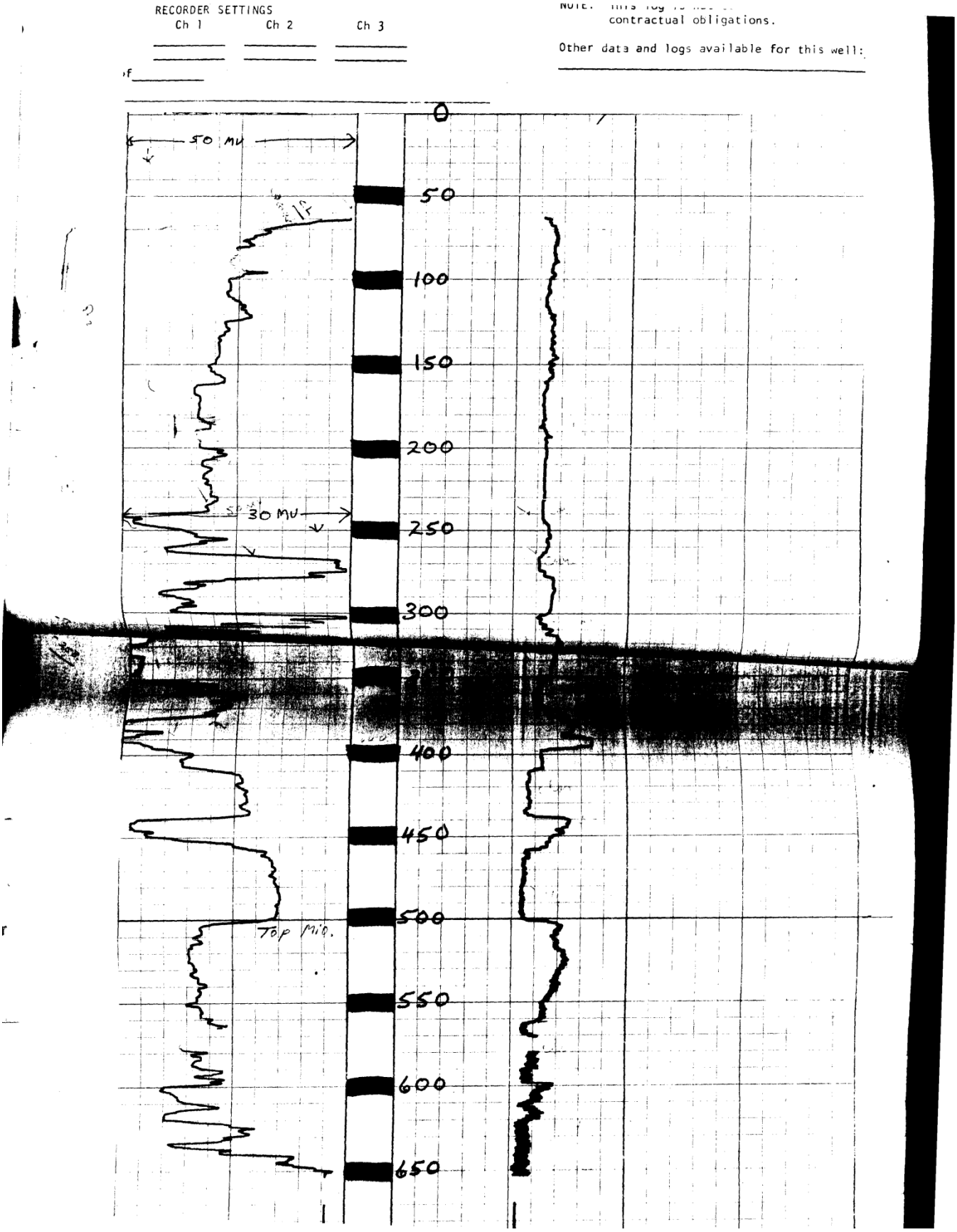

APPENDIX C: PEST OPTIMISATION RESULTS

| Parameter | Estimated value |
|---|---|
| ghb_1 | 441.93131 |
| ghb_10 | 12.614347 |
| ghb_100 | 12.314308 |
| ghb_101 | 12.968946 |
| ghb_102 | 10 |
| ghb_11 | 407.58954 |
| ghb_12 | 342.57874 |
| ghb_13 | 196.82477 |
| ghb_14 | 97.621045 |
| ghb_15 | 8.9287762 |
| ghb_16 | 156.61286 |
| ghb_17 | 252.5887 |
| ghb_18 | 83.541517 |
| ghb_19 | 303.7129 |
| ghb_2 | 790.98448 |
| ghb_20 | 117.82514 |
| ghb_21 | 72.656212 |
| ghb_22 | 705.04041 |
| ghb_23 | 1.12E-03 |
| ghb_24 | 655.56799 |
| ghb_25 | 475.2734 |
| ghb_26 | 608.62994 |
| ghb_27 | 676.1199 |
| ghb_28 | 512.06274 |
| ghb_29 | 455.55687 |
| ghb_3 | 959.96358 |
| ghb_30 | 431.8179 |
| ghb_31 | 773.05508 |
| ghb_32 | 613.88382 |
| ghb_33 | 2892.952 |
| ghb_34 | 50000 |
| ghb_35 | 3168.5986 |
| ghb_36 | 2341.4996 |
| ghb_37 | 1530.2654 |
| ghb_38 | 1473.6354 |
| ghb_39 | 648.63413 |
| ghb_4 | 371.22664 |
| ghb_40 | 1001.0886 |
| ghb_41 | 369.26594 |
| ghb_42 | 409.91361 |
| ghb_43 | 524.20942 |

| | |
|---|---|
| ghb_44 | 730.24537 |
| ghb_45 | 596.02637 |
| ghb_46 | 278.89168 |
| ghb_47 | 194.22887 |
| ghb_48 | 171.1716 |
| ghb_49 | 265.30284 |
| ghb_5 | 8.872647 |
| ghb_50 | 62.993065 |
| ghb_51 | 500 |
| ghb_53 | 13.875694 |
| ghb_54 | 16.365861 |
| ghb_55 | 32.62784 |
| ghb_56 | 14.742959 |
| ghb_57 | 41.629067 |
| ghb_58 | 51.164911 |
| ghb_59 | 8.914682 |
| ghb_6 | 228.01663 |
| ghb_60 | 17.758575 |
| ghb_61 | 8.0735334 |
| ghb_62 | 2.2576366 |
| ghb_63 | 3.0623813 |
| ghb_64 | 9.709913 |
| ghb_65 | 24.267146 |
| ghb_66 | 17.943991 |
| ghb_67 | 40.249577 |
| ghb_68 | 10 |
| ghb_69 | 224.47141 |
| ghb_7 | 0.10239064 |
| ghb_70 | 381.32909 |
| ghb_71 | 172.03987 |
| ghb_72 | 69.213972 |
| ghb_73 | 218.48964 |
| ghb_74 | 39.172586 |
| ghb_75 | 0.10054368 |
| ghb_76 | 0.10031118 |
| ghb_77 | 2.08E-03 |
| ghb_78 | 0.10151253 |
| ghb_79 | 0.10017474 |
| ghb_8 | 12.892553 |
| ghb_80 | 0.10017959 |
| ghb_81 | 0.10078728 |
| ghb_82 | 0.10068801 |
| ghb_83 | 0.10053862 |

| | |
|---|---|
| ghb_84 | 3.00E-03 |
| ghb_85 | 20.74345 |
| ghb_87 | 10.817351 |
| ghb_88 | 12.069243 |
| ghb_89 | 13.252351 |
| ghb_9 | 13.239947 |
| ghb_90 | 11.731347 |
| ghb_91 | 13.610794 |
| ghb_92 | 13.714432 |
| ghb_93 | 9.8967494 |
| ghb_94 | 11.017843 |
| ghb_95 | 7.9051159 |
| ghb_96 | 4.7810046 |
| ghb_97 | 6.1831021 |
| ghb_98 | 10.56619 |
| ghb_99 | 13.027445 |
| hk_10 | 112.88023 |
| hk_12 | 32.919957 |
| hk_2 | 87.272242 |
| hk_3 | 1.36E-02 |
| hk_4 | 200 |
| hk_5 | 30 |
| hk_6 | 200 |
| hk_7 | 48.424287 |
| hk_8 | 30 |
| hk_9 | 200 |
| rch_1 | 2.01E-03 |
| rch_10 | 1.73E-02 |
| rch_101 | 6.44E-03 |
| rch_102 | 6.09E-03 |
| rch_103 | 5.46E-03 |
| rch_104 | 1.23E-03 |
| rch_105 | 3.59E-04 |
| rch_106 | 3.59E-04 |
| rch_108 | 3.59E-04 |
| rch_11 | 1.43E-02 |
| rch_110 | 3.59E-04 |
| rch_111 | 3.59E-04 |
| rch_112 | 3.59E-04 |
| rch_113 | 3.12E-03 |
| rch_115 | 7.04E-04 |
| rch_117 | 3.59E-04 |
| rch_119 | 3.59E-04 |

| | |
|---|---|
| rch_12 | 2.45E-03 |
| rch_120 | 7.11E-03 |
| rch_121 | 3.48E-03 |
| rch_122 | 3.59E-03 |
| rch_13 | 4.13E-03 |
| rch_14 | 5.49E-04 |
| rch_15 | 3.59E-04 |
| rch_16 | 3.59E-04 |
| rch_17 | 1.00E-03 |
| rch_2 | 3.76E-03 |
| rch_20 | 3.59E-02 |
| rch_21 | 3.15E-02 |
| rch_22 | 2.87E-02 |
| rch_23 | 3.59E-02 |
| rch_24 | 2.65E-02 |
| rch_25 | 6.95E-03 |
| rch_26 | 3.59E-04 |
| rch_27 | 3.59E-04 |
| rch_28 | 1.10E-03 |
| rch_29 | 3.59E-04 |
| rch_3 | 3.08E-03 |
| rch_30 | 7.32E-03 |
| rch_31 | 2.01E-02 |
| rch_32 | 1.39E-02 |
| rch_33 | 1.77E-02 |
| rch_34 | 1.53E-02 |
| rch_35 | 2.09E-02 |
| rch_36 | 1.97E-03 |
| rch_4 | 3.06E-04 |
| rch_5 | 7.66E-03 |
| rch_6 | 1.93E-03 |
| rch_60 | 3.19E-02 |
| rch_61 | 3.13E-02 |
| rch_62 | 2.73E-02 |
| rch_63 | 2.53E-02 |
| rch_64 | 3.59E-02 |
| rch_65 | 2.21E-02 |
| rch_66 | 1.19E-02 |
| rch_67 | 5.57E-03 |
| rch_68 | 5.54E-03 |
| rch_69 | 6.31E-03 |
| rch_7 | 4.83E-03 |
| rch_70 | 4.63E-03 |

| | |
|---|---|
| rch_71 | 1.19E-03 |
| rch_72 | 1.10E-03 |
| rch_73 | 3.59E-04 |
| rch_74 | 3.59E-04 |
| rch_75 | 8.72E-03 |
| rch_76 | 3.62E-03 |
| rch_8 | 1.96E-02 |
| rch_80 | 5.59E-04 |
| rch_81 | 3.93E-04 |
| rch_82 | 9.02E-04 |
| rch_83 | 4.79E-03 |
| rch_84 | 4.93E-03 |
| rch_85 | 5.20E-03 |
| rch_86 | 6.77E-03 |
| rch_87 | 3.31E-03 |
| rch_88 | 4.79E-03 |
| rch_89 | 3.59E-03 |
| rch_9 | 1.75E-02 |
| rch_90 | 1.43E-03 |
| rch_91 | 3.55E-03 |
| rch_92 | 6.82E-03 |
| rch_93 | 5.60E-03 |
| rch_94 | 3.59E-04 |
| rch_95 | 1.39E-03 |
| rch_96 | 3.58E-03 |
| vk_11 | 2 |
| vk_12 | 200 |
| vk_123 | 124.11758 |
| vk_13 | 5.00E-02 |
| vk_14 | 200 |
| vk_15 | 6.25E-05 |
| vk_16 | 16.284173 |
| vk_17 | 1.75E-02 |
| vk_18 | 13.875194 |
| vk_19 | 2.67E-04 |
| vk_20 | 5.0514518 |
| vk_21 | 5.66E-03 |
| vk_22 | 200 |
| vk_23 | 175.27364 |
| vk_24 | 200 |
| vk_25 | 200 |
| vk_26 | 0.5 |
| vk_27 | 21.582171 |

| | |
|---|---|
| vk_28 | 191.27967 |
| vk_30 | 200 |

See file pestctl.sen for parameter sensitivities.

| Observation | Group | Measured | Modelled | Sensitivity |
|---|---|---|---|---|
| 1 | pm_default | 16.49022 | 16.51249 | 6.0019182E-02 |
| 2 | pm_default | 8.431901 | 8.426296 | 0.1345710 |
| 3 | pm_default | 4.296648 | 4.248219 | 0.1705080 |
| 4 | pm_default | 2.421609 | 2.423729 | 0.1191061 |
| 5 | pm_default | 7.340812 | 7.340909 | 5.3528793E-02 |
| 6 | pm_default | 5.850513 | 5.850950 | 6.3417701E-02 |
| 7 | pm_default | 16.09022 | 16.08946 | 5.1585710E-02 |
| 8 | pm_default | 7.819401 | 7.817667 | 0.1192891 |
| 9 | pm_default | 3.009148 | 3.008290 | 0.1447063 |
| 10 | pm_default | 1.771609 | 1.771591 | 0.1038799 |
| 11 | pm_default | 5.303312 | 5.303258 | 6.0659669E-02 |
| 12 | pm_default | 5.488012 | 5.488827 | 6.3639974E-02 |
| 13 | pm_default | 15.69022 | 15.69053 | 4.6415518E-02 |
| 14 | pm_default | 7.206901 | 7.204285 | 0.1191081 |
| 15 | pm_default | 1.721648 | 1.724014 | 0.1380381 |
| 16 | pm_default | 1.121609 | 1.121707 | 0.1062652 |
| 17 | pm_default | 3.265812 | 3.265740 | 6.2337935E-02 |
| 18 | pm_default | 5.125513 | 5.126021 | 6.3600911E-02 |
| 19 | pm_default | 15.29022 | 15.29995 | 3.9076259E-02 |
| 20 | pm_default | 6.594401 | 6.603068 | 0.1158120 |
| 21 | pm_default | 0.4341480 | 0.3642084 | 0.1643221 |
| 22 | pm_default | 0.4716087 | 0.4742114 | 0.1117662 |
| 23 | pm_default | 1.228312 | 1.228196 | 6.2395745E-02 |
| 24 | pm_default | 4.763012 | 4.763594 | 6.3487880E-02 |
| 25 | pm_default | 15.00000 | 14.99678 | 3.2956125E-02 |
| 26 | pm_default | 6.175152 | 6.175678 | 0.1147696 |
| 27 | pm_default | -0.3627759 | -0.3612195 | 0.1211296 |
| 28 | pm_default | 0.1486255 | 0.1523104 | 0.1412513 |
| 29 | pm_default | -0.5701165 | -0.5701342 | 9.4360972E-02 |
| 30 | pm_default | 4.408538 | 4.408616 | 6.3526065E-02 |
| 31 | pm_default | 15.00000 | 14.97421 | 2.5069654E-02 |
| 32 | pm_default | 6.266798 | 6.230834 | 5.8505771E-02 |
| 33 | pm_default | 0.1372241 | -0.2910717 | 5.2756859E-02 |
| 34 | pm_default | 0.6901686 | 0.6815465 | 7.9589823E-02 |
| 35 | pm_default | -1.736517 | -1.736730 | 8.0096578E-02 |
| 36 | pm_default | 4.075281 | 4.075020 | 6.3611327E-02 |
| 37 | pm_default | 15.00000 | 14.88227 | 2.9953759E-02 |
| 38 | pm_default | 6.358444 | 6.145974 | 5.1778989E-02 |
| 39 | pm_default | 0.6372241 | 2.495267 | 1.9807554E-02 |
| 40 | pm_default | 1.231712 | 1.161763 | 4.2995886E-02 |
| 41 | pm_default | -2.902918 | -2.903137 | 8.0508197E-02 |

| | | | | |
|---|---|---|---|---|
| 42 | pm_default | 3.742023 | 3.740555 | 6.3699869E-02 |
| 43 | pm_default | 15.00000 | 14.91037 | 2.4224348E-02 |
| 44 | pm_default | 6.450089 | 6.327650 | 0.1107750 |
| 45 | pm_default | 1.137224 | 2.383284 | 1.8783458E-02 |
| 46 | pm_default | 1.773255 | 1.727822 | 2.3520259E-02 |
| 47 | pm_default | -4.069318 | -4.069794 | 8.0598345E-02 |
| 48 | pm_default | 3.591234 | 3.590561 | 6.3712845E-02 |
| 49 | pm_default | 15.00000 | 14.96835 | 2.5014348E-02 |
| 50 | pm_default | 6.541735 | 6.502151 | 0.1007524 |
| 51 | pm_default | 1.122892 | 0.5145683 | 2.9482402E-02 |
| 52 | pm_default | 2.314798 | 2.308838 | 1.7103628E-02 |
| 53 | pm_default | -5.235719 | -5.236037 | 9.1873791E-02 |
| 54 | pm_default | 3.924491 | 3.923737 | 6.3836315E-02 |
| 55 | pm_default | 15.00000 | 14.85763 | 2.2452774E-02 |
| 56 | pm_default | 6.633380 | 6.389386 | 8.8623233E-02 |
| 57 | pm_default | -0.2511676 | 2.566380 | 1.4958517E-02 |
| 58 | pm_default | 2.856341 | 2.765512 | 1.8596125E-02 |
| 59 | pm_default | -6.402119 | -6.403071 | 0.1013493 |
| 60 | pm_default | 4.257748 | 4.256067 | 6.3917047E-02 |
| 61 | pm_default | 15.09101 | 15.08953 | 2.0134511E-02 |
| 62 | pm_default | 6.671448 | 6.670786 | 8.9538456E-02 |
| 63 | pm_default | -1.128653 | -1.130333 | 5.4691552E-02 |
| 64 | pm_default | 2.981533 | 2.981108 | 1.6636068E-02 |
| 65 | pm_default | -6.976375 | -6.977116 | 0.1079309 |
| 66 | pm_default | 4.295050 | 4.295207 | 6.3770740E-02 |
| 67 | pm_default | 15.42426 | 15.42379 | 2.3568296E-02 |
| 68 | pm_default | 6.566891 | 6.564315 | 7.2248126E-02 |
| 69 | pm_default | -0.6842891 | -0.6858571 | 8.5774464E-02 |
| 70 | pm_default | 1.998424 | 1.991529 | 1.3982511E-02 |
| 71 | pm_default | -5.974377 | -5.974092 | 0.1019246 |
| 72 | pm_default | 3.544537 | 3.544651 | 6.3674548E-02 |
| 73 | pm_default | 15.75752 | 15.75772 | 3.1767541E-02 |
| 74 | pm_default | 6.462335 | 6.465666 | 6.7251827E-02 |
| 75 | pm_default | -0.2399248 | -0.2427898 | 6.7340168E-02 |
| 76 | pm_default | 1.015315 | 0.7905028 | 1.9036845E-02 |
| 77 | pm_default | -4.972380 | -4.973040 | 9.4908632E-02 |
| 78 | pm_default | 3.036692 | 3.036507 | 6.3666528E-02 |
| 79 | pm_default | 16.00000 | 15.98207 | 3.2709265E-02 |
| 80 | pm_default | 6.357779 | 6.091078 | 7.3533707E-02 |
| 81 | pm_default | 0.2044394 | 0.3068777 | 7.4735282E-02 |
| 82 | pm_default | 0.3000000 | 0.9791253 | 1.4346981E-02 |
| 83 | pm_default | -3.970382 | -3.970935 | 8.8141912E-02 |
| 84 | pm_default | 3.170385 | 3.169908 | 6.4045692E-02 |
| 85 | pm_default | 16.00000 | 16.06674 | 3.3275602E-02 |
| 86 | pm_default | 6.253222 | 6.955706 | 5.7953640E-02 |
| 87 | pm_default | 0.6488037 | -0.1463500 | 6.7073145E-02 |
| 88 | pm_default | 0.3000000 | 1.918166 | 1.5777826E-02 |

| | | | | |
|---|---|---|---|---|
| 89 | pm_default | -2.968384 | -2.968883 | 7.8423707E-02 |
| 90 | pm_default | 3.304078 | 3.303802 | 6.3889805E-02 |
| 91 | pm_default | 16.00000 | 16.00019 | 3.1710795E-02 |
| 92 | pm_default | 6.148666 | 6.147924 | 8.7531076E-02 |
| 93 | pm_default | 1.093168 | 1.092913 | 8.9158807E-02 |
| 94 | pm_default | 0.3000000 | 0.3000344 | 4.0275944E-02 |
| 95 | pm_default | -1.966386 | -1.966856 | 7.4107220E-02 |
| 96 | pm_default | 3.437772 | 3.437722 | 6.5716955E-02 |

See file pestctl.res for more details of residuals in graph-ready format.
See file pestctl.seo for composite observation sensitivities.

OPTIMISATION RESULTS

Covariance matrix and parameter confidence intervals cannot be determined:-
Number of parameters exceeds non-zero-weighted observations plus prior information.

Objective function ----->

Sum of squared weighted residuals (ie phi) = 35.62

Correlation Coefficient ----->

Correlation coefficient = 0.9949

Analysis of residuals ----->

All residuals:-
Number of residuals with non-zero weight = 96
Mean value of non-zero weighted residuals = -7.9493E-02
Maximum weighted residual [observation "87"] = 1.219
Minimum weighted residual [observation "57"] = -3.249
Standard variance of weighted residuals = 0.3710
Standard error of weighted residuals = 0.6091
Note: the above variance was obtained by dividing the objective function by the number of system degrees of freedom (ie. number of observations with non-zero weight plus number of prior information articles with non-zero weight minus the number of adjustable parameters.)
If the degrees of freedom is negative the divisor becomes the number of observations with non-zero weight plus the number of prior information items with non-zero weight.

APPENDIX D - PEST PARAMETER VALUES

| | | | |
|---|---|---|---|
| ghb_1 | 441.9313100000000 | 1.000000 | 0.000000 |
| ghb_10 | 12.61434700000000 | 1.000000 | 0.000000 |
| ghb_100 | 12.31430800000000 | 1.000000 | 0.000000 |
| ghb_101 | 12.96894600000000 | 1.000000 | 0.000000 |
| ghb_102 | 10.00000000000000 | 1.000000 | 0.000000 |
| ghb_11 | 407.5895400000000 | 1.000000 | 0.000000 |
| ghb_12 | 342.5787400000000 | 1.000000 | 0.000000 |
| ghb_13 | 196.8247700000000 | 1.000000 | 0.000000 |
| ghb_14 | 97.62104500000000 | 1.000000 | 0.000000 |
| ghb_15 | 8.928776200000000 | 1.000000 | 0.000000 |
| ghb_16 | 156.6128600000000 | 1.000000 | 0.000000 |
| ghb_17 | 252.5887000000000 | 1.000000 | 0.000000 |
| ghb_18 | 83.54151700000000 | 1.000000 | 0.000000 |
| ghb_19 | 303.7129000000000 | 1.000000 | 0.000000 |
| ghb_2 | 790.9844800000000 | 1.000000 | 0.000000 |
| ghb_20 | 117.8251400000000 | 1.000000 | 0.000000 |
| ghb_21 | 72.65621200000000 | 1.000000 | 0.000000 |
| ghb_22 | 705.0404100000000 | 1.000000 | 0.000000 |
| ghb_23 | 1.1231100000000000E-03 | 1.000000 | 0.000000 |
| ghb_24 | 655.5679900000000 | 1.000000 | 0.000000 |
| ghb_25 | 475.2734000000000 | 1.000000 | 0.000000 |
| ghb_26 | 608.6299400000000 | 1.000000 | 0.000000 |
| ghb_27 | 676.1199000000000 | 1.000000 | 0.000000 |
| ghb_28 | 512.0627400000000 | 1.000000 | 0.000000 |
| ghb_29 | 455.5568700000000 | 1.000000 | 0.000000 |
| ghb_3 | 959.9635800000000 | 1.000000 | 0.000000 |
| ghb_30 | 431.8179000000000 | 1.000000 | 0.000000 |
| ghb_31 | 773.0550800000000 | 1.000000 | 0.000000 |
| ghb_32 | 613.8838200000000 | 1.000000 | 0.000000 |
| ghb_33 | 2892.952000000000 | 1.000000 | 0.000000 |
| ghb_34 | 50000.00000000000 | 1.000000 | 0.000000 |
| ghb_35 | 3168.598600000000 | 1.000000 | 0.000000 |
| ghb_36 | 2341.499600000000 | 1.000000 | 0.000000 |
| ghb_37 | 1530.265400000000 | 1.000000 | 0.000000 |
| ghb_38 | 1473.635400000000 | 1.000000 | 0.000000 |
| ghb_39 | 648.6341300000000 | 1.000000 | 0.000000 |
| ghb_4 | 371.2266400000000 | 1.000000 | 0.000000 |
| ghb_40 | 1001.088600000000 | 1.000000 | 0.000000 |
| ghb_41 | 369.2659400000000 | 1.000000 | 0.000000 |
| ghb_42 | 409.9136100000000 | 1.000000 | 0.000000 |
| ghb_43 | 524.2094200000000 | 1.000000 | 0.000000 |
| ghb_44 | 730.2453700000000 | 1.000000 | 0.000000 |
| ghb_45 | 596.0263700000000 | 1.000000 | 0.000000 |
| ghb_46 | 278.8916800000000 | 1.000000 | 0.000000 |
| ghb_47 | 194.2288700000000 | 1.000000 | 0.000000 |
| ghb_48 | 171.1716000000000 | 1.000000 | 0.000000 |

| | | | |
|---|---|---|---|
| ghb_49 | 265.3028400000000 | 1.000000 | 0.000000 |
| ghb_5 | 8.872647000000002 | 1.000000 | 0.000000 |
| ghb_50 | 62.99306500000000 | 1.000000 | 0.000000 |
| ghb_51 | 500.0000000000000 | 1.000000 | 0.000000 |
| ghb_53 | 13.87569400000000 | 1.000000 | 0.000000 |
| ghb_54 | 16.36586100000000 | 1.000000 | 0.000000 |
| ghb_55 | 32.62784000000000 | 1.000000 | 0.000000 |
| ghb_56 | 14.74295900000000 | 1.000000 | 0.000000 |
| ghb_57 | 41.62906700000000 | 1.000000 | 0.000000 |
| ghb_58 | 51.16491100000000 | 1.000000 | 0.000000 |
| ghb_59 | 8.914682000000002 | 1.000000 | 0.000000 |
| ghb_6 | 228.0166300000000 | 1.000000 | 0.000000 |
| ghb_60 | 17.75857500000000 | 1.000000 | 0.000000 |
| ghb_61 | 8.073533400000002 | 1.000000 | 0.000000 |
| ghb_62 | 2.257636600000000 | 1.000000 | 0.000000 |
| ghb_63 | 3.062381300000000 | 1.000000 | 0.000000 |
| ghb_64 | 9.709913000000000 | 1.000000 | 0.000000 |
| ghb_65 | 24.26714600000000 | 1.000000 | 0.000000 |
| ghb_66 | 17.94399100000000 | 1.000000 | 0.000000 |
| ghb_67 | 40.24957700000000 | 1.000000 | 0.000000 |
| ghb_68 | 10.00000000000000 | 1.000000 | 0.000000 |
| ghb_69 | 224.4714100000000 | 1.000000 | 0.000000 |
| ghb_7 | 0.1023906400000000 | 1.000000 | 0.000000 |
| ghb_70 | 381.3290900000000 | 1.000000 | 0.000000 |
| ghb_71 | 172.0398700000000 | 1.000000 | 0.000000 |
| ghb_72 | 69.21397200000000 | 1.000000 | 0.000000 |
| ghb_73 | 218.4896400000000 | 1.000000 | 0.000000 |
| ghb_74 | 39.17258600000001 | 1.000000 | 0.000000 |
| ghb_75 | 0.1005436800000000 | 1.000000 | 0.000000 |
| ghb_76 | 0.1003111800000000 | 1.000000 | 0.000000 |
| ghb_77 | 2.0837500000000000E-03 | 1.000000 | 0.000000 |
| ghb_78 | 0.1015125300000000 | 1.000000 | 0.000000 |
| ghb_79 | 0.1001747400000000 | 1.000000 | 0.000000 |
| ghb_8 | 12.89255300000000 | 1.000000 | 0.000000 |
| ghb_80 | 0.1001795900000000 | 1.000000 | 0.000000 |
| ghb_81 | 0.1007872800000000 | 1.000000 | 0.000000 |
| ghb_82 | 0.1006880100000000 | 1.000000 | 0.000000 |
| ghb_83 | 0.1005386200000000 | 1.000000 | 0.000000 |
| ghb_84 | 2.9996700000000000E-03 | 1.000000 | 0.000000 |
| ghb_85 | 20.74345000000000 | 1.000000 | 0.000000 |
| ghb_87 | 10.81735100000000 | 1.000000 | 0.000000 |
| ghb_88 | 12.06924300000000 | 1.000000 | 0.000000 |
| ghb_89 | 13.25235100000000 | 1.000000 | 0.000000 |
| ghb_9 | 13.23994700000000 | 1.000000 | 0.000000 |
| ghb_90 | 11.73134700000000 | 1.000000 | 0.000000 |
| ghb_91 | 13.61079400000000 | 1.000000 | 0.000000 |
| ghb_92 | 13.71443200000000 | 1.000000 | 0.000000 |

| | | | |
|---|---|---|---|
| ghb_93 | 9.896749400000000 | 1.000000 | 0.000000 |
| ghb_94 | 11.01784300000000 | 1.000000 | 0.000000 |
| ghb_95 | 7.905115900000000 | 1.000000 | 0.000000 |
| ghb_96 | 4.781004600000000 | 1.000000 | 0.000000 |
| ghb_97 | 6.183102100000000 | 1.000000 | 0.000000 |
| ghb_98 | 10.56619000000000 | 1.000000 | 0.000000 |
| ghb_99 | 13.02744500000000 | 1.000000 | 0.000000 |
| hk_10 | 112.8802300000000 | 1.000000 | 0.000000 |
| hk_12 | 32.91995700000000 | 1.000000 | 0.000000 |
| hk_2 | 87.27224200000002 | 1.000000 | 0.000000 |
| hk_3 | 1.3609400000000000E-02 | 1.000000 | 0.000000 |
| hk_4 | 200.0000000000000 | 1.000000 | 0.000000 |
| hk_5 | 30.00000000000000 | 1.000000 | 0.000000 |
| hk_6 | 200.0000000000000 | 1.000000 | 0.000000 |
| hk_7 | 48.42428700000000 | 1.000000 | 0.000000 |
| hk_8 | 30.00000000000000 | 1.000000 | 0.000000 |
| hk_9 | 200.0000000000000 | 1.000000 | 0.000000 |
| rch_1 | 2.0101753000000000E-03 | 1.000000 | 0.000000 |
| rch_10 | 1.7278758000000002E-02 | 1.000000 | 0.000000 |
| rch_101 | 6.4436188000000000E-03 | 1.000000 | 0.000000 |
| rch_102 | 6.0907285000000000E-03 | 1.000000 | 0.000000 |
| rch_103 | 5.4596293000000000E-03 | 1.000000 | 0.000000 |
| rch_104 | 1.2254771000000000E-03 | 1.000000 | 0.000000 |
| rch_105 | 3.5900000000000000E-04 | 1.000000 | 0.000000 |
| rch_106 | 3.5900000000000000E-04 | 1.000000 | 0.000000 |
| rch_108 | 3.5900000000000000E-04 | 1.000000 | 0.000000 |
| rch_11 | 1.4348859000000000E-02 | 1.000000 | 0.000000 |
| rch_110 | 3.5900000000000000E-04 | 1.000000 | 0.000000 |
| rch_111 | 3.5900000000000000E-04 | 1.000000 | 0.000000 |
| rch_112 | 3.5900000000000000E-04 | 1.000000 | 0.000000 |
| rch_113 | 3.1214887000000000E-03 | 1.000000 | 0.000000 |
| rch_115 | 7.0439223000000000E-04 | 1.000000 | 0.000000 |
| rch_117 | 3.5900000000000000E-04 | 1.000000 | 0.000000 |
| rch_119 | 3.5900000000000000E-04 | 1.000000 | 0.000000 |
| rch_12 | 2.4527322000000000E-03 | 1.000000 | 0.000000 |
| rch_120 | 7.1115328000000000E-03 | 1.000000 | 0.000000 |
| rch_121 | 3.4812084000000000E-03 | 1.000000 | 0.000000 |
| rch_122 | 3.5897900000000000E-03 | 1.000000 | 0.000000 |
| rch_13 | 4.1325860000000000E-03 | 1.000000 | 0.000000 |
| rch_14 | 5.4909569000000008E-04 | 1.000000 | 0.000000 |
| rch_15 | 3.5900000000000000E-04 | 1.000000 | 0.000000 |
| rch_16 | 3.5900000000000000E-04 | 1.000000 | 0.000000 |
| rch_17 | 1.0000000000000000E-03 | 1.000000 | 0.000000 |
| rch_2 | 3.7563424000000000E-03 | 1.000000 | 0.000000 |
| rch_20 | 3.5900000000000000E-02 | 1.000000 | 0.000000 |
| rch_21 | 3.1476933000000000E-02 | 1.000000 | 0.000000 |
| rch_22 | 2.8730659000000000E-02 | 1.000000 | 0.000000 |

| | | | |
|---|---|---|---|
| rch_23 | 3.5900000000000000E-02 | 1.000000 | 0.000000 |
| rch_24 | 2.6497538000000000E-02 | 1.000000 | 0.000000 |
| rch_25 | 6.9483622000000000E-03 | 1.000000 | 0.000000 |
| rch_26 | 3.5900000000000000E-04 | 1.000000 | 0.000000 |
| rch_27 | 3.5900000000000000E-04 | 1.000000 | 0.000000 |
| rch_28 | 1.1047420000000000E-03 | 1.000000 | 0.000000 |
| rch_29 | 3.5900000000000000E-04 | 1.000000 | 0.000000 |
| rch_3 | 3.0764762000000000E-03 | 1.000000 | 0.000000 |
| rch_30 | 7.3238125000000000E-03 | 1.000000 | 0.000000 |
| rch_31 | 2.0103164000000000E-02 | 1.000000 | 0.000000 |
| rch_32 | 1.3918783000000000E-02 | 1.000000 | 0.000000 |
| rch_33 | 1.7652053000000000E-02 | 1.000000 | 0.000000 |
| rch_34 | 1.5273095000000000E-02 | 1.000000 | 0.000000 |
| rch_35 | 2.0948327000000000E-02 | 1.000000 | 0.000000 |
| rch_36 | 1.9653740000000004E-03 | 1.000000 | 0.000000 |
| rch_4 | 3.0574181000000000E-04 | 1.000000 | 0.000000 |
| rch_5 | 7.6617415000000000E-03 | 1.000000 | 0.000000 |
| rch_6 | 1.9293933000000000E-03 | 1.000000 | 0.000000 |
| rch_60 | 3.1887739999999996E-02 | 1.000000 | 0.000000 |
| rch_61 | 3.1286230000000000E-02 | 1.000000 | 0.000000 |
| rch_62 | 2.7344391000000000E-02 | 1.000000 | 0.000000 |
| rch_63 | 2.5344608000000000E-02 | 1.000000 | 0.000000 |
| rch_64 | 3.5900000000000000E-02 | 1.000000 | 0.000000 |
| rch_65 | 2.2117901000000000E-02 | 1.000000 | 0.000000 |
| rch_66 | 1.1908710000000000E-02 | 1.000000 | 0.000000 |
| rch_67 | 5.5743048000000000E-03 | 1.000000 | 0.000000 |
| rch_68 | 5.5388968000000000E-03 | 1.000000 | 0.000000 |
| rch_69 | 6.3085232999999992E-03 | 1.000000 | 0.000000 |
| rch_7 | 4.8285791999999992E-03 | 1.000000 | 0.000000 |
| rch_70 | 4.6283931000000000E-03 | 1.000000 | 0.000000 |
| rch_71 | 1.1893049000000000E-03 | 1.000000 | 0.000000 |
| rch_72 | 1.0963311000000000E-03 | 1.000000 | 0.000000 |
| rch_73 | 3.5900000000000000E-04 | 1.000000 | 0.000000 |
| rch_74 | 3.5900000000000000E-04 | 1.000000 | 0.000000 |
| rch_75 | 8.7230341000000000E-03 | 1.000000 | 0.000000 |
| rch_76 | 3.6200100000000000E-03 | 1.000000 | 0.000000 |
| rch_8 | 1.9641805000000000E-02 | 1.000000 | 0.000000 |
| rch_80 | 5.5892450000000000E-04 | 1.000000 | 0.000000 |
| rch_81 | 3.9283964000000000E-04 | 1.000000 | 0.000000 |
| rch_82 | 9.0210490000000000E-04 | 1.000000 | 0.000000 |
| rch_83 | 4.7929845000000000E-03 | 1.000000 | 0.000000 |
| rch_84 | 4.9292241000000000E-03 | 1.000000 | 0.000000 |
| rch_85 | 5.1998900000000008E-03 | 1.000000 | 0.000000 |
| rch_86 | 6.7709369000000000E-03 | 1.000000 | 0.000000 |
| rch_87 | 3.3076361000000000E-03 | 1.000000 | 0.000000 |
| rch_88 | 4.7863721000000000E-03 | 1.000000 | 0.000000 |
| rch_89 | 3.5935610000000000E-03 | 1.000000 | 0.000000 |

| | | | |
|---|---|---|---|
| rch_9 | 1.7503285000000000E-02 | 1.000000 | 0.000000 |
| rch_90 | 1.4289728000000000E-03 | 1.000000 | 0.000000 |
| rch_91 | 3.5469542000000000E-03 | 1.000000 | 0.000000 |
| rch_92 | 6.8230148000000000E-03 | 1.000000 | 0.000000 |
| rch_93 | 5.6025804000000000E-03 | 1.000000 | 0.000000 |
| rch_94 | 3.5900000000000000E-04 | 1.000000 | 0.000000 |
| rch_95 | 1.3933470999999998E-03 | 1.000000 | 0.000000 |
| rch_96 | 3.5800000000000000E-03 | 1.000000 | 0.000000 |
| vk_11 | 2.000000000000000 | 1.000000 | 0.000000 |
| vk_12 | 200.0000000000000 | 1.000000 | 0.000000 |
| vk_123 | 124.1175800000000 | 1.000000 | 0.000000 |
| vk_13 | 5.0000000000000000E-02 | 1.000000 | 0.000000 |
| vk_14 | 200.0000000000000 | 1.000000 | 0.000000 |
| vk_15 | 6.2497589999999992E-05 | 1.000000 | 0.000000 |
| vk_16 | 16.28417300000000 | 1.000000 | 0.000000 |
| vk_17 | 1.7471362000000000E-02 | 1.000000 | 0.000000 |
| vk_18 | 13.87519400000000 | 1.000000 | 0.000000 |
| vk_19 | 2.6701328000000000E-04 | 1.000000 | 0.000000 |
| vk_20 | 5.051451800000000 | 1.000000 | 0.000000 |
| vk_21 | 5.6562533000000000E-03 | 1.000000 | 0.000000 |
| vk_22 | 200.0000000000000 | 1.000000 | 0.000000 |
| vk_23 | 175.2736400000000 | 1.000000 | 0.000000 |
| vk_24 | 200.0000000000000 | 1.000000 | 0.000000 |
| vk_25 | 200.0000000000000 | 1.000000 | 0.000000 |
| vk_26 | 0.5000000000000000 | 1.000000 | 0.000000 |
| vk_27 | 21.58217100000000 | 1.000000 | 0.000000 |
| vk_28 | 191.2796700000000 | 1.000000 | 0.000000 |
| vk_30 | 200.0000000000000 | 1.000000 | 0.000000 |

APPENDIX E: MODEL PREDICTION PUMPING RATES

**Table E1:** All the pumping rates for the wells used for the model are listed by year. The final three rows are the values used for the each of first three predictive models.

| Year | Gul-50 | Gul-45 | Gul-22 | zz-43 | Gul-23 | Gul-5 | Gul-50b | Gul-23b | Daily Sum |
|---|---|---|---|---|---|---|---|---|---|
| 1996 | -15000 | -100000 | -44000 | -66000 | -30000 | -96192 | -15000 | -70000 | -436192 |
| 1997 | -15000 | -102000 | -46000 | -68000 | -32000 | -96192 | -15000 | -72000 | -446192 |
| 1998 | -15000 | -104000 | -48000 | -70000 | -34000 | -96192 | -15000 | -74000 | -456192 |
| 1999 | -15000 | -121733 | -50150 | -65089 | -34114 | -96192 | -15000 | -76474 | -473752 |
| 2000 | -15000 | -102978 | -60892 | -70915 | -28882 | -96192 | -15000 | -103365 | -493224 |
| 2001 | -15000 | -56942 | -38995 | -42092 | -13673 | -96192 | -15000 | -91410 | -369304 |
| 2002 | -15000 | -18120 | -21946 | -36093 | -13895 | -96192 | -15000 | -86916 | -303162 |
| 2003 | -15000 | -16280 | -9910 | -62289 | -4938 | -96192 | -15000 | -71907 | -291516 |
| 2004 | -15000 | -29900 | -4311 | -61373 | -4987 | -96192 | -15000 | -80215 | -306978 |
| 2005 | -15000 | -12607 | -2668 | -56406 | -3048 | -96192 | -15000 | -81128 | -282049 |
| 2006 | -15000 | -56938 | -3242 | -58507 | -3520 | -96192 | -15000 | -79595 | -327994 |
| 2007 | -15000 | -77509 | -4496 | -47471 | -5221 | -96192 | -15000 | -71218 | -332107 |
| 2008 | -15000 | -66225 | -8957 | -45715 | -11072 | -96192 | -15000 | -68515 | -326676 |
| 2009 | -15000 | -66425 | -5792 | -45571 | -7261 | -96192 | -15000 | -70368 | -321609 |
| 2010 | -15000 | -65994 | -3871 | -35388 | -5118 | -96192 | -15000 | -61903 | -298466 |
| 2011 | -15000 | -73542 | -20721 | -51947 | -9378 | -96192 | -15000 | -65995 | -347775 |
| 2012 | -15000 | -73040 | -20654 | -53637 | -19868 | -96192 | -15000 | -91619 | -385010 |
| Average | -15000 | -67307.8 | -23212.1 | -55087.8 | -15351.5 | -96192 | -15000 | -77448.7 | -364599.9 |
| Minimum | -15000 | -12607 | -2668 | -35388 | -3048 | -96192 | -15000 | -61903 | -241806 |
| Maximum | -15000 | -102978 | -60892 | -70915 | -28882 | -96192 | -15000 | -103365 | -493224 |